High-Efficient Wideband Spectrum Measurement based on FFT for Dynamic Spectrum Access

Hiroki Iwata

Department of Electronic and Information Engineering

Tokyo University of Agriculture and Technology

A thesis is submitted for the degree of

Doctor of Philosophy

March 2019

Supervised by

Associate Professor Kenta Umebayashi

Reviewed by

Professor Toru Uno

Associate Professor Takuji Arima

Associate Professor Takehito Suzuki

Visiting Associate Professor Soichi Watanabe

Day of the Predefense: November 26, 2018.

Day of the Final Defense: February 7, 2019.

Abstract

The scarcity of spectrum resources is a pressing challenging problem in the field of wireless communications. This is due mainly to the current static and exclusive spectrum allocation. In fact, many spectrum measurement results all over the world reveal the allocated spectrum to existing wireless systems are not fully utilized or under-utilized. For this issue, dynamic spectrum access (DSA) has been extensively investigated globally. In DSA, secondary users (SUs), which have lower priority to use the spectrum, can use the spectrum owned by primary users (PUs) without causing harmful interference to PUs. For achieving the concept of DSA, several practical approaches have been proposed. These approaches are roughly classified into sensing-based DSA, database-based DSA, and these hybrid version. Among them, smart spectrum access (SSA), which is DSA based on spectrum measurement, modeling, database, management, and sensing is a promising approach to an advanced and practical DSA. Conceptually, SSA exploits useful *a priori* information regarding spectrum usage via spectrum measurements for achieving smart DSA. Therefore, one important aspect in SSA is spectrum measurement with efficiency and high accuracy since the results of spectrum measurements may affect the performance and operation of SUs.

Spectrum measurements are performed by several spectrum sensors which are distributed over wide geographical area. Each spectrum sensor observes surrounding radio environment, acquires the radio signal such as I/Q signal, detects spectrum occupancies, and send their occupancy data to a fusion center. Previous spectrum measurements utilize energy detector (ED) based on the fast Fourier transform(FFT) to detect spectrum usage. There is one most important issue with ED regardless of how it is implemented: its limited detection performance. To overcome this, Welch FFT-based ED (Welch FFT-ED) is an effective approach. Welch FFT consists of three steps: segmentation

of the data sequence with a specific FFT size, calculation of multiple power spectra and averaging of the power spectra. Here, the number of segments defines over how many segments the averaging is performed and more averaging provides better detection performance. Due to the the Welch FFT operation, there is a trade-off between the detection performance and frequency resolution in terms of FFT size. Thus, this trade-off affects awareness performance of spectrum usage at each spectrum sensor.

In this dissertation, we investigate FFT size setting problem in Welch FFT-ED by considering the above trade-off. The first part of this dissertation formulates the optimum FFT size as the one that allows the accurate detection of spectrum occupancy while maintaining target DC estimation accuracy and a small enough target false alarm rate. In addition, we also define a sub-optimum FFT size which is obtained analytically. The analysis reveals that the FFT size depends on SNR and true DC value. This indicates that FFT size setting is challenging problem since prior knowledge of SNR and actual DC value is impractical.

The second part of this dissertation proposes two practical adaptive FFT size setting methods which utilizes outputs of noise floor (NF) estimation instead of SNR and DC information. Thus, the proposed methods are very practical and easy to use. The first method uses NF estimation outputs for all possible FFT sizes in Welch FFT. Thus, this method is expected to achieve a high performance in terms of RMSE of DC estimation and WSDR metric, but to also have a relatively high computational cost. For reducing the computational cost of the first method, the second method is proposed. This method achieve both reasonable RMSE and WSDR performances and low computational complexity since it searches the proper segment size while limiting the searchable segment sizes. These two methods can adaptively select the proper FFT size in real time without human intervention. Therefore, we expect to the contributions in this dissertation are helpful for developing the real-time and automatic spectrum measurement systems.

Acknowledgements

This thesis is a summary of my doctoral study at the Tokyo University of Agriculture and Technology, Tokyo, Japan. I am grateful to a large number of people who have helped me to accomplish my work. First of all, I would like to express my deepest gratitude to my supervisors, Associate Professor Kenta Umebayashi and former Professor Yasuo Suzuki, for guiding my throughout my work. His motivations and encouragements immensely helped me throughout my life in the Tokyo University of Agriculture and Technology. I also would like to give my special thanks to Adjunct Professor Janne Lehtomaki and Lecturer Miguel Lopez Benitez for their valuable guidance, instructions and continuous support. I grateful to all the members of Umebayashi Lab. Finally, I would like to have my family to thank for their words, attitudes, and every supports.

Contents

[1]This chapter is based on "Welch FFT Segment Size Selection Method for Spectrum Awareness System" [2] in Publications, by the same authors, which appeared in IEICE Transactions on Communications, Copyright(C)2016 IEICE.

[2]This chapter is based on "Welch FFT Segment Size Selection Method for FFT Based Wide Band Spectrum Measurement" [1] in Publications, by the same authors, which appeared in IEICE Transactions on Communications, Copyright(C)2018 IEICE.

List of Figures

List of Tables

Nomenclature

Roman Symbols

Scalar	Roman italic letters（e.g., n)
Vector	Bold-face lower-case Roman letters（e,g,, $\boldsymbol{w}$)
行列	Bold-face upper-case Roman letters （e.g., $\boldsymbol{H}$)

Greek Symbols

j	Imaginary number
$\blacksquare^*$	Complex conjugate
$\blacksquare^H$	Complex conjugate transpose of a complex matrix
$\blacksquare^T$	Transpose of a matrix
$\lvert\blacksquare\rvert$	Absolute value of a scalar

Acronyms / Abbreviations

A

B

C

CFAR	Constant False Alarm Rate
COR	Channel Occupancy Rate
CR	Cognitive Radio

D

DC	Duty Cycle

DSA	Dynamic Spectrum Access
DSAS	Dynamic Spectrum Spectrum Access System

E

ED	Energy Detection
E-SS	Exhaustive Search-based FFT Size Setting

F

FBMC	Filter Bank Multi Carrier
FCME	Forward Consecutive Mean Excision
FFT	Fast Fourier Transform
fOFDM	Filtered Orthogonal Frequency Division Multiplexing

G

GFDM	Generalized Frequency Division Multiplexing
ISM	Industrial Scientific and Medical

I

IEEE	Institute of Electrical and Electronics Engineers
I/Q	In-phase/Quadrature
ITU	International Telecommunication Union

L

L-SS	Limited Search-based FFT Size Setting

M

MAC	Media Access Control
MAE	Mean Absolute Error
MIMO	Multiple Input Multiple Output
MTC	Machine-type Communication

N

NF	Noise Floor
NOMA	Non-Orthogonal Multiplex Access

O

OFDM	Orthogonal Frequency Division Multiplexing

P

PHY	PHYsical
PS	Power Spectrum
PSD	Power Spectrum Density
PU	Primary User

R

RMSE	Root Mean Square Error

S

SAS	Spectrum Awareness System
SNR	Signal-to-Noise Ratio
SSA	Smart Spectrum Access
SU	Secondary User

T

TCP/IP	Transmission Control Protocol/Internet Protocol
TDMA	Time Division Multiple Access

U

UHF	Ultra High Frequency
USRP	Universal Software Radio Peripheral

W

VHF	Very high Frequency
WLAN	Wireless Local Area Network
WS	White Space
WSDR	White Space Detection Rate

Chapter

1

Introduction

1.1 Background

1.1.1 Demand and Scarcity of Spectrum Resources

About 120 years have passed since German physicist, Heinrich Rudolf Hertz confirmed the existence of electromagnetic spectrum experimentally. After that, an Italian inventor, Guglielmo Marconi, invented a practical system for wireless telegraphy capable to use electromagnetic waves to send information; it is the beginning of wireless communication via electromagnetic spectrum (especially radio spectrum). On this occasion, remarkable progress has been made in the wireless communication field and the wireless communication has become indispensable to our now. Especially, data traffic has significantly increased during the last decade due to the spread of high-function mo-

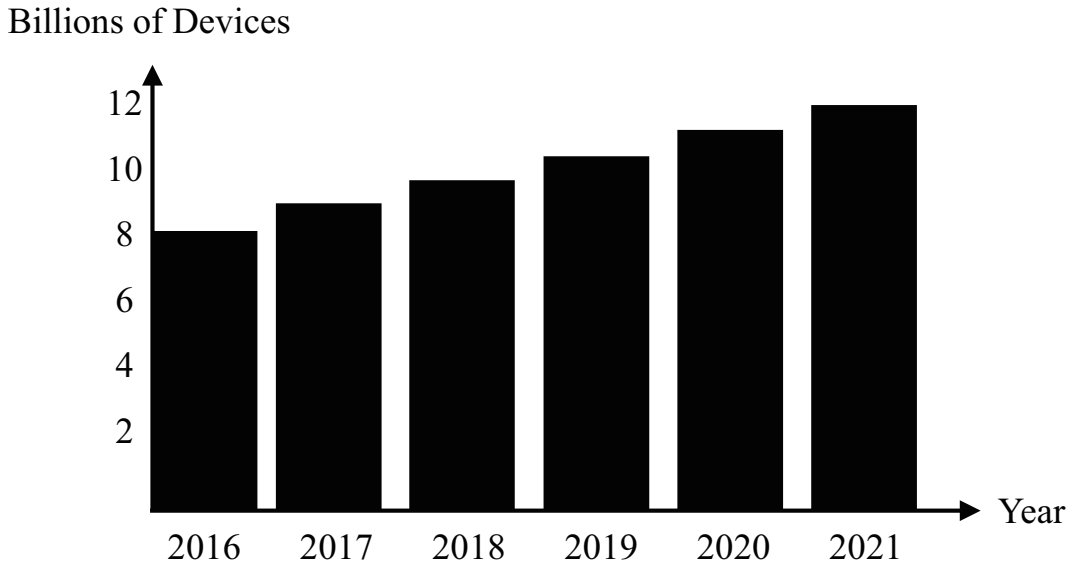

Fig. 1.1: Forecasts by Cisco about number of devices, 2016 to 2021 [1]

bile terminals such as smart phones and table terminals and the growth content-rich services, etc. In fact, the number of devices is expected a 1.5-fold increase between 2016-2021 (7.6 billion in 2016 and 11.6 billion in 20121) [1]. [1] predicts an exponential increase in data traffic that corresponds to a 7-fold increase in traffic between 2016-2021, as shown in Fig. 1.2. This is due mainly to the diversification of usage scenes; they mainly include cellular, wireless local area network (WLAN), bluetooth, machine-type communications (MTC). This means wireless communication is an indispensable lifeline and the demand for spectrum resources continues to increase. In addition, radio spectrum, which are one of the wireless resources have to be exploited efficiently since they are limited and precious resources.

However, although the demands for wireless communications are explosively expanding, we face a fundamental, but critical problem: severe scarcity of the spectrum resources. Due to the propagation properties of radio waves, the signal transmitted by an antenna interferes with the other communication systems that share the same spectrum at the same time and location. Therefore, spectrum have been statically and exclusively assigned to each specific system for a long term and over a large geographical area in order to avoid the unintended degradation (interference) of the communication

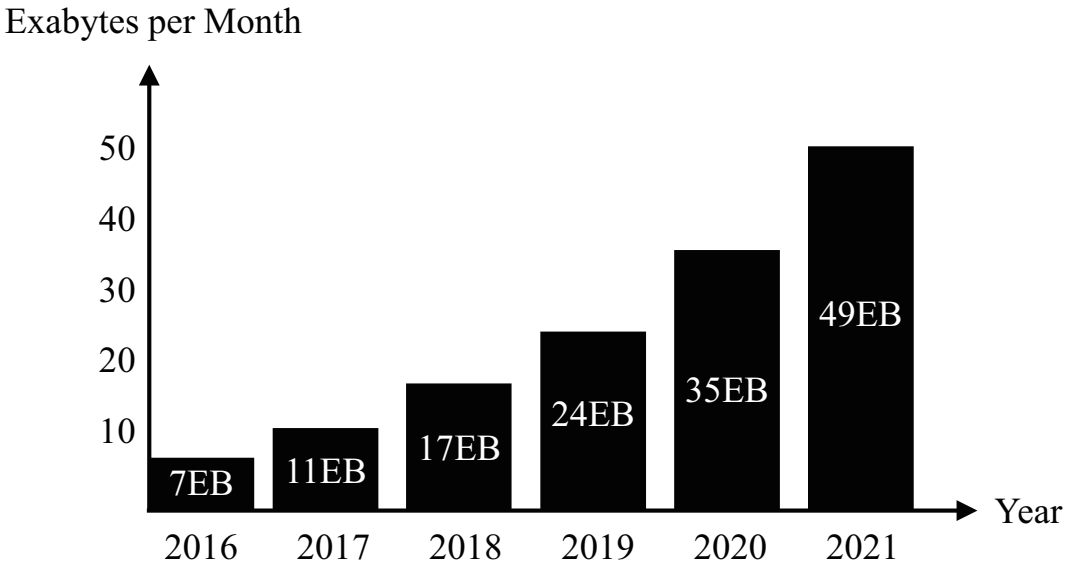

Fig. 1.2: Forecasts by Cisco about global mobile data traffic, 2016 to 2021 [1]

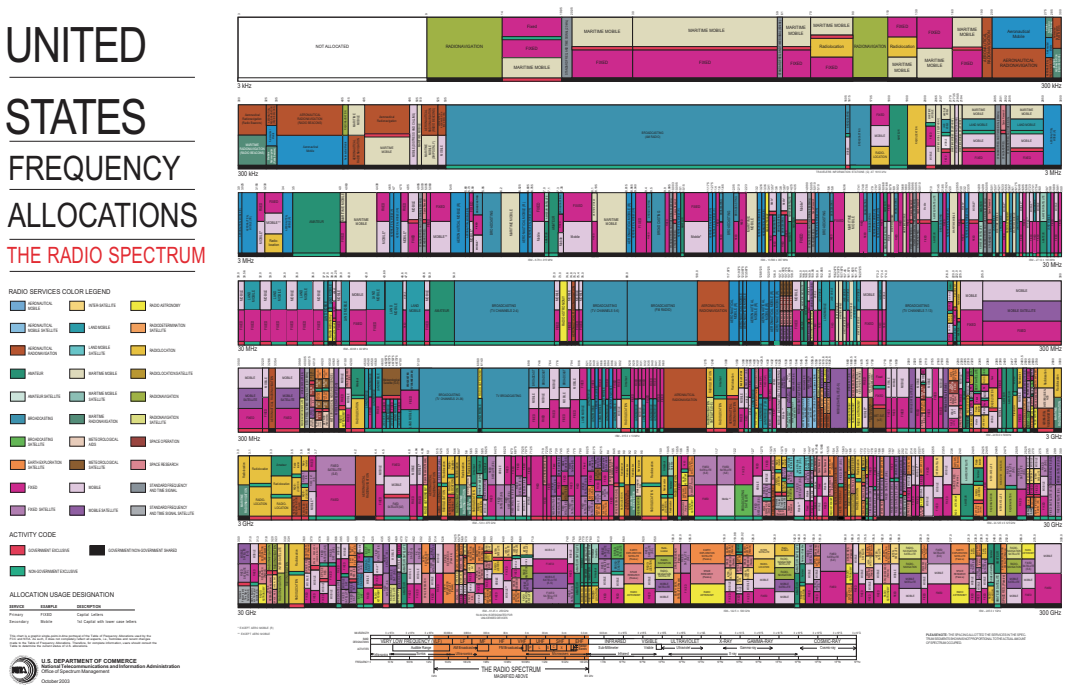

Fig. 1.3: Frequency Allocation Chart in U.S. [2]

quality.

Figure 1.3 summarizes the spectrum allocation in U.S. [2]. The figure clearly explains that almost all bands from several kHz to several hundred GHz have been already

allocated to any wireless systems. In particular, in several hundred MHz to several GHz bands, which are suitable for mobile communication systems from the viewpoint of antenna design and radio propagation, several wireless communications systems even share the same spectrum. Thus, it is clear that there is almost not the spectrum allocatable to new wireless systems appearing in the future if the current spectrum allocation or management strategy is not changed.

Furthermore, many researchers and wireless companies reported some wireless systems such as wireless local area networks (WLANs) and cellular networks are overcrowded and the desired quality of service of communication can not be satisfied. This means the overcrowded wireless systems require more spectrum to alleviate the congestion.

1.1.2 Potential Solutions to Spectrum Scarcity Problem

The scarcity of spectrum resources is one of the most important problem in the field of wireless communication and it has to be solved early. Therefore, many researches have attacked the problem from different viewpoint, and today's countermeasures for the problem can mainly be classified into three approaches as follows.

Development of High-Spectral Efficient Techniques

A simple direction is to improve the spectral efficiency via new radio techniques in the framework of the current frequency allocation (statical and exclusive allocation). This direction includes massive MIMO, new waveform such as fOFDM [4–6], FBMC [7, 8], spatial modulation [9–11], full-duplex radio [12–14], non-orthogonal multiple access (NOMA) [15–17], coded MAC [18, 19], and new error correction coding such as polar codes [20, 21]. The improvement of spectrum efficiency may be solve the congestion in the crowded wireless systems since more users are accommodated compared to the current using the same spectrum resources. Moreover, it can create the spectrum allocatable to new wireless systems while satisfying the demand of spectrum resources for existing wireless systems as the spectrum should be allocated to the existing wireless systems is compressed.

Opening of additional frequency band

As mentioned above, the spectrum in several hundred MHz to several GHz bands, say below 6GHz has been already allocated to some wireless systems. However, most of higher frequency bands, say above 6GHz such as mm-wave band and THz band are not allocated to any wireless systems yet due to the poor propagation characteristic compared to the lower frequency bands. So, many researchers attempt to develop their higher frequency bands for bandwidth-hungry wireless systems and new wireless systems. Especially, mm-wave communications are very important for the next-generation cellular mobile communication systems (the 5G systems). However, there are several difficult problems. These include path loss, blocking, atmospheric and rain absorption, link acquisition and development of new transceiver architectures.

Spectrum Sharing with Existing Wireless Systems

Most of the frequency bands suitable for mobile communication have already been allocated exclusively to some system as shown above. However, many experimental results show that the spatio-temporal usage rates in these bands are very low, and the other spectra are not used effectively. Therefore, spectrum sharing which uses these free bands while guaranteeing the communication quality of existing communication systems is also widely discussed over the last decades. There are several spectrum sharing models and they will be introduced in the next section.

In summary, all these approaches can deal with the spectrum scarcity today. However, from the viewpoint of fundamental physical characteristics such as antenna size and radio propagation, the frequencies below several GHz, say 6 GHz undoubtedly are exploited for wireless communications and/or non-wireless communications in the future. Thus, the spectrum sharing with existing wireless systems is a most appropriate approach in sub-6GHz spectrum since these frequency bands have been allocated to any wireless systems and there is no room for accommodating new wireless systems.

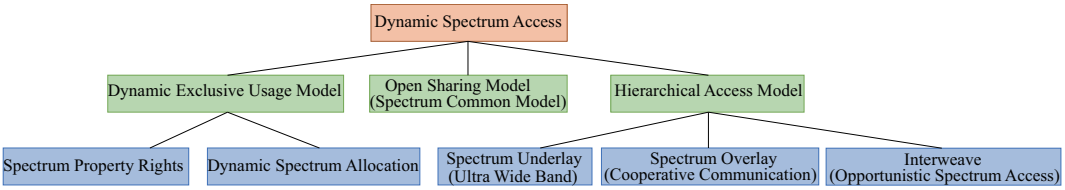

Fig. 1.4: Dynamic Spectrum Access Model

1.1.3 Dynamic Spectrum Access

Spectrum sharing with the existing wireless systems are called as Dynamic Spectrum Access (DSA) and have been investigated from the various aspects over about 20 years. The concept of DSA has a potential to bring to the ultimate spectrum usage over several frequency bands regardless of the wireless services. Although spectrum sharing is not a new idea, it has gained popularity for a long time. With this background, several DSA models have been proposed and some new models recently appear. There are many DSA models, but the models can be broadly are broadly classified into three models as shown in Fig. 1.4 following the survey papers [22–25]. We will describe their models in detail below.

Dynamic Exclusive Use Model [26–28]

This model maintains the basic structure of the current spectrum regulation policy, but some flexibility is introduced to improve spectrum efficiency. There are two approaches under this model: Spectrum property rights [26] and *dynamic spectrum allocation [27, 28]*. The former approach allows licensees to sell and trade own spectrum. The purchasers can freely choose technology. The fields of economy and market will thus play a more important role in this approach. Note that even though licensees have the right to lease or share the spectrum for profit, such sharing is not mandated by the regulation policy.

The second approach, dynamic spectrum allocation, was brought forth by the European DRiVE (Dynamic Radio for IP-Services in Vehicular Environments) project. It is aimed at managing the spectrum utilized by a converged radio system and share it between participating Radio Access Networks (RANs) over

space and time to increase overall spectrum efficiency. Similar to the current static spectrum allocation policy, such approach allocates, at a given time and region, a portion of the spectrum to a RAN for its exclusive use. However, this allocation varies at a much faster scale than the current policy, where the period of allocation in the current policy is several years, but dynamic spectrum allocation can vary every one hour or one minute.

Open Sharing Model [29, 30]

This model is referred to as spectrum commons and its history is relatively long compared with other models. It employs open sharing among peer users as the basis for managing a spectral region. Advocates of this model draw support from the phenomenal success of wireless services operating in the unlicensed industrial, scientific, and medical (ISM) radio band (e.g., WiFi, bluetooth, etc.). Spectrum commons proponents assert that wireless transmissions can be regulated by baseline rules that allow users to coordinate their use, to avoid collisions. Centralized and distributed spectrum sharing strategies have been investigated to address technological challenges under this spectrum management model. For example, WiFi systems (IEEE 802.11 family) operate in a distribute manner, i.e., CSMA/CA (Carrier Sense Multiple Access/Collision Avoidance) protocol. In recent year, the latest IEEE 802.11 standard (IEEE 802.11 ax) adopts a centralized mechanism since the unlicensed ISM band has become highly congested due to the success of WiFi and bluetooth.

Hierarchical Access Model

This model adopts a hierarchical access structure depending on the right to access the spectrum. Typical model consists of two layer structure: primary users (PUs) and secondary users (SUs). PUs have highest right to access the own spectrum and SUs have lower right to access than PUs. The basic idea is to open licensed spectrum to SUs while limiting the interference towards PUs. Three approaches to spectrum sharing between PUs and SUs have been considered: Spectrum underlay, Spectrum overlay, Interweave.

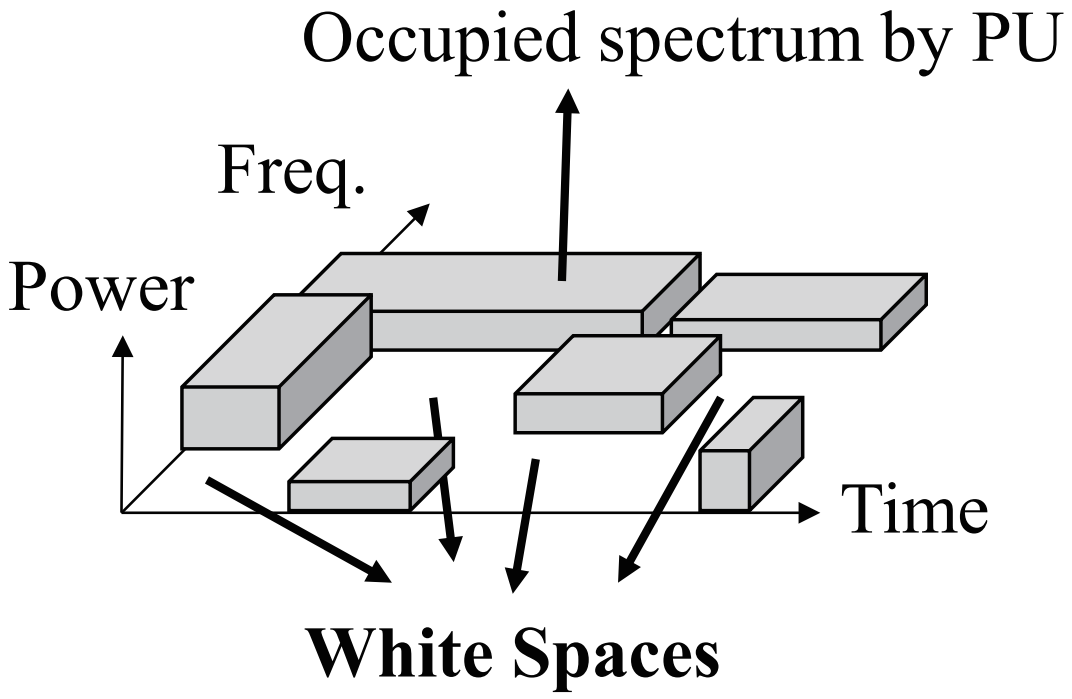

Fig. 1.5: Opportunistic Spectrum Access Concept

The underlay approach allows concurrent transmissions for SUs but imposes constraints on their transmission power so that they operate below the noise floor of PUs. To meet such requirements, SUs can use some technologies such as Code Division Multiple Access (CDMA) or Ultra Wide Band (UWB). This approach allows SUs to potentially achieve short-range high data-rates with extremely low transmission power. Based on a worst-case assumption that PUs transmit all the time, this approach does not rely on detection of spectrum white space (WS). Another advantage is that the activity of PUs does not need to be tracked by SUs since secondary transmissions are allowed provided that power constraints are met. Despite the aforementioned benefits, this approach suffers from some practical drawbacks that mitigate its importance [19], the most important one being that the low transmission power still limits the applicability of spectrum underlays to short-range applications.

The overlay approach also allows concurrent transmission for SUs at the same time, frequency and location. The knowledge sharing and cooperation between

the SUs and PUs is critical in this model. Specifically, the interference imposed on the PUs can be offset by using part of the SUs' power for relaying the PUs' information. Some SUs assist the PUs to free up some spectrum bands. These vacant spectrum bands would then be used by other CUs for their secondary transmission. Thus, This type of approach is also referred as to cooperation communication between PUs and SUs.

The interweave approach is also referred to as opportunistic spectrum access (OSA) and is basically based on cognitive radio technology [3, 31]. Differing from spectrum underlay, this approach is not necessarily characterized by severe restrictions on the transmission power of SUs. The restriction on this approach is that when and where SUs may transmit. Thus, the basic idea of this approach is to explore spatial and temporal spectrum gaps not occupied by PUs, referred to as spectrum holes or white spaces, and exploit such spaces for secondary transmissions. This idea allows SUs to harvest the spectrum resources for own transmissions without causing harmful interference towards PUs. The main subject of this approach is therefore to explore and exploit local and instantaneous spectrum availability in a non-intrusive and opportunistic manner as illustrated in Figure 1.5. Compared to the dynamic exclusive use and open sharing models, this hierarchical model is perhaps the most compatible with the current spectrum management policies and legacy wireless systems due to no PUs intervention. Furthermore, these three approaches can be employed simultaneously to further improve spectrum efficiency.

Although the dynamic exclusive use model is able to improve the spectrum efficiency without changing legacy management policies, this approach cannot completely eliminate white spaces resulting from the bursty nature of wireless traffic. The interest of the open sharing model has recently been decreasing due to the increased amount of interference among multiple wireless technologies on the band adopting the model.

On the other hand, the hierarchical access model is perhaps the most promising alternative because it does not require the change of current spectrum management policies and legacy wireless systems and it can be strictly managed the spectrum and

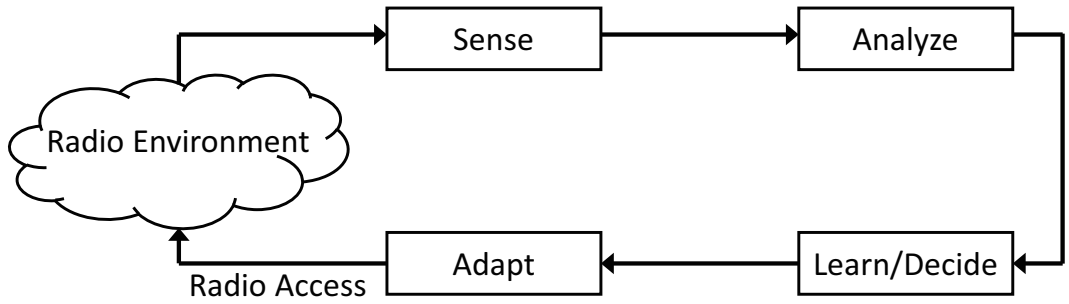

Fig. 1.6: Simplified Cognitive Cycle [3]

the interference. In particular, the spectrum overlay or OSA approach is one of the most popular frameworks nowadays. The spectrum overlay/OSA scheme has received large attention during the last years and also constitutes the DSA model considered in this dissertation.

1.1.4 Cognitive Cycle for Opportunistic Spectrum Access

As mentioned above, in the interweave or OSA model in the hierarchical access model, SUs can share the spectrum owned by PUs exploiting WS if SUs do not interfere to PUs significantly. Therefore, SUs may be able to access to the shared spectrum based on a cognitive cycle as shown in Fig. 1.6. The cognitive cycle is consisted of spectrum sensing (awareness of spectrum usage), spectrum decision, spectrum sharing and spectrum mobility [3]. We will describe each component of the cognitive cycle in detail below.

Spectrum Sensing

The role of this function is determining which portions of the spectrum are available to secondary users for opportunistic use, i.e., exploring WS. Also, it provides basic information or data to capture the parameters related to sensing bands (e.g., cumulative power levels, PUs' activities, etc.). Spectrum sensing becomes a function of paramount importance to enable spectrum sharing between PUs and SUs since it is the foremost functionality in the cognitive cycle and its performance affects subsequent cognitive functions as shown in Fig. 1.6.

Spectrum sensing may be performed in cooperative and non-cooperative fashions. In non-cooperative schemes, SUs detect the primary transmitter signal independently based on locally sensed spectrum information. The sensed spectrum information must be accurate high enough to reach accurate conclusions regarding the radio environment. Furthermore, spectrum sensing must be fast in order to track the temporal variations of the radio environment. Such requirements of spectrum sensing puts stringent requirements on the hardware implementation of cognitive radios in terms of the sensing bandwidth, the processing power, the radio frequency (RF) circuitry, etc. Existing spectrum sensing techniques include matched filter detection, energy detection, feature detection. The difference of these techniques is the amount of information regarding PUs and matched filter detection has highest performance because it exploits full information of PUs. On the other, energy detection can operate without any information of PUs leading to its applicability, but it cannot achieve high sensing performance. The future detection ranks between matched filter detection and energy detection in terms of sensing performance and the amount of information required. In general, this non-cooperative schemes are very susceptible to surrounding radio environment such as path loss, shadowing, multi-path fading.

For this issue, cooperative spectrum sensing schemes have been considered. It relies on the exchange of sensing information from multiple SUs. Cooperation among secondary users is theoretically more accurate due to spatial diversity which mitigated the negative effects of multi-path fading and shadowing. In addition, it allows individual secondary terminals to relax the detection performance requirements. However, cooperation also has some disadvantages. First, it requires a reliable control channel to exchange sensing information. Second, it introduces additional signaling overhead, which might be significant depending on the amount of cooperating nodes and the type of information exchanged (e.g., binary busy/idle decisions or signal statistics). Third, cooperation implies additional energy consumption, which is an important aspect in battery-powered terminals. Forth, cooperation may produce security issues due to e.g., the existing

malicious users and emulation attacks.

Spectrum Analysis

This function is in charge of characterization of the spectrum holes and the surrounding radio environment that are measured through spectrum sensing. Specifically, the characteristics of the spectrum holes detected in different spectrum bands are analyzed in terms of interference level, path loss, channel error rate, link layer delay, expectable vacancy duration, and other appropriate parameters.

Spectrum Decision

This function decides the most suitable spectrum band to meet the communication requirements of the SU based on spectrum analysis results. Specifically, based on spectrum analysis results, the operating band is selected based on the user Quality of Service (QoS) requirements (e.g., data rate, error rate, delay, etc.) and the spectrum characteristics. This function is also aimed at providing a fair spectrum access to the coexisting SUs by coordinating the access to the available WS. Therefore, the problem of spectrum decision shows some analogies with the Medium Access Control (MAC) problem in traditional communication systems. However, there are some substantially different challenges which are described in [64].

Adaptation/Reconfiguration of Transmission Parameters

The last step for access to WS is the adaptation of reconfiguration of transmission parameters. This function distinguishes a cognitive radio from a traditional one, and is essential part for complete the cognitive cycle depicted in Fig. 1.6. Specifically, it is its ability to re-tune its transceiver parameters on the fly based on its assessment of the surrounding radio environment (spectrum decision functionality). While today's radios have considerable flexibility in terms of their ability to reconfigure some transmission parameters such as the transmission rate and power, they are typically designed to operate over certain frequency band(s) according to a certain communication protocol. On the other hand, transceiver for realizing OSA concept should be more flexible than just this in order to be able to

exploit emerging WS over a wider spectrum range. For example, the transceiver must be able to configure the transmission bandwidth to adapt to spectral opportunities of different sizes. Furthermore, it must determine the appropriate communication protocol based on the characteristic of WS and surrounding radio environment.

Spectrum Mobility

To avoid harmful interference towards PUs, SUs must vacate a communicating channel when a PU is detected and move to an alternative available channel. Perhaps, the requirement of the movement to an alternative available channel occurs by other reasons such as preserving or improvement of the QoS. Such transition from one spectrum band to another is referred to as spectrum handover or mobility. The objective of the spectrum mobility function is to maintain seamless wireless connectivity for avoiding harmful interference to PUs and preserving or improvement of own QoS, etc. This function involves not only the change of parameters in physical layer, but also the change of parameters in higher layers and their changes should be performed rapidly.

By the cognitive cycle OSA concept can be realized, but its cycle speed should be fast enough so that it can track the dynamics of spectrum usage by PUs. Furthermore, the high-reliable cognitive cycle is required. Therefore, we must seek the new approach to solve the very difficult task for cognitive cycle.

1.1.5 Smart Spectrum Access

During the last years, the OSA concept has gained popularity as a promising solution to conciliate the existing conflicts between the ever-increasing spectrum demand growth and the demonstrated spectrum underutilization. As explained in Sects. 1.1.3 and 1.1.4, the basic idea of the OSA is that SUs are aware of WSs exploiting spectrum sensing techniques and then opportunistically exploit them for achieving the spectrum sharing with PUs though spectrum analysis, spectrum decision and adaptation of transmission parameters. In addition, SUs have to vacate the channel as soon as a primary

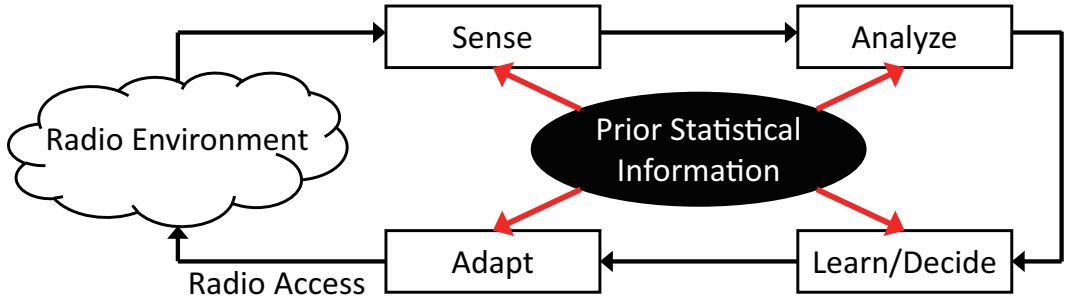

Fig. 1.7: Realizing the Reliable and efficient Cognitive Cycle by SAS

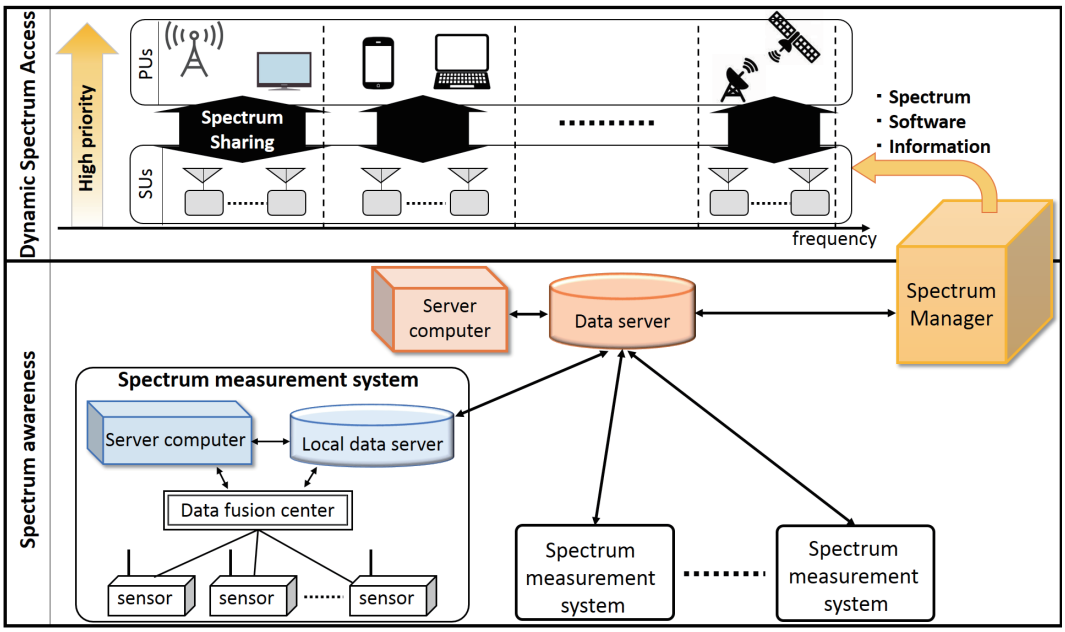

Fig. 1.8: Conceptual Diagram of Smart Spectrum Access

user reappears to avoid harmful interference to PUs based on spectrum mobility functionality.

While conceptually simple, the realization of the OSA poses great difficulties in practice because of very difficult and complicated task in cognitive cycle as mentioned previous section. Thus, many critical aspects in terms of the cognitive cycle still remain open. Especially that is, *How to enable the cognitive cycle with high-reliability and high-efficiency.* More efforts must therefore be devoted to the development of new concepts realizing the reliable and efficient cognitive cycle, leading to ultimate spectrum usage.

For enabling this vision, *smart spectrum access (SSA)* is a promising concept. SSA

exploits *a prior* useful information such as statistical information regarding spectrum usage by PUs for realizing the reliable and efficient cognitive cycle as shown in Fig. 1.7. SSA consists of the typical OSA approach using CR techniques in combination with an external *spectrum awareness system (SAS)* as shown in Fig. 1.8. The SAS is responsible for spectrum measurement, modeling, database, and spectrum management.

The SAS provides useful statistical spectrum usage information to SUs based on spectrum measurements so that SUs in DSA can be relieved of having to perform energy and time consuming SPU measurements. The SPU information, based on long term, wide band,and broad area spectrum measurements, is stored in a data base. The long term information is processed by adequate spectrum occupancy modeling to extract a set of parameters sufficiently characterizing the full information (which would be impractical to share).

As will be described in the following section, there are many works which show exploiting information regarding spectrum usage by PUs is very useful for enabling the cognitive cycle with high-reliability and high-efficiency

1.1.6 Survey Related to Smart Spectrum Access

As mentioned before, SSA exploits *a prior* useful information such as statistical information regarding spectrum usage by PUs for realizing the reliable and efficient cognitive cycle. Exploiting information regarding spectrum usage by PUs itself is not new since the behavior of SUs depends strongly on PUs' spectrum usage. Thus, there exist a lot of works related to smart spectrum access. In this section, we provide a comprehensive literature review related to smart spectrum access. Specifically, we survey the dynamic spectrum access techniques exploiting *a prior* statistical information regarding spectrum usage by PUs.

Physical Layer Spectrum Sensing [32–35]

In spectrum sensing in physical layer, it is important to set a decision threshold properly. It determines the sensing performance evaluated by detection probability and false alarm rate. Previous works show the statistical information in terms of spectrum usage can improve the sensing/detection performance. This is

achieved to properly set the decision threshold based on duty cycle or transition probability for Markov chain model. Intuitively, the threshold should be lower when the sensing band is expected to have a high traffic to improve the detection probability. On the other hand, the threshold should be higher when the sensing band is expected to have a lower traffic to reduce the false alarms. This can be realized if SUs know the spectrum usage model and its corresponding parameters.

MAC Layer Spectrum Sensing [36–38]

The role of spectrum sensing in MAC layer is to decide which and how frequently band/channel sensing is done. In addition, the channel order of performing the sensing is also important factor. Several works exploit statistical information regarding spectrum usage such as to determine above parameters.

Spectrum Decision [39–46]

In spectrum decision, statistical information regarding spectrum usage has very important role. As mentioned in Sect. 1.1.4, spectrum decision is done based on the spectrum sensing results. However, the function of spectrum sensing is to detect instantaneous/local WS over time, frequency and space dimensions leading to insufficient information about spectrum usage. As the complementary role, statistical information is very useful since this information provides more global interpretation about spectrum usage. Perhaps, ultimately spectrum sensing function can be excluded by exploiting statistical information if SUs decide the available channel exploiting only statistical information [47]. This situation would correspond to one that the spectrum usage can be easily predicted.

Spectrum Mobility [39, 41, 44, 48]

Perhaps statistical information become most useful resource in spectrum mobility function since it allows SUs to proactively change the channel. This results in low channel switching delay, lower interference to PUs, and higher spectrum utilization efficiency. Eventually, exploiting statistical information can improve overall agility of cognitive cycle.

In summary, statistical information regarding spectrum usage can contribute all the cognitive functions. However, most of previous works do not explicitly consider *"How to obtain useful statistical information"*. On the other hand, SSA approach explicitly deals with this issue and the spectrum awareness system is responsible for this role as shown in Fig. 1.8.

1.2 Thesis Motivation and Contributions

In SAS, one of the important aspects is spectrum measurement part is the spectrum awareness system. This is because spectrum measurement performance strongly affects subsequent spectrum usage modeling performance, eventually spectrum sharing performance. For this reason, we focus on the signal processing part each spectrum sensor in the spectrum measurement system.

To data, there have been many spectrum measurement campaigns all over the world [references]. Many spectrum occupancy studies reported in the literature have been conducted with a single device at a fixed location, focusing on the time and frequency dimensions since the characterization of spectrum occupancy in spatial domain involves several spectrum sensors leading to expensive and difficult tasks. Most of their spectrum measurement campaigns aim at quantifying duty cycle (DC) or channel occupancy rate (COR), i.e., the proportion of time when a certain frequency channel or frequency band is occupied in a given area. Measurements can be used to assess the current status of the spectrum use and the availability of the spectrum for other users. Some spectrum measurement studies give us detailed spectrum occupancy models in time, frequency, space domains and their mixtures. These detailed spectrum occupancy models are beneficial for SUs, which attempt to share the spectrum owned by PUs by exploiting these models effectively; This is certainly the idea of smart spectrum access. In addition, measurement campaigns also give valuable information to administrators each country about the efficiency of the current spectrum allocations.

In most spectrum measurements, energy detection (ED) has been utilized energy detector (ED) to detect spectrum usage as it does not require a prior signal information of PUs and its implementation and computational costs are low compared with cyclostationary feature based detection and matched filter detection. Conventionally, the ED has been implemented with swept-frequency spectrum analyzers as spectrum sensor. This type of sensor can miss signals that occur between the sweeps and it may lead to inaccurate spectrum measurements. On the other hand, we focus on the ED with real-time spectrum analyzers such as in [10], [11]. This type of sensor can observe large instantaneous bandwidths without any time domain gaps between the outputs unlike

the swept-frequency counterpart. In general, the outputs correspond to I/Q baseband samples and a spectrum analysis such as fast Fourier transform (FFT) over the I/Q baseband samples is performed as a first step of signal processing. After that, the ED detects spectrum usage based on power spectrum estimated by FFT. There is one main issue with ED regardless of how it is implemented which is not deeply considered to date in the field of spectrum measurement. That is, time and frequency resolutions setting issue and detection performance of ED. In FFT-based spectrum measurement, both time and frequency resolutions depend on FFT size. Moreover, the detection performance of ED is closely related with time and frequency resolutions.

Therefore, the main contribution of this dissertation is the realization of accurate spectrum measurement in FFT-based spectrum measurements considering time and frequency resolutions as well as the detection performance of ED. The detailed contributions of this dissertation follow:

[**C1**] We define the optimum FFT size as the one that allows the accurate detection of the spectrum occupancy in time and frequency domains while maintaining target DC estimation accuracy and a small enough target false alarm rate. The DC estimation accuracy is quantified in terms of its root mean squared error (RMSE), which is related to signal detection performance without considering the frequency resolution. On the other hand, the detection accuracy of the spectrum occupancy in time and frequency domains is quantified by means of the white space detection ratio (WSDR), defined as the ratio of true WS to estimated WS, which also includes the effect of the frequency resolution.

[**C2**] We also define a sub-optimum FFT size which is obtained analytically. The analysis reveals that the FFT size depends on SNR and DC. This indicates that FFT size selection is challenging problem since prior knowledge of SNR and DC is impractical.

[**C3**] We propose two practical FFT size setting methods which do not require SNR and DC information. Both method exploit a relationship between output of NF estimation based on FCME algorithm and the FFT size for proper FFT size set-

ting. The difference between the two is mainly the computational complexity By the extensive numerical evaluations, we show both methods can achieve a comparative WSDR performance compared with optimal one while meeting RMSE constraint in terms of DC estimation.

1.3 Thesis Outline

Figure 1.9 shows the organization of this dissertation. We survey related works regarding smart spectrum access (SSA) comprehensively in chapter 2. Next, chapter 3 describes a spectrum measurement system model in SSA. After we formulate an optimization problem in terms of FFT size setting from the view point of wideband spectrum measurement in chapter 4. This chapter corresponds to the contributions [C1] and [C2]. In chapter 5, we propose two practical FFT size setting methods and evaluate/compare their performances and the contributions in this chapter correspond to [C3]. Finally, we conclude the dissertation and point out the future directions in chapter 6.

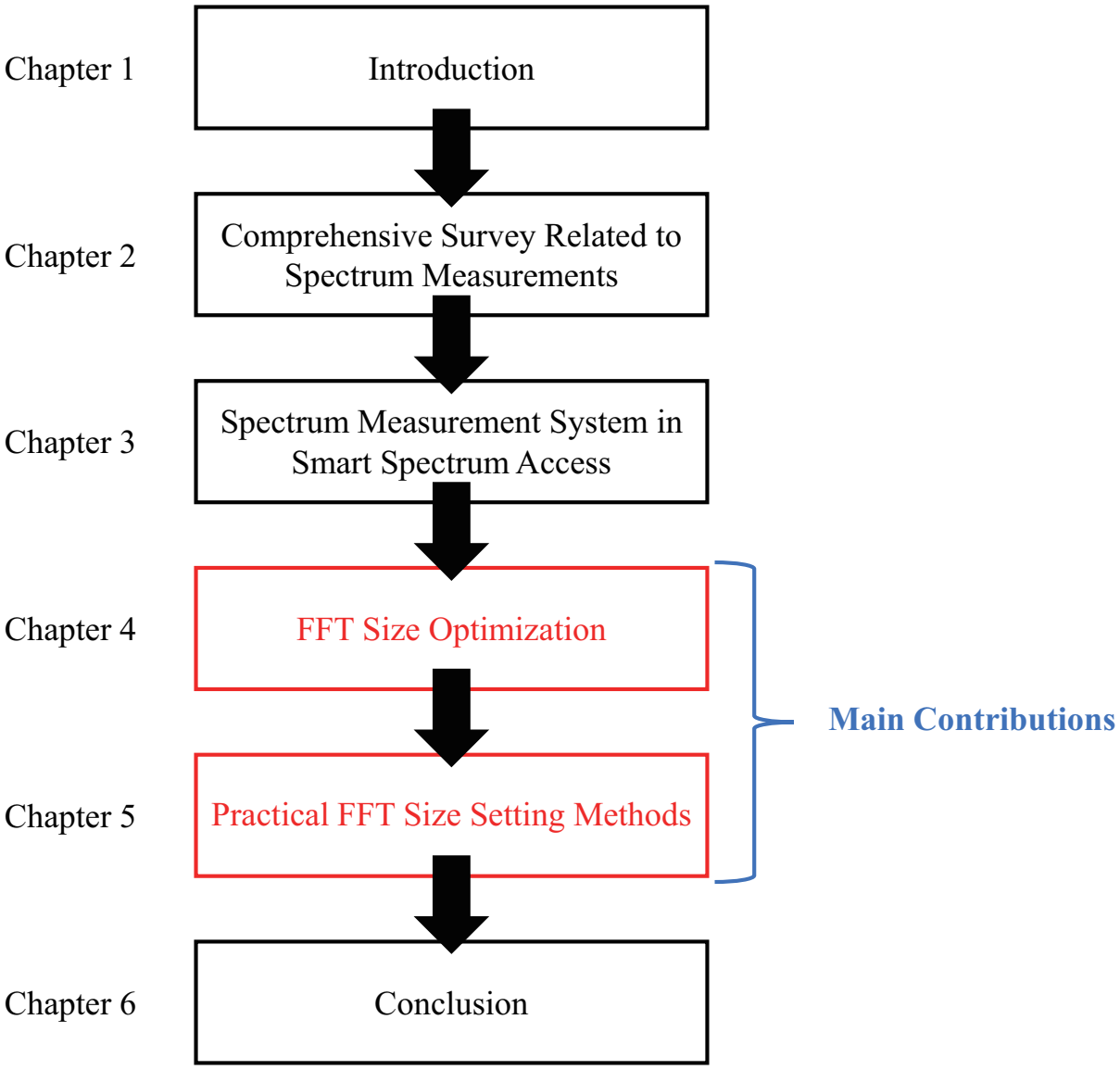

Fig. 1.9: Organization of this dissertation.

Chapter

2

Comprehensive Survey Related to Spectrum Measurements

This chapter provides a comprehensive literature review related to spectrum measurements. Specifically, we survey their works from the viewpoint of spectrum measurement parameters setting since it is one of our subjects in this dissertation.

2.1 Introduction

In OSA which is a promising approach to solving the spectrum resource scarcity, a SU senses the spectrum availability, learns from the spectrum and changes its parameters according to the surroundings based on CR technology. To make the SSA and OSA

concepts successful, spectrum measurement is very essential. It estimates the PU activity on the different bands and indicates the amount of available spectrum for SUs. In fact, There have been a large number of measurement campaigns around the world including US, Europe, Singapore, China, and Japan to study the spectrum utilization in the context of DSA. Some of these measurement campaigns give detailed data analysis in terms of statistical models in terms of spectrum usage. On the other hand, other measurement campaigns only give simple but important sample statistics such as power, duty cycle (DC), spectrum occupancy. Before proceeding to survey several important spectrum measurement campaigns, we claim a few common aspects regarding these campaigns.

First, most of these campaigns have been conducted by using an omnidirectional antenna that measures surrounding radio signals, a spectrum analyzer acquires data such as I/Q data and power data and a computer that processes and analyses measured data. A few measurement campaigns exploit a directional antenna to investigate the spectrum occupancy in the space domain. Furthermore, a spectrum analyzer is in general installed at a fixed point, but some measurement campaigns use a vehicle to investigate the spatial distribution of spectrum usage. The acquired data in a spectrum analyzer also are different each measurement campaigns. In general, the type of the acquired data is classified into I/Q data or power data depending on the type of exploited spectrum analyzers. Most of measurements use a swept-frequency type spectrum analyzer and this type of spectrum analyzer outputs power data on the principle of its operation. Some of measurements use a real-time spectrum analyzer and this basically outputs I/Q data.

Second, Most of these campaigns consider either outdoor or indoor locations. As for the outdoor scenario, the measured locations are basically chosen on the roof of a high building in order to reduce the effect of radio propagation loss on the measurements []. Some measurement campaigns perform the measurement at a ground level to reveal the realistic spectrum occupancy. As for the outdoor scenario, the measured locations are often chosen in an office building, a typical application environment for wireless communications. Some of the measurements use several spectrum analyzer which are

installed at different geographical locations to investigate the location variations in terms of spectrum occupancy and power. However, introducing several analyzers is very expensive and complicated task

Finally but not all, different measurements apply different measurement parameters such as measurement time span, measurement cycle, measurement bandwidth, measurement frequency band, to name a few. The setting of measurement parameters are one of critical issues in spectrum measurements. Several works mention the methodological aspect and investigate the effect of measurement parameter setting to measurement accuracy. The measurement time span varies from a few hours in some campaigns to a few years in other campaigns. Intuitively, the longer the time span is, the more useful but also the more expensive the measurement campaign will be. Also, most of these campaigns focus on the frequency range between several dozen MHz (e.g., 20 MHz) and several GHz (e.g., 6 GHz). This range covers some of the very important applications of wireless communications, such as FM radio, TV broadcasting, cellular communications currently. And, it is especially important to realize DSA in this frequency range since many of the spectrum in this frequency range has already allocated to any wireless services. It will be also important to perform spectrum measurements over higher frequency range because it is expected the next generation mobile communication systems exploit very higher frequency bands such as mm-wave band. However, higher frequencies are more vulnerable to propagation loss and it makes the measurement over higher frequency bands very difficult.

In the next section, we will discuss several important measurement works. Finally, we make a few summary statements in this chapter.

2.2 Survey of Global Spectrum Measurement Campaigns

Following our survey, the initial spectrum measurement campaigns are performed in North America, specifically the US and the Canada [49, 50]. In these campaigns, their purpose is reveal the spectrum occupancy and the measured occupancy data are used to assist in the assignment of radio frequencies. To our best knowledge, there are two earliest measurement campaigns. First one is performed by Matheson for the In-

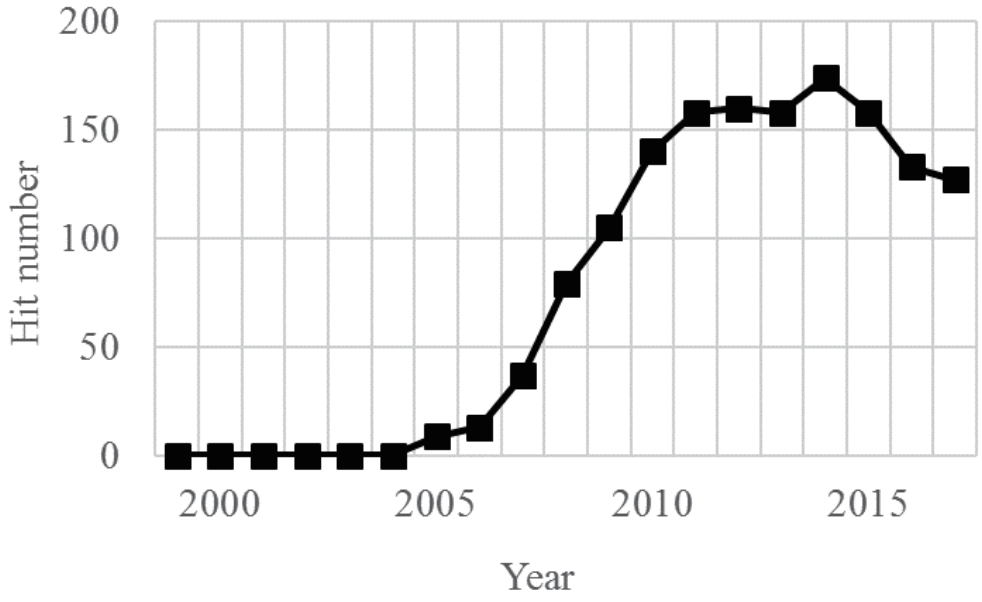

Fig. 2.1: Transition of the number of article published per year, Keywords: "Spectrum measurement" and "Cognitive radio".

stitute of Telecommunication Science in the US and second one is by Vaccani in the Canada. Matheson has provided basic guidelines for spectrum measurements through his experience and obtained results for 15 years. Especially, he argued the importance of spectrum occupancy in terms of five different dimensions called as "electrospace": time, frequency, location, direction and polarization. Finally, he emphasized that different measurement strategies or measurement parameters may lead to significantly different results through some experimental examples. Miguel et al. extended the basic guideline by Matheson and they argues the detailed measurement methodology including the measurement setup, time and frequency resolutions, and post-processing to obtain accurate measurement results.

On the other hand, Vaccani performed the measurements over land mobile radio band. In this measurement, average duty cycle (DC) for 16 hours each frequencies and time variation of DC every one hour are showed. And, in the DC measurement energy detection (ED) is exploited. His results indicate a maximum average DC is about 57% and the fluctuations of DC in time domain is small in the land mobile radio band.

After that many observations were conducted in the US and another countries such as UK [51], Sweden [52], Germany and Australia [53] and one of important broadband spectrum measurement is perhaps one by Sanders for the Institute of Telecommunication Science in the US [54]. In this work, Sanders measured the frequency bands from 108 MHz to 19.7 GHz in three different US cities, Denver, San Diego and Los Angeles, for two weeks. All the measurements were performed outdoors and all evaluations are based on power data. Using these measurements, it was found that San Diego has considerably more radio activities than Denver.

More extensive measurement campaign was done by McHenry et al. in the Chicago, US in 2006 [55]. In this era, the researches of cognitive radio and dynamic spectrum access spread all over the world. For this reason, the number of articles about spectrum measurement from the point of view of cognitive radio has been increased at that time. In fact, Fig. 2.1 shows the transition of the number of published articles per year. This figure shows the number of achievements such as conference papers, journal articles published within the year using "Cognitive Radio" and "Spectrum Measurement" as search words in the IEEE Xplore. In [55], measurements were taken from 30 MHz to 3 GHz for a few hours. The location was fixed to the roof of a multistory building in the Chicago. The results were presented in terms of the maximum power level and the duty cycle. From the results, a highest average DC is 70.9% at some TV bands. On the other hand, a lowest average DC is 0% at some satellite bands. Also, the cellular band also has a heavy occupancy with an average duty cycle of 55%. Furthermore, this article compares the spectrum occupancy in the Chicago with one in the New York. This comparative evaluations reveal a significant difference although two cities are large in the US.

In 2007 and 2008, three conference papers were published [56–58]. The measurement locations are respectively in German, in New Zealand and in Singapore. All these measurements use the swept-type spectrum analyzer and energy detection as a spectrum usage detection. Moreover, these measurements show duty cycle, distribution of power or amplitude mainly. Especially, [56] made comparisons the measurement result between outdoor scenario and indoor scenario.

In 2009, there are seven journal and conference papers [59–65]. Spectrum measurements are performed at the various locations including Spain, Qatar and China. All these measurements also use the swept-type spectrum analyzer and energy detection as a spectrum usage detection. Especially, [59] investigated the effect of frequency resolution setting into the spectrum occupancy results, but a concrete guideline for frequency resolution setting was given. Moreover, [60] considered a problem about adaptive energy detection threshold setting and claimed the importance of using the difference threshold each frequency band/channel.

Seven articles are explored in 2010 [66–73]. The location of these spectrum measurements include US, Spain and Finland. Almost all measurements also use the swept-type spectrum analyzer and energy detection as a spectrum usage detection. [72] used USRP (Universal Software Radio Peripheral) as a spectrum sensor, but basic structure is same as the swept-type spectrum analyzer In [72], a spectrum occupancy model based on independent Poisson process was proposed and the modeling method was introduced.

In 2011, five papers were published [74–78]. All these measurements also use the swept-type spectrum analyzer and energy detection as a spectrum usage detection. Especially, [75] reviewed past measurement campaigns performed by different research groups and analysis of empirical results from the viewpoint of cognitive radio. The conclusion was the past results show that the average occupancy of the spectrum is very low. Thus, there is a significant amount of spectrum available for the future deployment of cognitive radio. Further, it provided a spectrum occupancy measurement framework for the proposed spectrum measurement in India.

There are eight papers in 2012 [79–86]. All these measurements also use the swept-type spectrum analyzer and energy detection as a spectrum usage detection. [85] presented the first comprehensive study on the level of "usable" spectrum available to SUs based on RWTH data set, which include large amount of data measured at various locations including German and Netherlands. Their analysis shows that even with extensive statistical knowledge on PU's spectrum usage pattern, and while running optimal algorithms, secondary devices can only extract $20\% - 30\%$ of available spectrum in a channel. To provide better spectrum availability, they proposed *frequency*

bundling. It is a method that SUs build reliable channels by combining multiple unreliable frequencies into virtual frequency bundles.

In 2013, 17 papers were published [87–103]. The number is a maximum from 2006 to 2017 as far as I can see. In this year, several spectrum occupancy models were proposed based on real spectrum measurement results. [102] proposed the spectrum occupancy models in time dimension He considered the low-time resolution and high-time resolution spectrum usage models. Their model parameters were extracted from real-wold spectrum measurement data he obtained. He concluded almost all wireless systems can be modeled by a generalized Pareto distribution at long-time scale, but different models must be applied at short-time scale.

In 2014, there are six papers [104–109]. All these measurements also use the swept-type spectrum analyzer and energy detection as a spectrum usage detection. An important paper is [107]. In this paper, vehicle-based spectrum measurements were performed for enhancing whitespace spectrum databases. They proposed a system V-Scope, a measurement framework for TV whitespaces. The system leverages spectrum sensors mounted on public vehicles to collect spectrum measurements during the drive, where FFT-based spectrum measurements are adopted.

In 2015, nine papers were published [110–118]. An important paper is [114]. This paper surveys past spectrum measurement campaigns used in diverse locations by research campaigns worldwide. The detail analyses of the empirical results in different scenarios of measurement have been compared. The purpose of this survey was to evaluate up to what percentage the whole spectrum band is occupied by different services. They concluded that most of the bands are vacant worldwide which can be utilized for the DSA.

There are 16 papers in 2016 [119–134]. In these papers, two survey papers are included [126, 129]. [126] surveyed measurement-based spectrum occupancy modeling from the viewpoint of cognitive radio. In addition, they surveyed various models for spectrum occupancy prediction. Recently, spectrum occupancy prediction has gained popularity due to its ability of improvement of cognitive cycle efficiency [135]. They concluded most models are established based on the observations from the measure-

ments and are extracted by fitting them to the well-known theoretical models. This leads to a large number of different models for similar situations. Thus, we should investigate a point that whether a general model exists that can unify most existing models.

Finally, seven papers were published in 2017 [136–142]. Almost all measurements also use the swept-type spectrum analyzer and energy detection as a spectrum usage detection. [137] used USRP as a spectrum sensor. The USRP they used is similar to the real-time spectrum analyzer, but USRP basically adopts direct-conversion method as a frequency transformation unlike typical real-time spectrum analyzer adopting super-heterodyne method. The observe data is I/Q data and they applied FFT as a spectrum analysis. They concludes a high variability of the spectrum occupancy at different locations and notable differences between the values measured in the two locations.

2.3 Chapter Summary

In this chapter, we comprehensively surveyed past spectrum measurement campaigns. Many campaigns have revealed most of allocated frequency bands are underutilized and the vast about of available spectrum resources, i.e., white space. Most of the spectrum measurements exploit sweep-type spectrum analyzers and energy detection for investigation of spectrum occupancy and estimating the duty cycle. A few measurement campaigns exploit real-time spectrum analyzer in combination with FFT. Most important thing is that most of the spectrum measurements did not consider the frequency and time resolutions as well as detection performance. A few works investigated the effect of frequency resolution and detection performance (i.e., detection threshold setting) in terms of measurement results. These facts have motivated our to study the design and setting of FFT size which affects time and frequency resolutions setting and detection performance.

Chapter

3

Spectrum Measurement System in Smart Spectrum Access

In this chapter, we introduce the spectrum measurement system prototype we have developed for achieving smart spectrum access. Furthermore, we in detail describe the model of a spectrum sensor assumed throughout this dissertation.

3.1 Spectrum Measurement System

Figure 3.1 shows the implemented spectrum measurement prototype system. The system prototype consists of an antenna that can observe the target frequency band, cables, multiple spectrum sensors, a network-attached high-capacity hard disk, a mea-

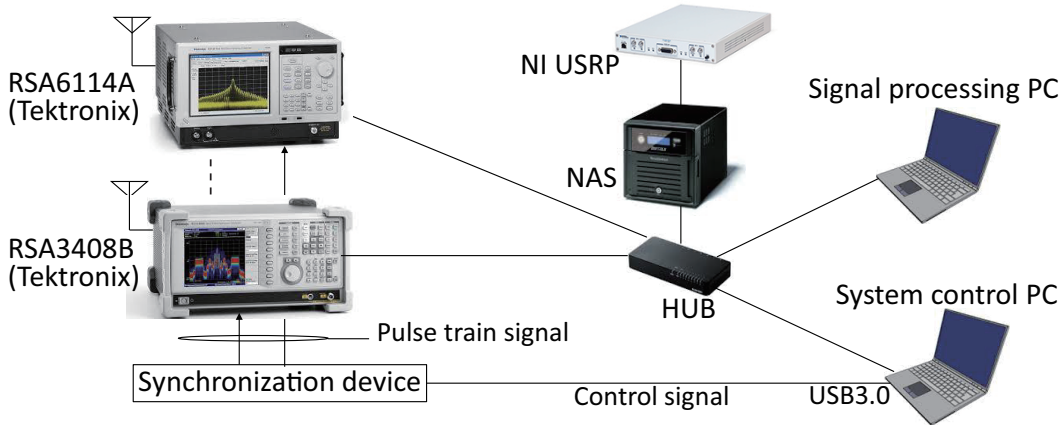

Fig. 3.1: Spectrum Measurement System Prototype

surement system manager, and a data analysis computer. In the system, spectrum sensors perform the spectrum measurement. Here, the synchronization device controls the measurement timing on spectrum sensors using a pulse train signal with a duty cycle given by system control PC. Each sensor performs the first function (PUs' signal acquisition) and transfers obtained data to storage device such as network attached storage (NAS). After that, signal processing PC performs the last three functions (Welch FFT, ED and DC estimation). The obtained information also are stored in storage device.

3.2 General Model for Spectrum Measurement in A Spectrum Sensor

The general measurement setup and methodology to obtain DC data in this section. The measurement system manager takes care of the measurement time scheduling, which is shown in Fig. 3.3. The number of days for spectrum measurement is denoted by D and we set $D = 24$ in the spectrum usage measurement. One day (24 hours) is divided into M time slots. The time duration for one time slot is denoted by T_S. One time slot consists of a measurement period and a data analysis period, whose time durations are denoted by T_M and T_A, respectively. Typically T_M depends on the capability of the spectrum sensor, such as internal buffer size and sampling rate. During one measurement period, the RSA continuously observes the target frequency

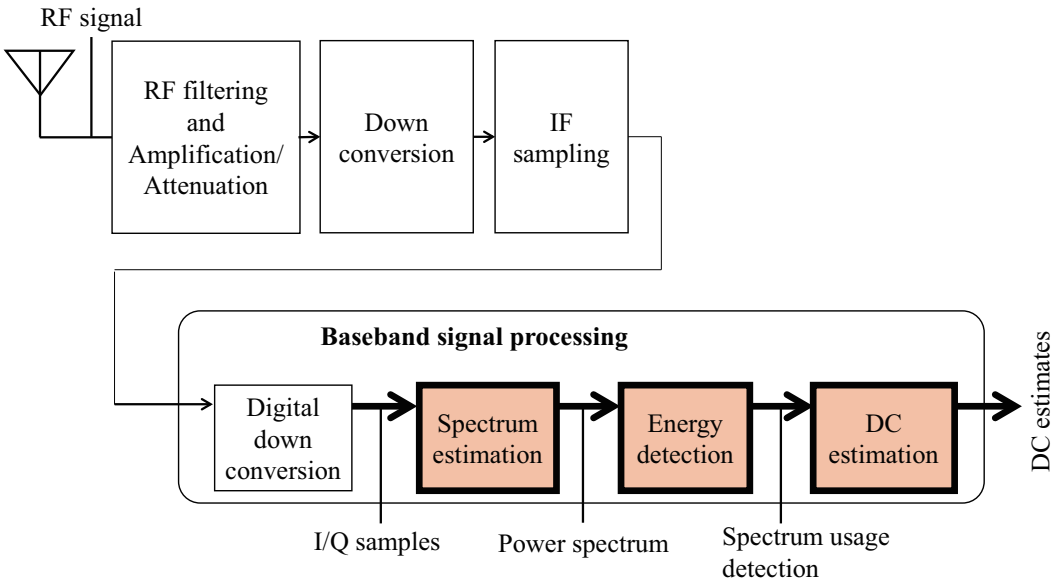

Fig. 3.2: General Model for Spectrum Measurement in A Spectrum Sensor

band for T_M seconds. Note that the observation of the RSA is continuous unlike typical swept spectrum analyzers. T_M has to be much longer than one continuous spectrum usage cycle, such as data packet, for proper DC estimation in the target frequency band. For example, the time durations for data packet in WLAN is at most about 0.87 ms, (corresponding to the time duration of the IEEE 802.11 PLCP (Physical Layer Convergence Procedure) protocol data unit). Based on this, we should set $T_M \gg 0.87$ ms.

The measured data (I/Q data in this spectrum measurement) is first stored in the hard disk and then transferred to the data analysis computer. The data analysis computer provides estimates of the DC by means of Welch FFT-based energy detection (Welch FFT-ED) and post processing to achieve accurate spectrum usage detection performance. The measurement period T_M is divided into M_S super fames and noise floor estimation is performed in each super frame as shown in Chapter 5. One super frame consists of M time frames. Each time frame has N_S I/Q samples and Welch FFT-ED is performed in each time frame. Then, N_S corresponds to time resolution and FFT size exploited in Welch FFT determines frequency resolution.

The spectrum usage detections are performed based on the $M \times N_F$ estimated power

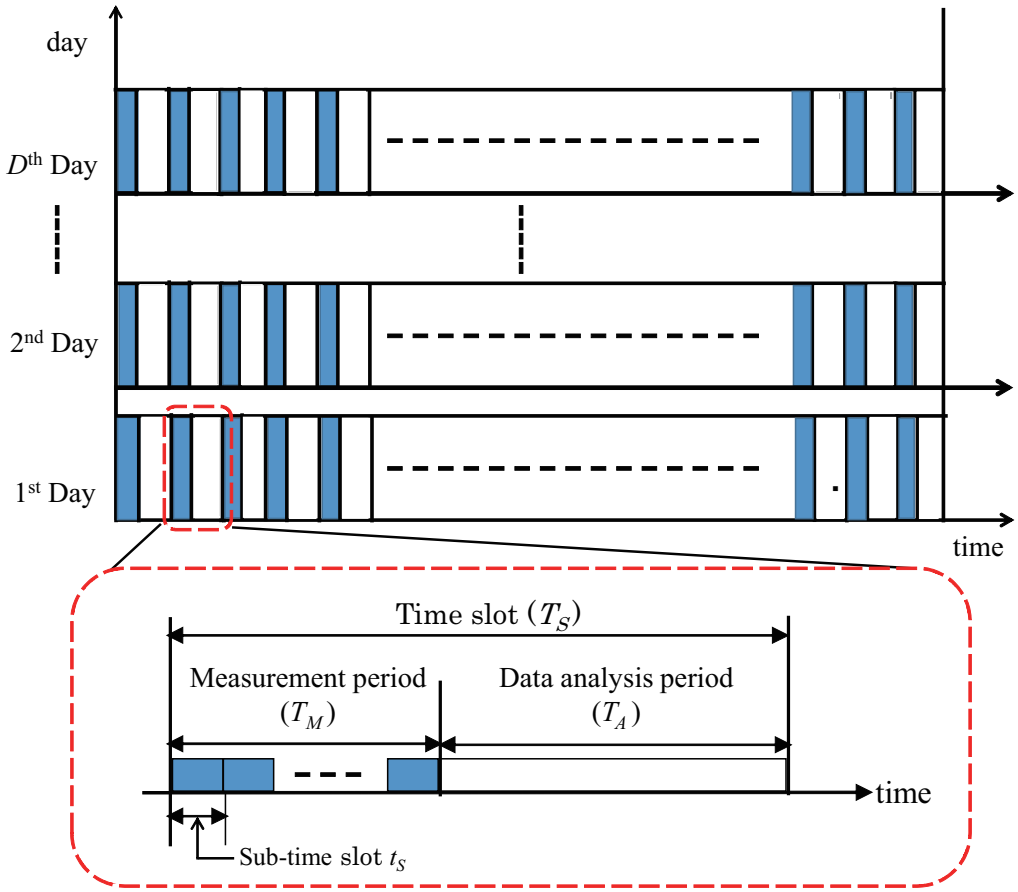

Fig. 3.3: Measurement time schedule

spectrum samples by Welch FFT at the data analysis computer. In this measurement, the spectrum usage detections consists of typical ED. We set the detection threshold based on constant false alarm rate criterion where the target false alarm rate is set to 0.01. In this criterion, we need noise floor information in order to set the threshold and we employ forward consecutive mean excision (FCME) algorithm for noise floor estimation. The description of FCME algorithm-based noise floor estimation will be provided in Chapter 5.

Finally the DC in each frequency bins are estimated by exploiting ED results. The detailed description of energy detection and DC estimation will be introduced in Chapters 4 and 5.

3.3 Chapter Summary

In this chapter, we have shown the spectrum measurement prototype system. In addition, a general model for spectrum measurement in a spectrum sensor is also introduced. Throughout this thesis, we use it as a basic measurement model.

Chapter

4

FFT Size Optimization[i]

4.1 Introduction

As mentioned in Chapter 2, most of previous spectrum usage measurements utilize energy detector (ED) to detect spectrum utilization. Furthermore, the ED has been implemented with swept-frequency spectrum analyzers or FFT-based spectrum analyzers. We assume FFT-based spectrum analyzer since it has an advantage that it can sample the I/Q samples continuously in one observation period without intermittent as swept-frequency spectrum analyzer. There are one important issue with ED regardless

[i]This chapter is based on "Welch FFT Segment Size Selection Method for Spectrum Awareness System" [2] in Publications, by the same authors, which appeared in IEICE Transactions on Communications, Copyright(C)2016 IEICE.

of how it is implemented: That is its limited detection performance.

To overcome the limited detection performance of FFT-based ED, Welch FFT is an effective approach [143]. Welch FFT consists of three steps: segmentation of the data sequence with a specific *FFT size*, calculation of multiple power spectra and averaging of the power spectra. Here, the number of segments define over how many segments the averaging is performed and more averaging provides better detection performance.

Due to the the above mentioned process of Welch FFT, there is a trade-off between the detection performance and frequency resolution in terms of FFT size. More specifically, large FFT sizes lead to poor detection performance due to insufficient averaging of power spectrum but better frequency resolution. Small FFT sizes can improve signal detection performance and also noise floor estimation accuracy because of the higher number of averages of the power spectra. However, decreasing the FFT size can lead to inaccurate recognition of bandwidth of occupied spectrum due to poor frequency resolution. As a result, the inaccurate recognition of bandwidth of occupied spectrum results in inaccurate detection of the spectrum occupancy in time and frequency domains.

In this chapter, we formulate a design criterion for FFT size setting in Welch FFT based spectrum usage measurements by considering the trade-off between detection performance and frequency resolution. Our main contributions in this chapter are as follows:

- We define the optimum FFT size as the one that allows the accurate detection of the spectrum occupancy in time and frequency domains while maintaining target DC estimation accuracy and a small enough target false alarm rate[1]. The DC estimation accuracy is quantified in terms of its root mean squared error (RMSE), which is related to signal detection performance without considering the frequency resolution. On the other hand, the detection accuracy of the spectrum occupancy in time and frequency domains is quantified by means of the white space detection ratio (WSDR), defined as the ratio of true WS to estimated WS, which also includes the effect of the frequency resolution.

[1]In fact, false alarm rate can be also optimized for DC estimation as shown in [144]. However it is beyond of this paper and we use constant false alarm rate approach instead.

- We also define a sub-optimum FFT size which is obtained analytically. The analysis reveals that the FFT size depends on SNR and DC. This indicates that FFT size selection is challenging problem since prior knowledge of SNR and DC is impractical.

- Numerical results demonstrate that the optimum FFT size can achieve optimum WSDR performance while satisfying the RMSE constraint if SNR value is known.

The remainder of the paper is organized as follows. The system model used in this paper is presented in Section 4.2. In Section 4.3, we introduce the FFT size design criterion. Specifically, we formulate optimization problem of FFT size. Additionally, we also formulate sub-optimization problem of FFT size because of difficulty in analysis of optimization problem. Performance evaluation based on computer simulation is presented in Section 4.4. Finally, chapter summaries are presented in Section 4.5.

4.2 System model

A detailed block diagram of signal processing for sampled I/Q data is shown in Fig. 4.2. Configuration of time frames for the spectrum usage measurement in the spectrum sensor is shown in Fig. 4.1. One consecutive measurement duration consists of M_s super frames, each super frame consists of M time frames, and one time frame of M time frames consists of N_s complex samples of observed signal with sampling rate f_s Hz at the spectrum sensor.

The block diagram of the spectrum usage measurement process in an spectrum sensor is shown in Fig. 4.2. The DC estimation process in the spectrum sensor consists of several components: Welch FFT, threshold setting, spectrum usage detection and DC estimation. In ED, the threshold setting is very important since it determines the detection performance (detection probability and false alarm rate). In general, the threshold is based on constant false alarm rate (CFAR) criterion. In this case, the threshold depends on noise floor information. The noise floor must generally be estimated since its level and shape are time-varying depending on surround environment. However, we assume a spectrum sensor knows the complete noise floor information for

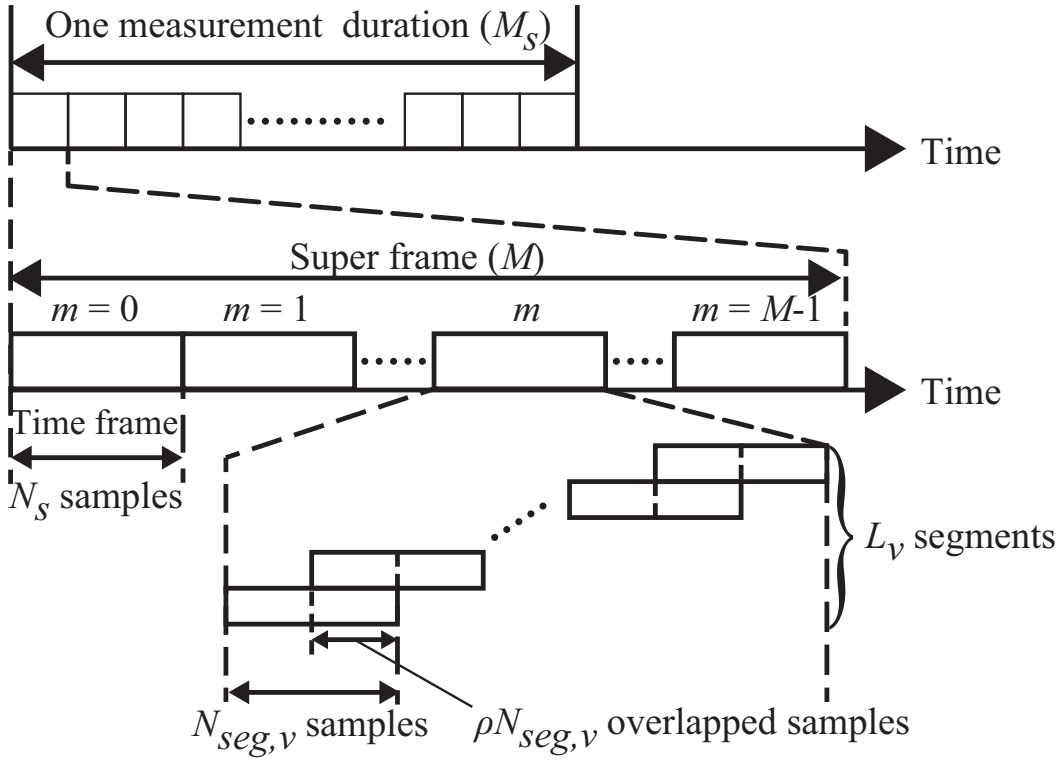

Fig. 4.1: The configuration of time frames in the measurement process

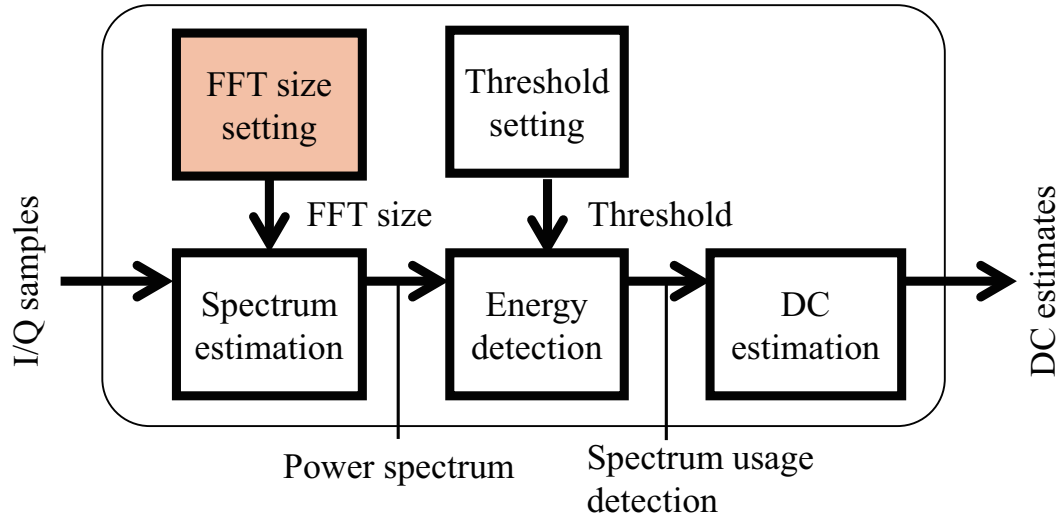

Fig. 4.2: Block diagram of the spectrum measurement process in the spectrum sensor

simplicity of future analysis in this chapter. In next chapter, we consider practical noise floor estimation method for achieving the practicality of this thesis. The DC estimation obtains M_s DC estimates during one measurement duration based on $M_s \times M$ signal

usage detection results.

Multiple PUs may randomly access any channel in the measurement bandwidth denoted by W_M (equivalent to f_s in this paper) and W_M is set to so as to enable the observation of multiple PU signals, where the bandwidth of one PU signal is denoted by W_S. We assume there are I communication physical channels with and/or without overlap between adjacent channels in the measurement bandwidth. We use the 30-dB bandwidth [145], so that the signal bandwidth is defined by the frequency bandwidth in which the signal power is 30 dB below its peak value. In addition, we assume that PU system parameters (e.g., center frequency, bandwidth, SNR, etc.) are not known at the SAS.

Now let us focus on the mth time frame ($m = 0, 1, \cdots, M-1$). The nth sampled complex baseband signal $y[n]$ ($n = mN_s, mN_s+1, \cdots, mN_s+N_s-1$) in the mth time frame is given by

$$y[n] = \begin{cases} z[n] & \text{(PU is not active)} \\ x[n] + z[n] & \text{(PU is active),} \end{cases} \tag{4.1}$$

where $x[n]$ represents the PU signal component and $z[n]$ represents the noise component which follows independent and identically distributed (i.i.d) circular symmetric complex Gaussian distribution with zero mean and variance σ_z^2, i.e., $z[n] \sim CN(0, \sigma_z^2)$. SNR is defined by SNR $= \sigma_x^2/\sigma_z^2$, where σ_x^2 and σ_z^2 are the average signal power and noise power in the observed spectrum, respectively.

In the Welch FFT, N_s samples are segmented into L_v segments with an overlap ratio ρ. In L_v, v denotes the index number of FFT size ($v = v_{\min}, v_{\min}+1, \cdots, v_{\max}$). Without loss of generality, N_s and FFT size ($N_{seg,v}$) are assumed to be powers of two, i.e., $N_s = 2^{v_{\max}}$ and $N_{seg,v} = 2^v$, namely v also indicates the exponent of the FFT size. In this case,

$$L_v = 2N_s/N_{seg,v} - 1. \tag{4.2}$$

After the segmentation, normal FFT is performed on each segment with respect to

each segment and the power spectrum averaged over L_v segments is given by

$$\begin{aligned} & P_{m,v}[f_v] \\ &= \frac{1}{L_v}\sum_{l=0}^{L_v-1}\left|\sum_{k=0}^{N_{seg,v}-1}\frac{(w_v[k]y[k+\frac{lN_{seg,v}}{2}]e^{-j\frac{2\pi k f_v}{N_{seg,v}}})}{\sqrt{N_{seg,v}}}\right|^2, \\ &= \frac{1}{L_v}\sum_{l=0}^{L_v-1}|Y_{m,v}[l,f_v]|^2, \end{aligned} \tag{4.3}$$

where f_v is the index number of the frequency bin ($f_v = 0, 1, \cdots, N_{seg,v}-1$), m is the index number of the time frame and $w_v[k]$ is the real-valued window coefficient.

Type of window affects the detection performance [146]. In [147], it has been shown that Hamming window can achieve slightly better performance compared to other windows. Therefore, we employ it and $w_v[k]$ is given by:

$$\begin{aligned} & w_v[k] \\ &= \begin{cases} 0.54 - 0.46\cos\left(\frac{2\pi k}{N_{seg,v}-1}\right) & (0 \le k < N_{seg,v}-1) \\ 0 & (\text{otherwise}). \end{cases} \end{aligned} \tag{4.4}$$

We assume that time resolution $\Delta t = N_s/f_s$ for the duration of a time frame is small enough compared to the time duration of one continuous signal, such as a data packet, and the time gap between string of two continuous signals as suggested in [148]. On the other hand, the frequency resolution Δf_v is determined by the FFT size as $\Delta f_v = f_s/N_{seg,v}$. We also assume that considered PU signal is composed of multiple frequency bins, i.e., $W_S/\Delta f_{v_{\max}} \ge 2$ to enable the averaging of power spectrum in Welch FFT.

Let $f_{v_{\mathrm{P}}(m)}$ denote the index number of the frequency bin in the mth time frame. Detection result at the mth time frame and the $f_{v_{\mathrm{P}}(m)}$th frequency bin is obtained by the ED as:

$$\hat{D}_{m,v_{\mathrm{P}}(m)}[f_{v_{\mathrm{P}}(m)}] = \begin{cases} 1 \ (\text{if } P_{m,v_{\mathrm{P}}(m)}[f_{v_{\mathrm{P}}(m)}] > \dot{\eta}_{v_{\mathrm{P}}(m)}) & \text{(4.5a)} \\ 0 \ (\text{otherwise}), & \text{(4.5b)} \end{cases}$$

where (4.5a) and (4.5b) correspond to the decisions of occupied spectrum ($\mathcal{H}_1$) and vacant spectrum ($\mathcal{H}_0$), respectively. The occupied spectrum ($\mathcal{H}_1$) indicates that PU signal exists in the frequency bin partially or completely and vacant spectrum ($\mathcal{H}_0$) otherwise. In general, the detection performance is summarized in two probabilities

[149]: probability of detection $P_{\mathrm{D}} = \Pr(P_{m,v_{\mathrm{P}}(m)}[f_{v_{\mathrm{P}}(m)}] > \dot{\eta}_{v_{\mathrm{P}}(m)}|\mathcal{H}_1)$ and false alarm rate $P_{\mathrm{FA}} = \Pr(P_{m,v_{\mathrm{P}}(m)}[f_{v_{\mathrm{P}}(m)}] > \dot{\eta}_{v_{\mathrm{P}}(m)}|\mathcal{H}_0)$, where $\Pr(x)$ indicates the probability of event x. In this paper, the threshold $\dot{\eta}_{v_{\mathrm{P}}(m)}$ is set according to the true noise floor $\sigma^2_{z,\mathrm{F}}$ and the selected FFT size in the mth time frame to satisfy a certain target false alarm rate, $P_{\mathrm{FA,target}}$. The reader is referred to [146] for the derivation of the threshold for Welch FFT based ED based on CFAR criterion. Moreover, we can get P_{D} for Welch FFT based ED in [144].

In this chapter, we consider FFT size can change each time frame. Thus, the number of frequency bins may change each time frame. Since possible number of bins is however always a power of two, we can map the detection results with selected FFT size to detection results with the maximum FFT size as

$$\hat{D}_{m,v_{\max}}[f] = \hat{D}_{m,v_{\mathrm{P}}(m)}[f_{v_{\mathrm{P}}(m)}], \tag{4.6}$$

where

$$\frac{\Delta f_{v_{\mathrm{P}}(m)}}{\Delta f_{v_{\max}}} f_{v_{\mathrm{P}}(m)} \leq f \leq \frac{\Delta f_{v_{\mathrm{P}}(m)}}{\Delta f_{v_{\max}}} (f_{v_{\mathrm{P}}(m)} + 1) - 1. \tag{4.7}$$

Finally, DC estimation is performed for every super frame and the DC at the fth bin is given by

$$\hat{\Psi}[f] = \frac{1}{M} \sum_{m=0}^{M-1} \hat{D}_m[f]. \tag{4.8}$$

where M indicates the DC estimation period (equivalent to length of median filter).

In this paper, we use $m_{\mathcal{H}_1}$-*out-of-M* model[2] to define the true DC as $\Psi[f] = m_{\mathcal{H}_1}[f]/M$, where $m_{\mathcal{H}_1}[f]$ denotes the number of $\mathcal{H}_1$ hypotheses in the fth frequency bin and M denotes the number of time frames in one super frame.

4.3 FFT size design criterion

Larger FFT size $N_{seg,v}$ can achieve high frequency resolution Δf_v, however it results in reduced signal detection sensitivity due to small L_v in (4.2) and vice versa. To set a

[2] In [144], $m_{\mathcal{H}_1}$-*out-of-M* model is denoted by *m-out-of-M* model.

proper FFT size, we define the evaluation criterion for the design of the optimum FFT size by

$$
\begin{aligned}
v_{\mathrm{OPT}} = & \underset{v \le v_{\max}}{\arg\min} \, |1 - \mathrm{WSDR}(v)|, \\
& \text{s.t. Worst RMSE}(\Psi[f]) \le \delta, \\
& \quad P_{\mathrm{FA}} = P_{\mathrm{FA,target}},
\end{aligned}
\tag{4.9}
$$

where optimum FFT size is given by $N_{seg,v_{\mathrm{OPT}}} = 2^{v_{\mathrm{OPT}}}$, $\mathrm{WSDR}(v)$ and δ denote the WSDR and allowable RMSE for DC estimate, respectively. Moreover, Worst $\mathrm{RMSE}(\Psi[f]) = \min\{\mathrm{RMSE}(\Psi[f_{\mathrm{CH}i}]), i \in \{1, 2, \cdots, I\}\}$ indicates the minimum (worst) DC estimation error among I PU channels, where $\mathrm{RMSE}(\Psi[f_{\mathrm{CH}i}])$ is RMSE in terms of DC estimation at the center frequency $f_{\mathrm{CH}i}$ for ith PU channel.

In the following sub-sections, the details of $\mathrm{RMSE}(\Psi[f_{\mathrm{CH}i}])$ and $\mathrm{WSDR}(v)$ are described. In addition, the trade-off with $\mathrm{WSDR}(v)$ is shown.

4.3.1 RMSE in terms of DC estimation

The RMSE of DC estimation error in the $m_{\mathcal{H}_1}$ -out-of-M model is given by [144]

$$
\mathrm{RMSE}(\Psi[f_{\mathrm{CH}i}]) = \sqrt{\mathbb{E}[(\hat{\Psi}[f_{\mathrm{CH}i}] - \Psi[f_{\mathrm{CH}i}])^2]},
\tag{4.10}
$$

where $\mathbb{E}[\cdot]$ denotes expectation, $\Psi[f_c]$ is the true DC, and $\hat{\Psi}[f_c]$ is the estimated DC. Based on [144], analysis of RMSE is as follows

$$
\begin{aligned}
& \mathrm{RMSE}\left(\Psi[f_{\mathrm{CH}i}]\right) \\
= \; & \Big\{ \frac{1}{M} \left[(1 - \Psi[f]) \, P_{\mathrm{FA}} \, (1 - P_{\mathrm{FA}}) + \Psi[f_c] P_{\mathrm{D}} \, (1 - P_{\mathrm{D}}) \right] \\
& \qquad + \left[- \, (1 - P_{\mathrm{D}}) \, \Psi[f_c] + P_{\mathrm{FA}} \, (1 - \Psi[f_c]) \right]^2 \Big\}^{\frac{1}{2}},
\end{aligned}
\tag{4.11}
$$

Typically, $P_{\mathrm{FA,target}}$ should be set to a small value, such as 0.01. Therefore, P_{D} should be high enough to satisfy $\mathrm{RMSE}(\Psi[f_{\mathrm{CH}i}]) \le \delta$ with small δ. Since $f_{\mathrm{CH}i}$ is set to the center of the ith PU's channel in frequency domain, the frequency resolution is not considered in the RMSE which implies that the RMSE can be improved by setting small FFT size.

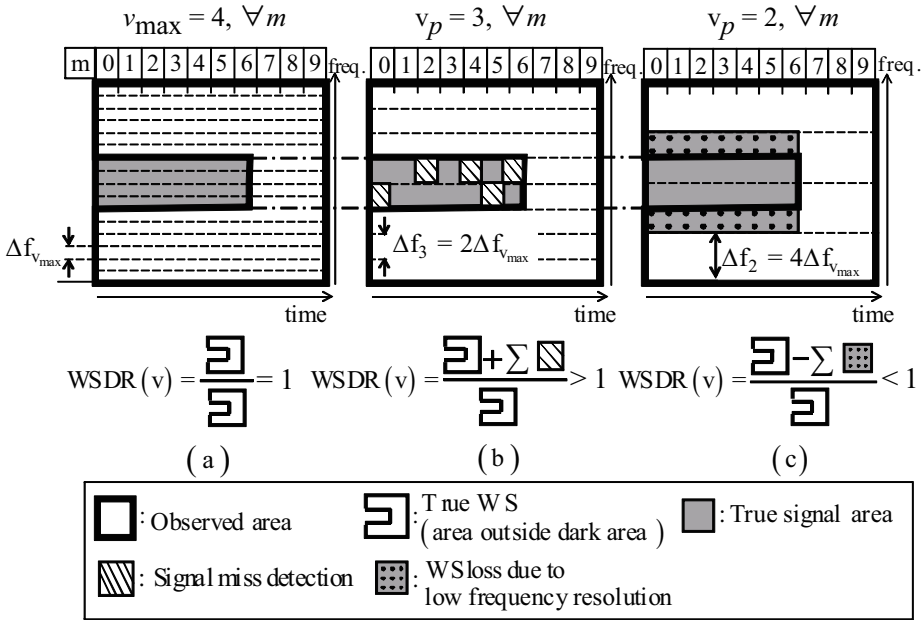

Fig. 4.3: Illustration of the trade-off relationship between RMSE($\Psi[f_c]$) and WSDR(v) as a function of v; (a) ideal case; (b) large FFT size case ($v_{\mathrm{P}} = 3,\ \forall m$); (c) small FFT size case ($v_{\mathrm{P}} = 2,\ \forall m$), $M = 10$

4.3.2 White Space Detection Rate

The criterion in terms of WSDR in (4.9) indicates a vacant spectrum detection capability in frequency and time domains. In other words, the criterion considers the frequency resolution. WSDR is defined by

$$\mathrm{WSDR}(v) = \frac{\sum_{f=0}^{N_{seg,v_{\max}}-1}(1 - \mathbb{E}[\hat{\Psi}[f]])}{\sum_{f=0}^{N_{seg,v_{\max}}-1}(1 - \Psi[f])}, \tag{4.12}$$

where the denominator and numerator indicate true WS and estimated WS, respectively. In this metric, values closer to one indicate more accurate detection performance. Note that in (4.12) the effect of frequency resolution is included in the estimated DC $\hat{\Psi}[f]$ as f is given by (4.7).

4.3.3 Trade-off regarding the FFT size

Different cases are studied in Fig. 4.3 to determine effects of FFT size on RMSE($\Psi[f_c]$) and WSDR. Specifically, they are (a) ideal case, (b) large FFT size case, such as

$v_{\mathrm{P}} = 3,\ \forall m$, i.e., $N_{seg,v_{\mathrm{P}}(m)} = N_{seg,3} = 2^3,\ \forall m$, and (c) small FFT size case, such as, $v_{\mathrm{P}} = 2,\ \forall m$, i.e., $N_{seg,v_{\mathrm{P}}(m)} = N_{seg,2} = 2^2,\ \forall m$. Note that each (a)-(c) in Fig. 4.3 is a special case so that same FFT size is assumed over all time frames to confirm the trade-off even though in a real case the WSDR in (4.12) is assumed different FFT size.

In all cases, effects of false alarms are assumed negligible, because $P_{\mathrm{FA,target}}$ is assumed to be sufficiently small. We define observed area as an outermost square in Fig. 4.3 where the vertical axis and the horizontal axis correspond to frequency and time, respectively.

In the ideal case (Fig. 4.3 (a)), maximum FFT size is assumed with $P_{\mathrm{D}} = 1$ and no false alarms within the signal area (dark area). Therefore, true WS and true signal area in the observed area are perfectly recognized, and $\mathrm{WSDR}(v) = 1$.

In practical cases ((b) and (c) in Fig. 4.3), the trade-off between the detection performance and the frequency resolution exists.

In the case of large FFT size (Fig. 4.3 (b)), miss detections (diagonal line areas in the figure) may be caused by insufficient averaging in Welch FFT. On the other hand, it has high enough frequency resolution and it results in no WS loss caused by the frequency resolution. Due to the miss detections, $\mathbb{E}[\hat{\Psi}[f]] < \Psi[f]$ in (4.12) and it leads to $\mathrm{WSDR}(v) > 1$. In fact, larger $\mathrm{WSDR}(v)$, larger DC estimation error due to the miss detections which is not good actually. However, the amount exceeding one on WSDR can be controlled by δ which can control probability of miss detection with a given false alarm rate.

Although the smaller FFT size in Fig. 4.3 (c) leads to better detection performance due to more averaging of power spectrum, it also leads to reduced frequency resolution. The reduced frequency resolution leads to overestimation of the occupied area, shown with dotted lines in Fig. 4.3 (c). The dotted lines correspond to time-frequency areas detected as occupied but in fact outside the actual signal bandwidth. Due to overestimation, $\mathrm{WSDR}(v) < 1$.

4.3.4 Analysis of sub-optimum FFT size

An index number of sub-optimum FFT size $v_{\mathrm{SUB-OPT}}$ is defined by

$$\begin{aligned} v_{\mathrm{SUB-OPT}} = & \max v \\ & \text{s.t. Worst RMSE}(\Psi[f]) \leq \delta, \\ & P_{\mathrm{FA}} = P_{\mathrm{FA,target}}, \end{aligned} \tag{4.13}$$

The solution of (4.13) means that the largest FFT size satisfying the constraint in terms of RMSE is selected. Selecting the largest allowed FFT size leads to the highest frequency resolution. However it does not consider the effect of detection performance, i.e., the relation between P_{D} and $P_{\mathrm{FA,target}}$ on the WSDR. In other words, the largest allowed FFT size does not necessarily achieve the optimum solution in (4.9). We will compare the results of $v_{\mathrm{SUB-OPT}}$ and v_{OPT} with numerical evaluation to show the validity of $v_{\mathrm{SUB-OPT}}$.

The sub-optimum FFT size is equivalent to the maximum FFT size which can get the probability of detection so that it satisfies $\mathrm{RMSE}(\Psi[f_c]) = \delta$ (for given $P_{\mathrm{FA,target}}$) according to (4.11). The rationale of this is that the probability of detection is sufficient to satisfy the RMSE constraint. Now, based on (4.11) and $\mathrm{RMSE}(\Psi[f_c]) = \delta$, we get $v_{\mathrm{SUB-OPT}}$ analytically as follows. Based on $\mathrm{RMSE}(\Psi[f_c]) = \delta$, the following quadratic equation

$$aP_{\mathrm{D}}^2 + bP_{\mathrm{D}} + c = 0, \tag{4.14}$$

where

$$\begin{cases} a = \Psi[f_c]^2 - \frac{\Psi[f_c]}{M} \\ b = 2[\left(P_{\mathrm{FA,target}} + \frac{1}{2M}\right)\Psi[f_c] \\ \qquad\qquad - \left(1 + P_{\mathrm{FA,target}}\right)\Psi[f_c]^2] \\ c = \frac{(1-\Psi[f_c])P_{\mathrm{FA,target}}\left(1-P_{\mathrm{FA,target}}\right)}{M} \\ \qquad\qquad + [P_{\mathrm{FA,target}}\left(1 - \Psi[f_c]\right) - \Psi[f_c]]^2 - \delta^2. \end{cases} \tag{4.15}$$

Two solutions for (4.14) are given by

$$\begin{cases} P_{\mathrm{D1}} = \frac{-b}{2a} - \frac{\sqrt{b^2-4ac}}{2a}, \\ P_{\mathrm{D2}} = \frac{-b}{2a} + \frac{\sqrt{b^2-4ac}}{2a}. \end{cases} \tag{4.16}$$

Since P_{D2} and P_{D1} are probability, both of them have to be between [0, 1]. However, $P_{\mathrm{D2}} \leq 1$ cannot be satisfied by $\delta^2 \geq 0$.

On the other hand, $P_{\mathrm{D1}} \leq 1$ can be satisfied under the following condition:

$$\delta \geq \sqrt{P_{\mathrm{FA,target}}^2 + \frac{P_{\mathrm{FA,target}}(1 - P_{\mathrm{FA,target}})}{M}}. \tag{4.17}$$

The condition implies that low probability of false alarm is required to satisfy $\mathrm{RMSE}(\Psi[f_c]) = \delta$ under sufficiently small δ. Moreover, $P_{\mathrm{D1}} \geq 0$ can be satisfied by the following condition:

$$\begin{aligned} \Psi[f_c] &\geq \frac{\left(2 - \frac{1}{M}\right) P_{\mathrm{FA,target}}^2 + \left(2 + \frac{1}{M}\right) P_{\mathrm{FA,target}}}{1 + P_{\mathrm{FA,target}}} \\ &\approx 2P_{\mathrm{FA,target}}. \end{aligned} \tag{4.18}$$

The condition (4.18) is not satisfied when DC is very small, such as $\Psi[f_c] < 2 \times 0.01$.

In conclusion, we consider P_{D1} as a solution for (4.14) when (4.17) and (4.18) are satisfied under small target false alarm rate. The conditions (4.17) and (4.18) are derived in Appendix.

Finally, $v_{\mathrm{SUB-OPT}}$ is given as

$$v_{\mathrm{SUB-OPT}} = \lfloor \log_2 \left[2N_s / (L_{\mathrm{SUB-OPT}} + 1) \right] \rfloor, \tag{4.19}$$

where $L_{\mathrm{SUB-OPT}}$ denotes the sub-optimum number of segments and it corresponds to the minimum number of segments satisfying $P_{\mathrm{D}} \geq P_{\mathrm{D1}}$.

According to the fact that $L_{\mathrm{SUB-OPT}}$ depends on P_{D1}, the sub-optimum FFT size can be selected based on real DC $\Psi[f]$, SNR and P_{FA}. For selecting the FFT size properly, we consider the worst case in terms of DC. In other words, if FFT size is selected in a way that the RMSE constraint is satisfied at $\Psi[f] = 1$ subject to (4.17), the selected FFT size can satisfy the RMSE constraint for any DC. Figure 4.4 shows the index number of sub-optimum FFT size $v_{\mathrm{SUB-OPT}}$ at different $\Psi[f]$ and δ as a function of SNR. This figure shows that sub-optimum FFT size has a stepwise property due to

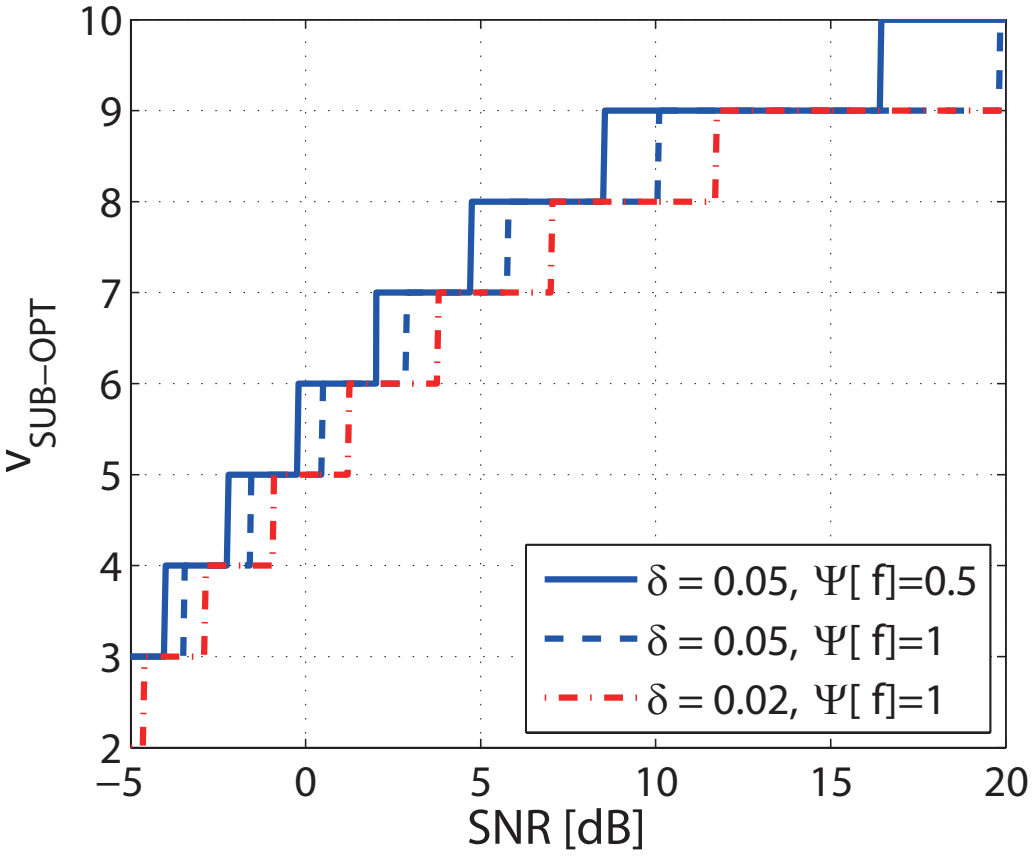

Fig. 4.4: The index number of sub-optimum FFT size as a function of SNR at different $\Psi[f]$ and δ

the fact that the number of v is integer. The RMSE characteristic for sub-optimum FFT size will be discussed in Section 4.4. Unfortunately, SNR is unavailable in typical spectrum measurements, therefore it is difficult to select the FFT size based on (4.19). For this issue, we propose ASSS method which can select a proper FFT size without SNR information in the next section.

4.4 Numerical evaluations

In this section, we show the validity of our ASSS method based on computer simulations. We assume the measurement bandwidth (equivalent to complex sampling rate) $W_M = f_s = 44$MHz and PU signal bandwidth $W_S = 22$MHz. This signal bandwidth corresponds to the RF channel bandwidth in IEEE 802.11g WLAN. In this case, six

Table. 4.1: Simulation parameters

Parameter name	**Parameter**
Modulation mode	Quadrature phase shift keying
Time frame size N_s	2^{10}
v	$\{v_{\min} = 3, 4, 5, 6, 7, 8, 9, v_{\max} = 10\}$
M	100
σ_z^2	1
SNR [dB]	[-3 10]
Window type	Hamming window
δ	0.05
$P_{\text{FA,target}}$	0.01
$\Psi[f],\ f \in \mathcal{H}_1$	0.5

WLAN channels are contained exactly within measurement bandwidth $W_M = 44$MHz, but for the sake of clarity we have assumed only one WLAN channel with $W_S = 22$MHz is used.

In addition, the durations of a packet and a time gap between string of two packets vary from several tens of microseconds to several milliseconds. Accordingly, we set the time frame size $N_s = 1024$ as in [148] where the time resolution $\Delta t = N_s/f_s$ corresponds to $\Delta t = 1024/44 \times 10^6 \approx 23\mu$sec, which is shorter than the time duration of distributed coordination function inter frame space (DIFS) with 28μsec. Then, N_s with 1024 is equal to the index number of maximum FFT size $v_{\max} = 10$.

Moreover, we set DC estimation period M to 100 as the RMSE constraint in terms of DC estimate with $\delta = 0.05$ is satisfied completely by this value. Common simulation parameters are summarized in Table 4.1.

At first, we verify the effect of the overlap ratio ρ in the Welch FFT and set the proper ρ through computer simulation. Figure 4.5 shows the probability of detection as a function of ρ with different values of SNR. For each SNR, the applied FFT size is the optimum FFT size, i.e., $N_{seg} = 2^4,\ 2^6,\ 2^8$ for SNR $= -3,\ 0,\ 6$ dB, respectively.

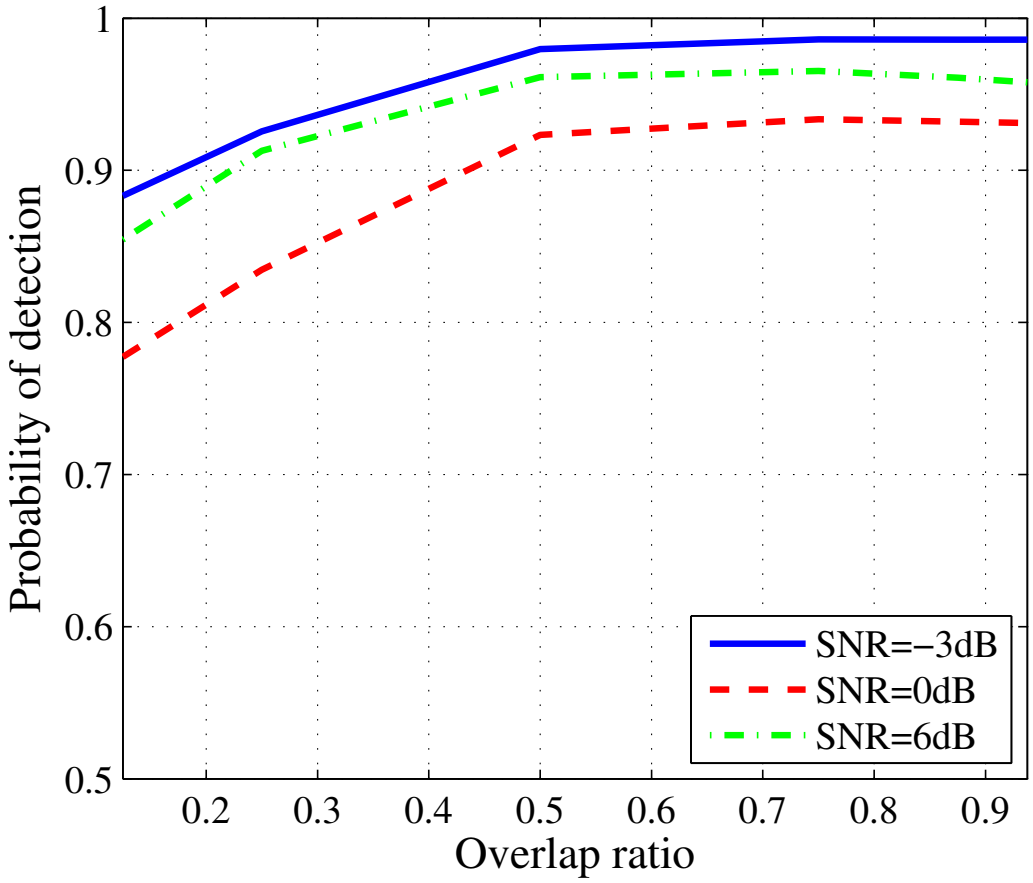

Fig. 4.5: Probability of detection as a function of ρ at different SNR

The result in Fig. 4.5 indicates that $\rho = 0.5$ is proper for any case because the probability of detection at $\rho = 0.5$ almost attains maximum probability. For this reason, we use $\rho = 0.5$ in subsequent computer simulations.

Finally, we verify the property of RMSE in terms of DC estimate and WSDR. Figure 4.6 shows RMSE($\Psi[f_c]$) as a function of SNR to confirm whether the RMSE constraint is satisfied. In Fig. 4.7, WSDR(v) as a function of SNR is shown to confirm the ability to find WS. In the results of Figs. 4.6 and 4.7, five methods are evaluated. The optimum result based on (4.9) represents upper bound performance in Fig. 4.7.

The sub-optimum result is obtained based on (4.19) and both optimum and sub-optimum, SNR information is assumed to be known. In results of $v = 3$ and $v = 7$, FFT sizes $N_{seg,v} = 2^3$ or $N_{seg,v} = 2^7$ are used during whole observation, respectively.

In the cases of fixed FFT size, $N_{seg,v} = 2^3$ and $N_{seg,v} = 2^7$, we can confirm the trade-off. In low SNR, such as SNR < 2 dB of Fig. 4.6, $v = 7$ is too large to satisfy the constraint of RMSE$(\Psi[f_c]) \leq 0.05$. On the other hand, in the case of $v = 3$ the RMSE constraint can be satisfied in any SNR. However, Fig. 4.7 reveals that WSDR(v) with $v = 3$ is less than 0.9 in high SNR region such as SNR < 4 dB. This indicates that WS cannot be found properly.

In Fig. 4.6, the optimum one, sub-optimum one and the result of ASSS method can always satisfy the RMSE constraint. In the sub-optimum method, the FFT size corresponds to the maximum one while it satisfies the RMSE constraint. Therefore, RMSE$(\Psi[f_c])$ of the sub-optimum method is always the closest to δ.

Moreover, we can see that optimum method and sub-optimum method have a bumpy property. This phenomenon is related to the result in Fig. 4.4 where v is an integer. In the region where $2 <$ SNR < 4 in dB, $v = 7$ is the sub-optimum but in the case SNR $= 5$ dB, now $v = 8$ is the sub-optimum. In principle, higher SNR leads to smaller RMSE and this can be confirmed in the region $2 <$ SNR < 4 in dB. On the other hand, in SNR $= 5$ dB, $v = 8$ is used and the larger FFT size leads to larger RMSE while the constraint is satisfied. In Fig. 4.7, we can confirm that WSDR(v) of the optimum method is always the closest to one. On the other hand, the sub-optimum and ASSS method are also very close to one for all SNR. These results verify the validity of our proposed methods.

4.5 Chapter Summary

In this chapter, we investigated the optimal design for FFT size in Welch FFT based energy detection. In Welch FFT based ED, time resolution, frequency resolution and spectrum usage detection sensitivity determine WS detection performance in the time and frequency domains. We focused on the trade-off between the detection sensitivity and achievable frequency resolution regarding the FFT size used in Welch FFT while

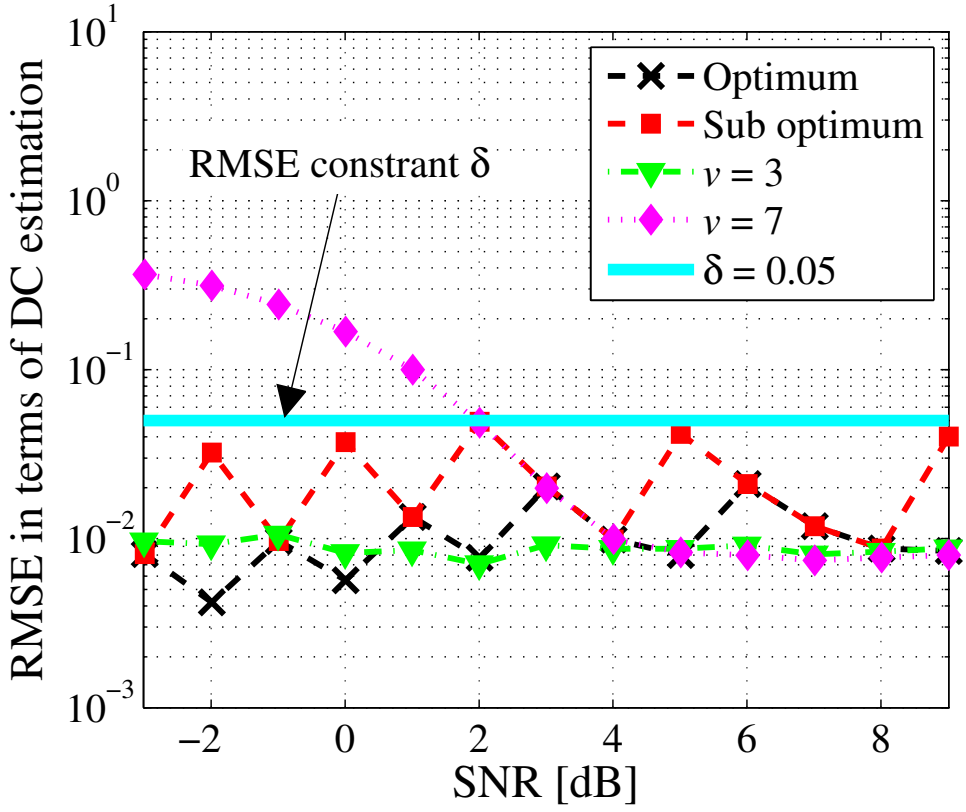

Fig. 4.6: RMSE($\Psi[f_c]$) against SNR

high enough time resolution is achieved.

We have formulated the optimum FFT size design criterion regarding WSDR with the constraint of RMSE. Due to the difficulty to derive the optimum FFT size analytically, we have also formulated the sub-optimum FFT size which is obtained analytically. However, the sub-optimum FFT size depends on the SNR which is an unknown parameter practically.

Extensive numerical evaluations showed the validity of the optimum design of FFT size. We revealed the importance of adaptively setting the FFT size according to the SNR value.

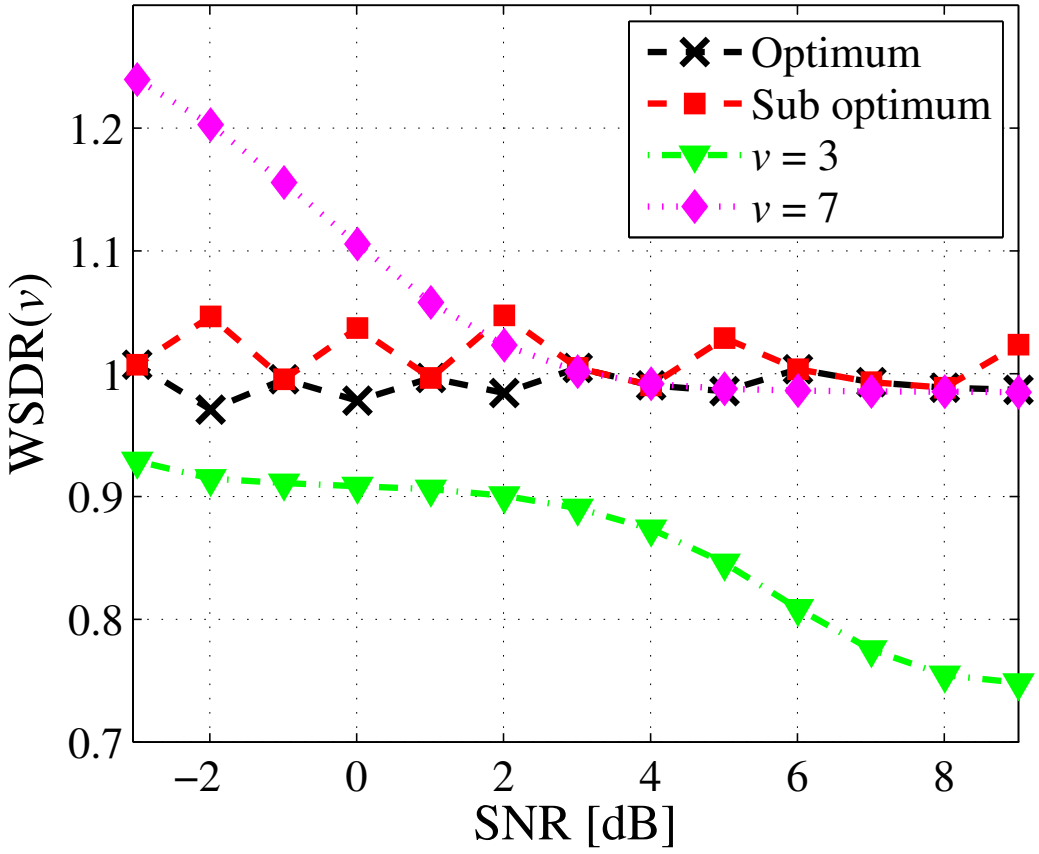

Fig. 4.7: WSDR(v) against SNR

Chapter

5

Practical FFT Size Setting Methods[ii]

5.1 Introduction

In previous chapter, Welch FFT-based ED is an effective method for achieving proper spectrum usage detection if FFT size is appropriately set. To this end, we formulated the optimum FFT size in terms of a criterion which is determined by white space detection ratio (WSDR) performance with a constraint determined by sensitivity required for spectrum usage detection. WSDR is defined by the ratio of estimated WS and actual WS in time and frequency domains, therefore WSDR = 1 indicates ideal situation,

[ii]This chapter is based on "Welch FFT Segment Size Selection Method for FFT Based Wide Band Spectrum Measurement" [1] in Publications, by the same authors, which appeared in IEICE Transactions on Communications, Copyright(C)2018 IEICE.

WSDR > 1 indicates overestimation of WS, and WSDR < 1 indicates underestimation of WS. The sensitivity in the constraint is quantified by root mean square error (RMSE) of DC estimation. In facr, if we know SNR and DC values, the optimum spectrum measurement performance can be achieved in terms of WSDC metric. Especially, if we know SNR and DC values, the optimum spectrum measurement performance can be achieved in terms of WSDC metric. Furthermore, the sub-optimum spectrum measurement performance can be achieved unless we know DC value; It is very difficult for a spectrum sensor to obtain the true DC value since the role of the spectrum sensor is just to estimate the true DC value. As for SNR information, its accurate acquisition is a difficult task since a spectrum sensor cannot know the channel information between observed PUs and the spectrum sensor. Therefore, this fact makes practical and optimum FFT size setting difficult.

Furthermore, in (Welch) FFT-based ED, there is another issue in addition to its detection limit as mentioned in the previous chapter. That is detection threshold setting. The threshold setting requires the noise floor information. In [84], the noise floor is measured in an anechoic chamber. In general, the threshold is set based on m-dB criterion in which the threshold is fixed at m decibels above the noise floor [150]. In the existing literature [56, 58, 73, 97], values such as $m = 3$, 5, 6, 20 dB have been employed, respectively. In fact, the noise floor should be estimated periodically due to its time dependency [151]. In [101, 152], threshold setting method based on noise floor estimation with forward consecutive mean excision (FCME) algorithm was proposed and it can achieve constant false alarm rate (CFAR) criterion to set threshold. In this chapter, we use the threshold setting method based on noise floor estimation with FCME algorithm since it can track the time varying noise floor, which makes a practical approach in this thesis.

For practicality of FFT size setting, we propose two FFT size setting methods to select a proper FFT size without SNR information. These are denoted by Exhaustive search based FFT Size Setting (E-SS) and Limited search based FFT Size Setting (L-SS). Both methods exploit a relationship between output of noise floor (NF) estimation based on FCME algorithm and the FFT size for proper FFT size setting. Our main

contributions in this chapter are as follows:

- We reveal the NF estimate by FCME algorithm depends on FFT size and SNR. This is due to the accuracy of NF estimate also depends on FFT size and SNR. Thus, the NF estimate which can be easily obtained in a spectrum sensor makes proper FFT size setting practical.

- E-SS exploits a relationship between output of NF estimation based on FCME algorithm and the FFT size for proper FFT size setting. E-SS uses NF estimation outputs for all possible segment sizes in Welch FFT, therefore it can achieve high WSDR performance but requires relatively high computational complexity. On the other hand, L-SS searches the proper FFT size while limiting the searchable FFT sizes. This limiting leads to low computational complexity in terms of FFT size setting.

- Numerical results show that E-SS and L-SS has comparable performances in terms of RMSE of DC estimate and WSDR, while computational complexity of L-SS has sufficiently lower than that of E-SS.

The remainder of the paper is organized as follows. The system model used in this paper is presented in Sect. 5.2. In Sect. 4.3, we introduce the FFT size design criterion leading an optimum FFT size by considering the trade-off between detection performance and frequency resolution. In Sect. 5.3, we introduce related works regarding FFT size selection. Specifically, we present the relationship between SNR, FFT size and NF estimate by FCME algorithm. After that, we propose two practical FFT size setting methods in Sects. 5.4 and refsec:L-SS, respectively. Performance evaluation based on computer simulation is presented in Sect. 5.6. Finally, chapter summaries are presented in Sect. 5.7.

5.2 System model

The block diagram of the signal processing used for spectrum usage measurement is shown in Fig. 5.1. The process consists of several components: Welch FFT with mem-

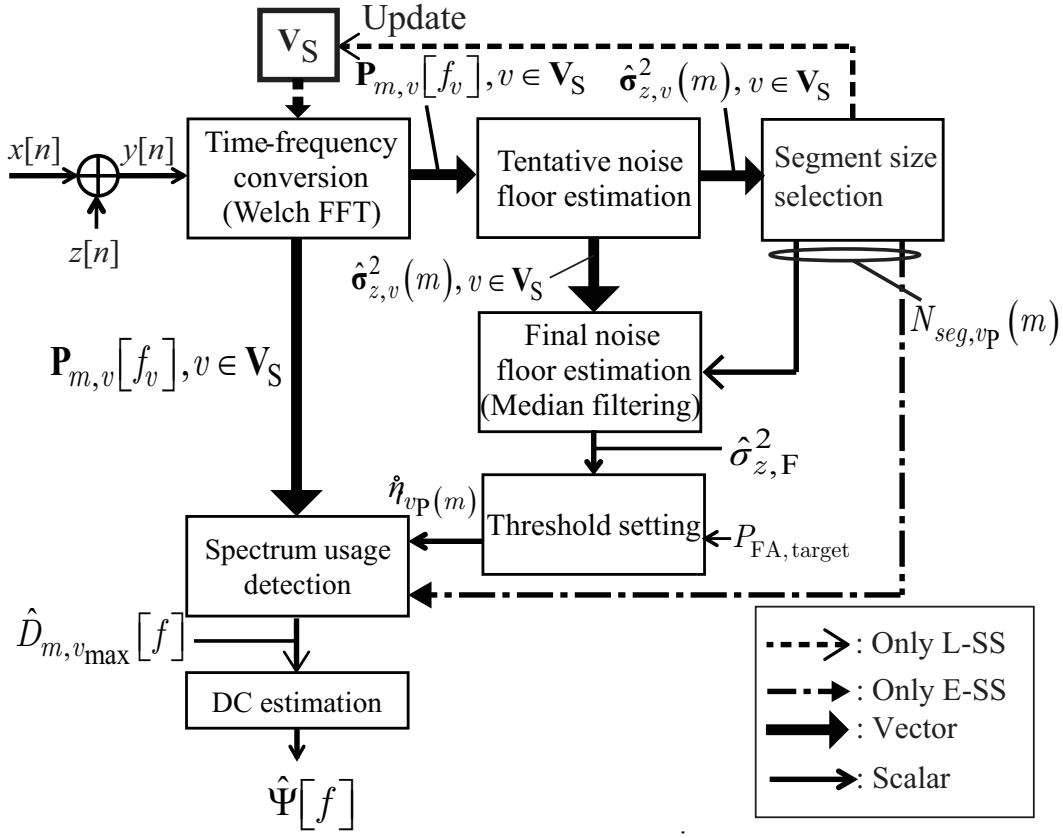

Fig. 5.1: Block diagram of the spectrum measurement process.

ory [143], NF estimation consisting of tentative NF estimation and final NF estimation, threshold setting, spectrum usage detection, FFT size selection, and DC estimation.

Configuration of time frames for the spectrum usage measurement is shown in Fig. 5.2. One consecutive spectrum usage measurement consists of M_s super frames and each super frame consists of M time frames. It is desirable to have sufficiently long measurement duration so that multiple primary user signals can be observed for accurately estimating DC. However, practically maximum duration is limited by the memory size in a spectrum sensor such as spectrum analyzer in SAS. Welch FFT, spectrum usage detection, and FFT size selection are performed to obtain signal usage detection results for every time frame. One time frame consists of N_s complex samples of received signal with sampling rate f_s Hz and this time frame corresponds to one Welch FFT size. The time frame length determines time resolution which is an important parameter to understand spectrum activity of PUs. The time frame length is set so that required

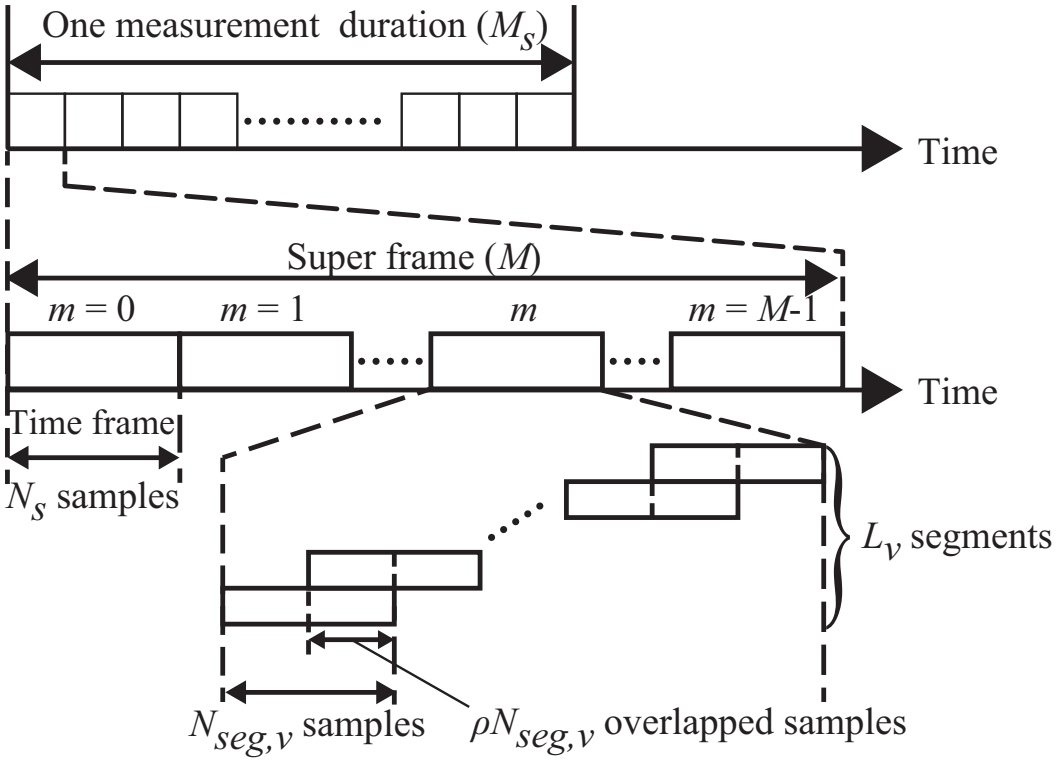

Fig. 5.2: The configuration of time frames in the measurement process.

time resolution can be met.

The tentative NF estimation using FCME algorithm [152] is performed in every time frame and the final NF estimation is obtained by median filtering the M tentative NF estimates [147]. The one super frame size M corresponds to median filter length for final NF estimation. NF estimation accuracy can be improved by using a median filter for NF estimation [153]. Optimization of super frame length (median filter length) is out of our scope and we determine the length according to [153]. The rationale for using the median filter for NF estimation is that NF is usually almost static at least a few minutes [151, 153]. The DC estimation is obtained based on $M_\mathrm{s} \times M$ signal usage detection results.

SAS observes the wide band spectrum in which several PUs may exist in the observed frequency band and bandwidth is denoted by W_M Hz. We assume that PU's signal bandwidth can vary with time, but the bandwidth is at most 90% of W_M Hz. The time duration and time interval of PU's signals can be also changed in time, but

time resolution of spectrum measurement has to be shorter than the time duration and time interval. The time resolution is determined by the time frame duration. The maximum signal length is assumed to be less than one measurement duration.

Now let us focus on the mth time frame ($m = 0, 1, \cdots, M-1$). The nth sample of the complex baseband signal $y[n]$ ($n = mN_{\rm s}, mN_{\rm s}+1, \cdots, mN_{\rm s}+N_{\rm s}-1$) in the mth time frame is given by

$$y[n] = \begin{cases} z[n] & \text{(PU is not active)} \\ x[n] + z[n] & \text{(PU is active),} \end{cases} \tag{5.1}$$

where $x[n]$ represents the PU signal component and $z[n]$ represents the noise component which follows independent and identically distributed (i.i.d) circular symmetric complex Gaussian distribution with zero mean and variance σ_z^2, i.e., $z[n] \sim CN(0, \sigma_z^2)$. We assume quasi static fading channel in which channel state is constant during one time frame. The instantaneous SNR is defined by SNR $= \sigma_x^2/\sigma_z^2$, where σ_x^2 and σ_z^2 are the instantaneous received PU signal power in spectrum sensor and noise power in the observed spectrum, respectively.

In the Welch FFT, $N_{\rm s}$ samples are segmented into L_v segments with an overlap ratio ρ. In the rest of the paper, we use $\rho = 0.5$ since the signal detection performance at $\rho = 0.5$ is appropriate as confirmed in previous chapter. In L_v, v denotes the index number of FFT size ($v = v_{\min}, v_{\min}+1, \cdots, v_{\max}$) and V denotes the number of all segment sizes as $V = v_{\max} - v_{\min} + 1$.

Without loss of generality, $N_{\rm s}$ and FFT size ($N_{{\rm seg},v}$) are assumed to be powers of two, i.e., $N_{\rm s} = 2^{v_{\max}}$ and $N_{{\rm seg},v} = 2^v$, namely v also indicates the exponent of the FFT size. In this case,

$$L_v = 2N_{\rm s}/N_{{\rm seg},v} - 1. \tag{5.2}$$

After the segmentation, normal FFT is performed with respect to each segment and the power spectrum averaged over L_v segments is given by [143]

$$\begin{aligned} &P_{m,v}[f_v] \\ &= \frac{1}{L_v} \sum_{l=0}^{L_v-1} \left| \sum_{k=0}^{N_{{\rm seg},v}-1} \frac{(w_v[k] y[k + \frac{lN_{{\rm seg},v}}{2}] e^{-j\frac{2\pi k f_v}{N_{{\rm seg},v}}})}{\sqrt{N_{{\rm seg},v}}} \right|^2, \end{aligned} \tag{5.3}$$

where f_v is an index number of the frequency bin ($f_v = 0, 1, \cdots, N_{\text{seg},v} - 1$), m is the index number of the time frame and $w_v[k]$ is the real-valued window coefficient. The type of window function also affects the detection performance [146]. Here, we use Hamming window because it has been shown that it can achieve slightly better performance compared to other window functions in [147].

Both FFT size selection methods, i.e., L-SS and E-SS perform Welch FFT with segment sizes specified by a set $\mathbf{V}_{\text{S}}$. In the case of E-SS, the elements in $\mathbf{V}_{\text{S}}$ are all segment sizes $\mathbf{V}_{\text{S}} = \{v_{\min}, v_{\min} + 1, \cdots, v_{\max}\}$ and Welch FFT is performed for each segment in $\mathbf{V}_{\text{S}}$ at once, thus, E-SS always performs Welch FFT V times.

On the other hand, in the case of L-SS, $\mathbf{V}_{\text{S}}$ always has only one element and is updated until a proper FFT size is found. For this reason, the number of Welch FFT operations can be less than the number in E-SS, i.e, V. The reason for the less number of Welch FFT operations in L-SS will be described in Sect. 5.6.2.

We assume that time resolution $\Delta t = N_{\text{s}}/f_{\text{s}}$ for the duration of a time frame is small enough compared to the minimum continuous signal length such as packet length and the minimum time gap between two consecutive signals, i.e., idle length [148]. On the other hand, the frequency resolution Δf_v is determined by the FFT size as $\Delta f_v = f_{\text{s}}/N_{\text{seg},v}$. We assume the maximum frequency resolution, i.e., $\Delta f_{v_{\max}} = f_{\text{s}}/N_{\text{seg},v_{\max}}$ is at least narrower than any PU signal bandwidth.

In the mth time frame, FFT size selection method (E-SS or L-SS) selects the proper FFT size. The background for performing FFT size selection every time frame is that in spectrum measurement over wide band including several primary systems, SNR may be changed by time frame basis and the optimum FFT size depends on SNR. The FFT size selection methods, E-SS and L-SS, will be presented in detail in Sects. 5.4 and 5.5, respectively. The FFT size selected is denoted by $N_{seg,v_{\text{P}}(m)}$, where $v_{\text{P}}(m)$ denotes the index number of the selected FFT size in the mth time frame.

The vector of the tentative NF estimates with the selected FFT size is

$$\hat{\boldsymbol{\sigma}}_z^2 = [\hat{\sigma}^2_{z,v_{\text{P}}(0)}, \hat{\sigma}^2_{z,v_{\text{P}}(1)}, \cdots, \hat{\sigma}^2_{z,v_{\text{P}}(M-1)}]^t,$$

where the superscript t denotes the vector transpose. The final NF estimate, denoted by $\hat{\sigma}^2_{z,\text{F}}$, is obtained by median filtering the elements in $\hat{\boldsymbol{\sigma}}_z^2$ [147].

Let $f_{v_{\mathrm{P}}(m)}$ denote the index number of the frequency bin in the mth time frame. Detection result at the mth time frame and the $f_{v_{\mathrm{P}}(m)}$th frequency bin is obtained by the ED as:

$$\begin{aligned}&\hat{D}_{m,v_{\mathrm{P}}(m)}[f_{v_{\mathrm{P}}(m)}]\\ &= \begin{cases} 1 & (\text{if } P_{m,v_{\mathrm{P}}(m)}[f_{v_{\mathrm{P}}(m)}] > \dot{\eta}_{v_{\mathrm{P}}(m)}) \\ 0 & (\text{otherwise}). \end{cases}\end{aligned} \tag{5.4}$$

where 1 and 0 respectively correspond to the decisions of occupied spectrum ($\mathcal{H}_1$) and vacant spectrum ($\mathcal{H}_0$), and $\dot{\eta}_{v_{\mathrm{P}}(m)}$ indicates the threshold for ED. $\mathcal{H}_1$ indicates that PU signal exists in the frequency bin partially or completely and $\mathcal{H}_0$ otherwise. In general, the detection performance can be summarized by two probabilities [149]: detection rate $P_{\mathrm{D}} = \Pr(P_{m,v_{\mathrm{P}}(m)}[f_{v_{\mathrm{P}}(m)}] > \dot{\eta}_{v_{\mathrm{P}}(m)}|\mathcal{H}_1)$ and false alarm rate $P_{\mathrm{FA}} = \Pr(P_{m,v_{\mathrm{P}}(m)}[f_{v_{\mathrm{P}}(m)}] > \dot{\eta}_{v_{\mathrm{P}}(m)}|\mathcal{H}_0)$, where $\Pr(x)$ indicates the probability of event x. The threshold $\dot{\eta}_{v_{\mathrm{P}}(m)}$ is set based on $\hat{\sigma}^2_{z,\mathrm{F}}$, the selected FFT size in the mth time frame, and a target false alarm rate $P_{\mathrm{FA,target}}$. In case of Welch FFT-based ED, proper threshold setting for $P_{\mathrm{FA,target}}$ or P_{D} is available [144, 146].

In the spectrum usage detection ($\hat{D}_{m,v_{\mathrm{P}}(m)}[f_{v_{\mathrm{P}}(m)}]$), the number of frequency bins varies every time frame due to the FFT size selection. For the DC estimation in each frequency bin, the number of frequency bins in each time frame is unified by the maximum number of frequency bins $N_{\mathrm{s}} = 2^{v_{\max}}$. This can be achieved by

$$\hat{D}_{m,v_{\max}}[f] = \hat{D}_{m,v_{\mathrm{P}}(m)}[f_{v_{\mathrm{P}}(m)}], \tag{5.5}$$

where

$$\frac{\Delta f_{v_{\mathrm{P}}(m)}}{\Delta f_{v_{\max}}} f_{v_{\mathrm{P}}(m)} \leq f \leq \frac{\Delta f_{v_{\mathrm{P}}(m)}}{\Delta f_{v_{\max}}} (f_{v_{\mathrm{P}}(m)} + 1) - 1, \tag{5.6}$$

and $\Delta f_{v_{\mathrm{P}}(m)}$ and $\Delta f_{v_{\max}}$ indicate the frequency resolution for FFT size $2^{v_{\mathrm{P}}(m)}$, i.e., $\Delta f_{v_{\mathrm{P}}(m)} = f_{\mathrm{s}}/N_{seg,v_{\mathrm{P}}(m)}$ and the frequency resolution for largest FFT size $N_{seg,v_{\max}} = N_{\mathrm{s}}$, i.e., $\Delta f_{v_{\max}} = f_{\mathrm{s}}/N_{\mathrm{s}}$, respectively.

DC estimation is performed for each super frame and each frequency bin and the estimated DC at the fth bin is

$$\hat{\Psi}[f] = \frac{1}{M} \sum_{m=0}^{M-1} \hat{D}_{m,v_{\max}}[f]. \tag{5.7}$$

We use $m_{\mathcal{H}_1}$-out-*of*-M model [144] to define the true DC as $\Psi[f] = m_{\mathcal{H}_1}[f]/M$, where $m_{\mathcal{H}_1}[f]$ denotes the number of $\mathcal{H}_1$ hypotheses in the fth frequency bin.

5.3 Noise Floor Estimation based on FCME Algorithm

In this section, at first we briefly introduce the noise floor estimation based on forward consecutive mean excision (FCME) algorithm. Then, we will show a relationship between SNR, FFT size and NF estimate by the tentative NF estimation with brief description of FCME algorithm. In fact, E-SS and L-SS exploit an aspect of the tentative NF estimate.

5.3.1 Brief Explanation of FCME algorithm

FCME algorithm [152] used in the tentative NF estimation is an iterative method that attempts to recognize clean power spectrum samples (noise-only samples) which correspond to $\mathcal{H}_0$ samples.

More specifically, the process of FCME algorithm is as follows. It first sorts the power spectrum samples in an ascending order. After that, it calculates the mean of the I smallest sorted samples. The NF estimation assumes that at least I smallest sorted samples are noise-only samples (clean samples). In general, $I = \lceil 0.1N \rceil$, where $\lceil \cdot \rceil$ is the ceiling function and N is the number of frequency bins (FFT size), and we also use $I = \lceil 0.1N \rceil$ throughout the paper according to the related works [147,153]. By assuming that the calculated mean is correct, the threshold that attains the target false alarm rate such as 0.01 with the calculated mean is obtained based on the distribution of noise power samples, which follows Chi-square distribution with degrees of freedom $2L_v$ [154]. Obviously, the threshold is more than the mean value and the clean samples are updated by adding samples which have value lower than the threshold. Then, the threshold is updated based on the updated clean samples and the target false alarm rate. The updating of clean samples continues as long as new samples are added from the set of non-clean samples (signal plus noise samples) obtained with the latest threshold. Finally, the tentative NF estimate is given by the average power of the estimated clean samples at the final iteration.

5.3.2 Relationship between SNR, FFT size and NF estimate

From process of FCME algorithm, NF estimation accuracy is determined by whether the algorithm can accurately divide the sorted power spectrum samples into clean samples and non-clean samples.[1] We explain this fact using Figs. 5.3 to 5.8.

Figures 5.3, 5.5 and 5.7 show the power spectrum samples with $v = 10$, 7 and 2 at SNR = 5dB, respectively. There is one signal from $f = -10$MHz to $f = 10$MHz and the true NF level is set to 0dB. Also, Figs. 5.4, 5.6 and 5.8 show the ascending sorted version of power spectrum samples with $v = 10$, 7 and 2 at SNR = 5dB, respectively.

In case of $v = 10$, the NF estimation algorithm cannot divide the sorted samples into clean samples and non-clean samples accurately as shown in Fig. 5.4. This is due to large fluctuations of power spectrum as shown in Fig. 5.3. Thus, this results in a poor NF estimation accuracy for $v = 10$.

On the other hand, from Fig. 5.6, in case of $v = 7$, the sorted samples can be divided into clean samples and non-clean samples via NF estimation based on FCME algorithm accurately. A gap can be confirmed at frequency bin number 65 in Fig. 5.6. The NF estimation can divide the samples by the gap. In $v = 7$, averaging process in Welch-FFT suppress the fluctuations due to noise, but in $v = 10$ there is no averaging. The averaging leads to accurate NF estimation in $v = 7$.

However, in $v = 2$, the power spectrum samples cannot clearly distinguish between the clean samples and the non-clean samples due to poor frequency resolution. Specifically, frequency bins $f = -20$ and 20MHz partially include the signal components in Fig. 5.7. For this reason, the sorted samples cannot be divided into clean samples and non-clean samples accurately as shown in Fig. 5.8 and this leads to deviation of the NF estimate with $v = 2$ from true NF level.

Figure 5.9 shows the average of tentative NF estimates in linear scale as a function of FFT size for different SNR, i.e. -3 dB, 0 dB and 5 dB. The real noise power is set to

[1] If the whole observed band is occupied by PU signals, it may cause overestimation of NF due to non clean samples. However, it may be a rare situation that PUs simultaneously occupy all frequency range since we are typically assuming to use a wide band observation equipment. In addition, median filter can be employed to suppress the effect of the overestimation [153].

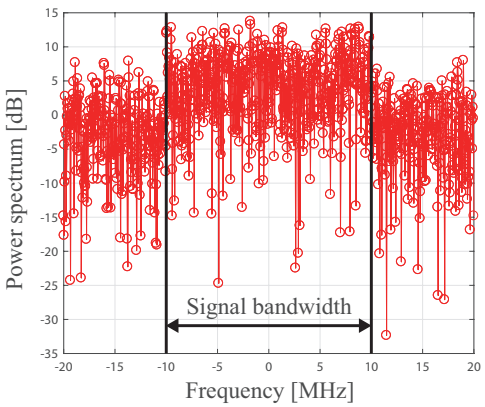

Fig. 5.3: Power spectrum with $v = 10$

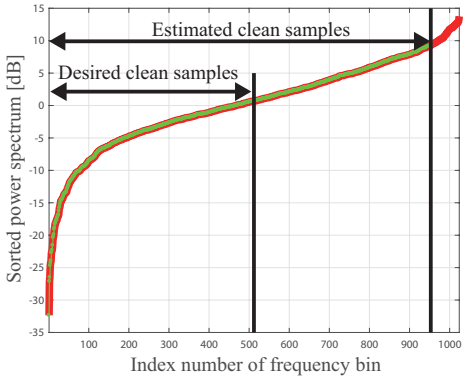

Fig. 5.4: Sorted power spectrum with $v = 10$

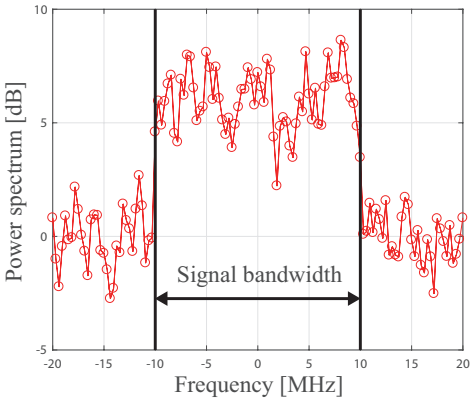

Fig. 5.5: Power spectrum with $v = 7$

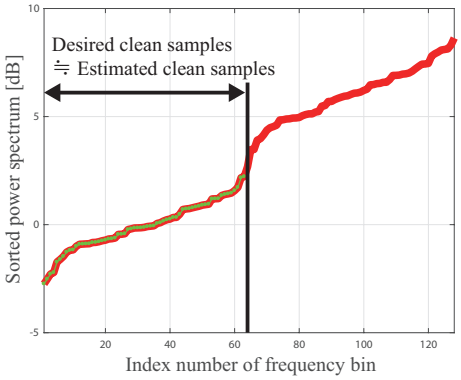

Fig. 5.6: Sorted power spectrum with $v = 7$

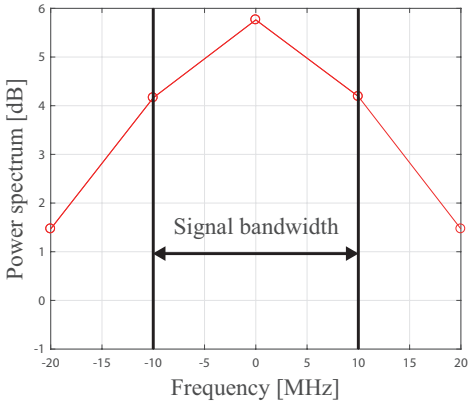

Fig. 5.7: Power spectrum with $v = 2$

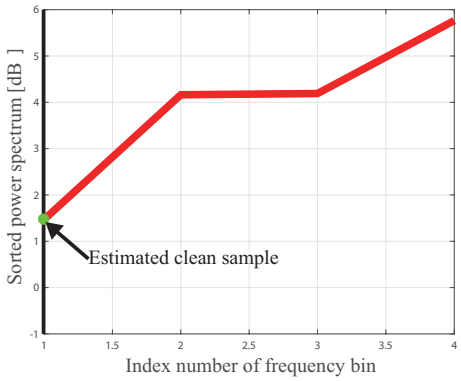

Fig. 5.8: Sorted power spectrum with $v = 2$

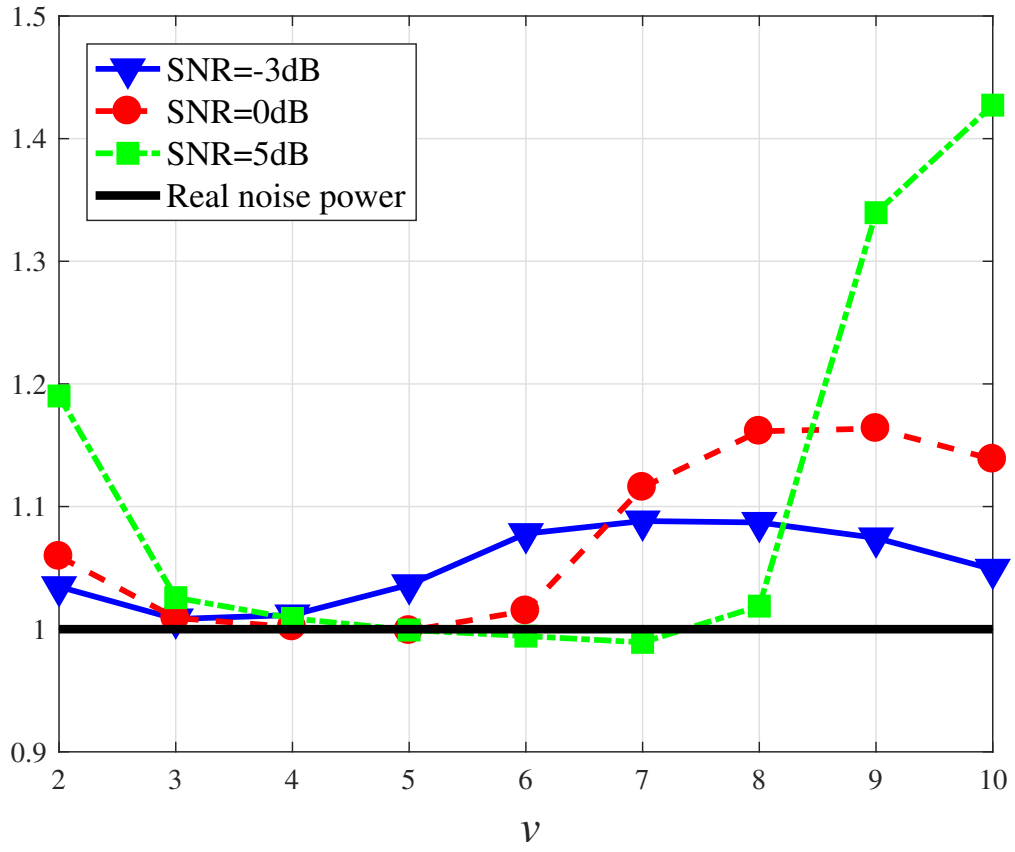

Fig. 5.9: The relationship between v and tentative NF estimate, SNR $= -3, 0, 5$ dB, the real noise power $\sigma_z^2 = 1$.

one. Throughout the paper, the index number of optimum FFT size v_{OPT} is a solution of the optimization problem (4.9) in which v is the parameter for the optimization problem. The optimum FFT size can achieve high enough detection performance while $|1 - \mathrm{WSDR}(v)|$ is minimized by a proper frequency resolution (larger FFT size). Figure 5.10 shows |1-WSDR(v)| as a function of the index number of FFT size v at SNR $= -3$, SNR $= 0$ and SNR $= 5$ dB. From this figure, the index number of optimum FFT size is $v = 4$ in SNR $= -3$ dB, $v = 6$ in SNR $= 0$ dB and $v = 7$ in SNR $= 5$ dB, respectively as |1-WSDR(v)| is minimized at the index number of optimum FFT size while the optimum segment sizes meet the constraint of the optimization problem (4.9).

FCME algorithm estimates NF by finding a set of clean samples while power spectrum samples are either clean samples or non-clean samples. Specifically, FCME algorithm attempts to find a gap between the clean samples and non-clean samples [155].

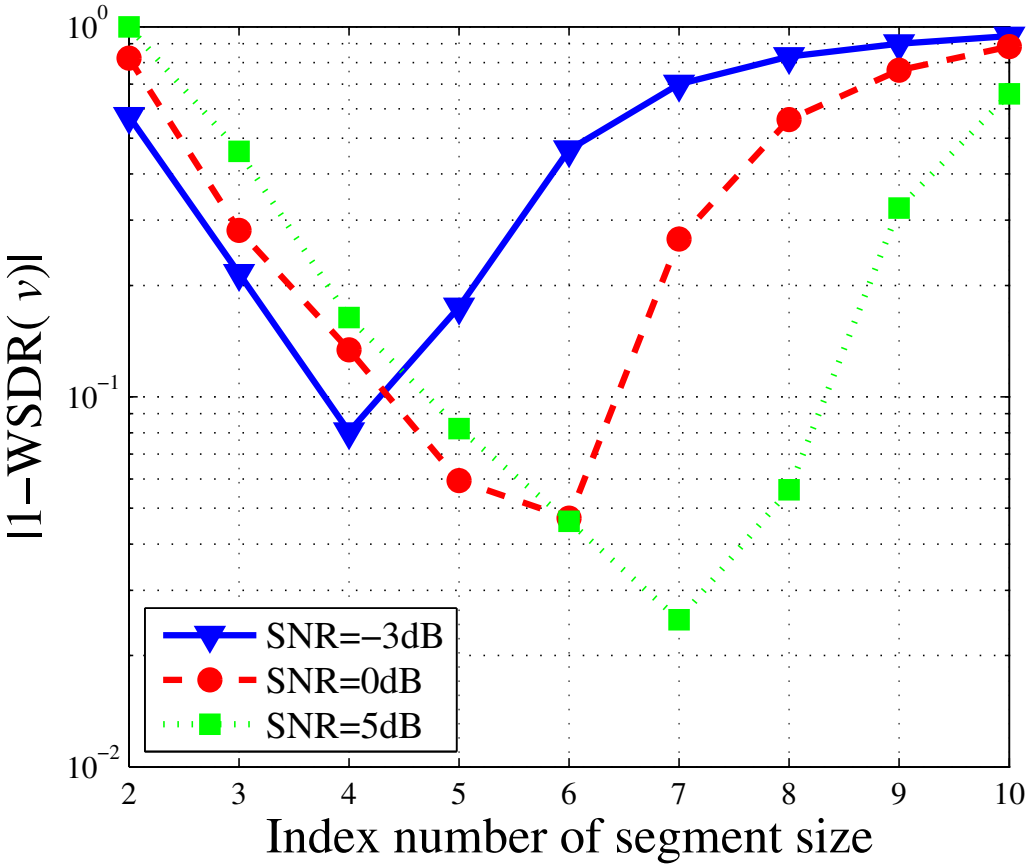

Fig. 5.10: |1-WSDR(v)| as a function of the index number of FFT size v, SNR $= -3, 0, 5$ dB.

In the case of $v = 10$, FCME algorithm estimates non-clean samples as clean samples due to no averaging in Welch FFT leading to large fluctuations of power spectrum and difficulty to find the gap [155]. Therefore, it leads to the overestimation of the NF estimate with $v = 10$ as shown in Fig. 5.9. In case of $v = 2$, NF estimation accuracy is also poor as shown in Fig. 5.9. This is reason that some of power spectrum samples (frequency bins) include signal components partially due to the poor frequency resolution and it cannot clearly distinguish between clean samples and non-clean samples. If the FFT size is proper ($3 \leq v \leq 8$ in SNR $= 5$ dB, $3 \leq v \leq 6$ in SNR $= 0$ dB and $3 \leq v \leq 5$ in SNR $= -3$ dB in Fig. 5.9), NF estimation accuracy is sufficiently high since averaging power spectrum can show the gap accurately.

Both E-SS and L-SS exploit above aspect of the tentative NF estimate, i.e., the

slope of tentative NF estimate against the FFT size. In fact, the most appropriate FFT size is such that it can achieve proper NF estimation with the largest possible FFT size to achieve a sufficiently high frequency resolution.

5.4 Exhaustive Search-based FFT Size Setting: E-SS

In E-SS, at first Welch FFT and the tentative NF estimation are performed with all segment sizes $N_{\mathrm{seg},v}$ for each time frame. This provides V tentative NF estimates for the set $\mathbf{V}_{\mathrm{S}} = \{v_{\min}, v_{\min}+1, \cdots, v_{\max}\}$, i.e., $[\hat{\sigma}^2_{z,v_{\min}}(m), \cdots, \hat{\sigma}^2_{z,v_{\max}}(m)]$. The increment of tentative NF estimates between adjacent segment sizes with a positive direction is given by

$$\Delta\hat{\sigma}^2_{z,v}(m) = \hat{\sigma}^2_{z,v+1}(m) - \hat{\sigma}^2_{z,v}(m). \tag{5.8}$$

Then, the index number of the FFT size maximizing the increment is given by

$$v_{\mathrm{MAX}}(m) = \arg\max_{v} \Delta\hat{\sigma}^2_{z,v}(m). \tag{5.9}$$

The tentative NF estimation with the index number $v_{\mathrm{MAX}}(m)$ can achieve relatively accurate estimation performance. However, it does not necessarily satisfy the RMSE constraint. Therefore, an adjustable integer parameter β is employed to achieve the RMSE constraint and the index number of FFT size selected by E-SS is

$$v_{\mathrm{P}}^{(\mathrm{E-SS})}(m) = v_{\mathrm{MAX}}(m) + \beta. \tag{5.10}$$

Thus, the FFT size selected by E-SS is $N_{seg,v_{\mathrm{P}}^{(\mathrm{E-SS})}(m)} = 2^{v_{\mathrm{MAX}}(m)+\beta}$.

5.5 Limited Search-based FFT Size Setting: L-SS

In this section, we present details of L-SS algorithm. A flowchart of the process of L-SS is shown in Fig. 5.11. It consists of three decisions: decision-1 (D-1), decision-2 (D-2) and decision-3 (D-3) to determine appropriate FFT size.

At the mth time frame, the initial value of $\mathbf{V}_{\mathrm{S}}$ is set by an index number of FFT size selected in the previous time frame $(m-1)$: $v_0(m) = v_{\mathrm{P}}(m-1)$, where subscript 0

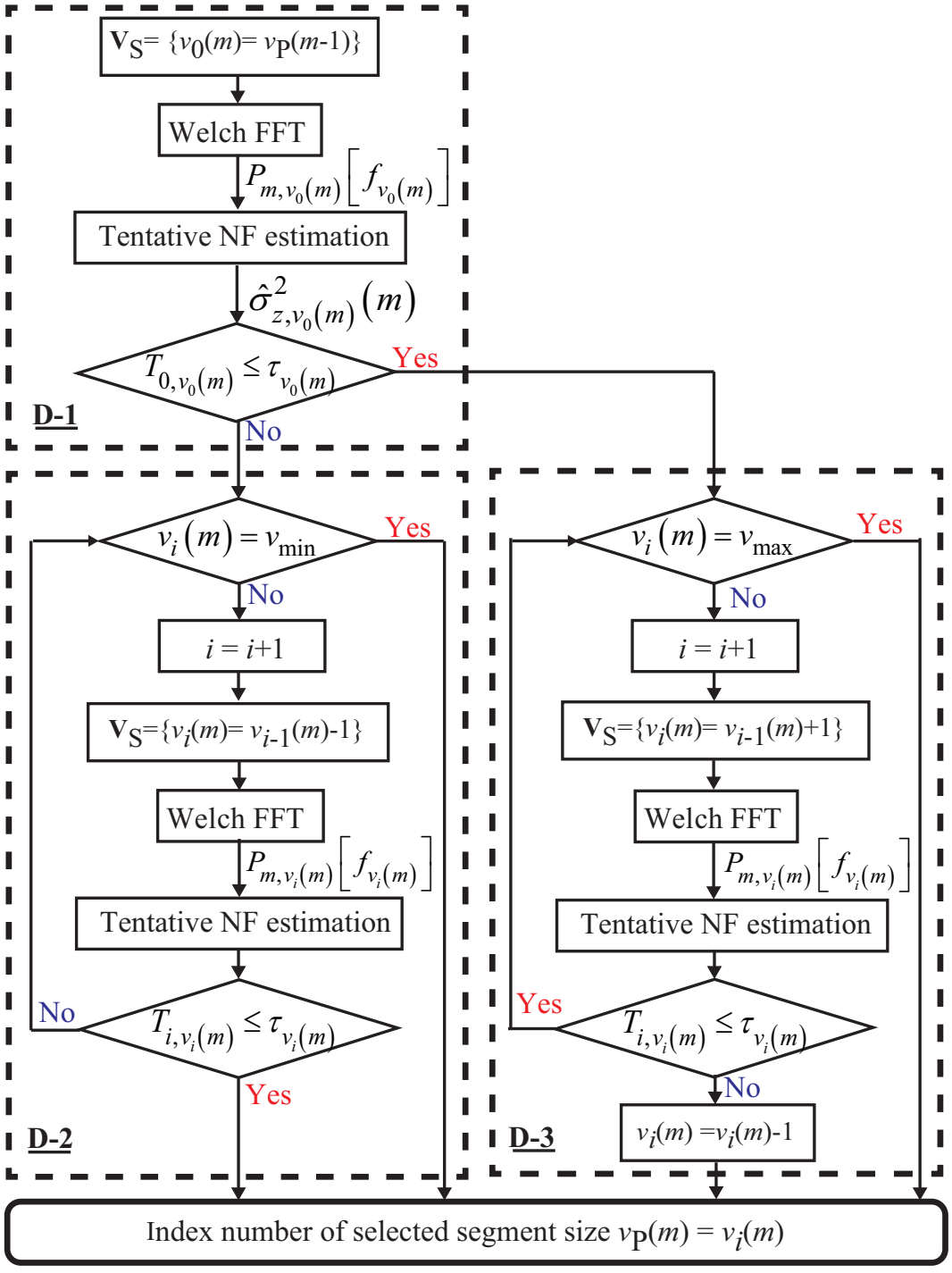

Fig. 5.11: Flowchart of L-SS.

indicates the initial value. In the case of $m = 0$, we can employ E-SS to select a proper FFT size.

Let $T_{i,v_i(m)}$ denote the ratio of the tentative NF estimate ($\hat{\sigma}^2_{z,v_i(m)}(m)$) to the final

NF estimate from the previous super frame ($\hat{\sigma}^2_{z,\mathrm{F}}$), i.e.,

$$T_{i,v_i(m)} = \frac{\hat{\sigma}^2_{z,v_i(m)}(m)}{\hat{\sigma}^2_{z,\mathrm{F}}}, i = 0, 1, \cdots, V-1, \tag{5.11}$$

where the subscript i indicates the index number of FFT size updating.

Typically, the changing rate of NF is very slow and relatively accurate NF estimate is available by $\hat{\sigma}^2_{z,\mathrm{F}}$. In fact, it has been shown that NF is usually almost static at least a few minutes [151, 153]. Considering this aspect, in the case that $\hat{\sigma}^2_{z,v_0(m)}(m)$ is significantly larger than $\hat{\sigma}^2_{z,\mathrm{F}}$, i.e., $T_{0,v_0(m)} > \tau_{v_0(m)}$, it is considered that the current checked FFT size $2^{v_0(m)}$ is large compared with a proper FFT size. This leads to the fact D-1 is "No". Then, the threshold $\tau_{v_0(m)}$ is determined by a significance level regarding whether $\hat{\sigma}^2_{z,v_0(m)}(m)$ is too large compared with $\hat{\sigma}^2_{z,\mathrm{F}}$. More detailed description about the threshold setting will be presented at the end of this subsection.

Specifically, in the case that the decision is "No" in D-1, the index number of FFT size is updated by $v_i(m) = v_{i-1}(m) - 1,\ i = 1, \cdots, V-1$, i.e., the set $\mathbf{V}_{\mathrm{S}} = \{v_{i-1}(m) - 1\}$ in D-2. The update is repeated until it achieves an appropriate FFT size so that $T_{i,v_i(m)} \leq \tau_{v_i(m)}$ or that it reaches the smallest FFT size $N_{seg,v_{\min}}$.

On the other hand, the decision "Yes" in D-1 indicates that the FFT size is not too large and proper NF estimation performance may be achievable. However, there is a possibility that the FFT size is too small, for example due to increase of SNR. In this case, it goes to D-3 and the FFT size is updated in the increasing direction until an inappropriate FFT size is found or that it reaches the largest FFT size $N_{\mathrm{seg},v_{\max}}$. Once the inappropriate FFT size is found by the decision "No" in D-3, the index number of selected FFT size is given by $v_{\mathrm{P}}(m) = v_i(m) - 1$ since the last updated FFT size is the most appropriate FFT size.

We set $\tau_{v_i(m)}$ so that the following probability equals to a given target probability $P_{\mathrm{L-SS}}$.

$$\begin{aligned} P_{\mathrm{L-SS}} &= \Pr(T_{i,v_i(m)} > \tau_{v_i(m)} | \hat{\sigma}^2_{z,\mathrm{F}} = \sigma^2_z, \mathcal{H}_0) \\ &= \int_{\tau_{v_i(m)}}^{\infty} p(T_{i,v_i(m)} | \hat{\sigma}^2_{z,\mathrm{F}} = \sigma^2_z, \mathcal{H}_0) dT_{i,v_i(m)}, \end{aligned} \tag{5.12}$$

where $p(T_{i,v_i(m)} | \hat{\sigma}^2_{z,\mathrm{F}} = \sigma^2_z, \mathcal{H}_0)$ is the conditional probability density function (PDF) of $T_{i,v_i(m)}$ under $\hat{\sigma}^2_{z,\mathrm{F}} = \sigma^2_z$ and $\mathcal{H}_0$ and it is obtained via Monte Carlo simulations. $P_{\mathrm{L-SS}}$

means a significance level regarding whether $\hat{\sigma}^2_{z,v_i(m)}(m)$ is too large compared with $\hat{\sigma}^2_{z,\mathrm{F}}$, thus whether the current checked FFT size is too large compared with a proper FFT size.

5.6 Numerical evaluations

In this section, we will evaluate two FFT size selection methods, i.e., L-SS and E-SS. The evaluated metrics are as follows: RMSE in terms of DC, $|1 - \mathrm{WSDR}(v)|$ and computational complexity. In addition, we will also evaluate the adaptivity of FFT size selection with time, i.e., the behavior of L-SS and E-SS in case that SNR is varied in time of L-EE and E-SS.

We assume that the measurement bandwidth (equivalent to complex sampling rate) is set to $W_{\mathrm{M}} = f_{\mathrm{s}} = 44$ MHz and the PU signal bandwidth $W_{\mathrm{S}} = 22$ MHz, such as the bandwidth in IEEE 802.11g WLAN. In addition, the duration and interval of PU signals are constant and the DC Ψ is 0.5. Specifically, the time duration and the time interval are about 230μsec. The time frame size is set to $N_{\mathrm{s}} = 1024$ [148] and the time resolution $\Delta t = N_{\mathrm{s}}/f_{\mathrm{s}}$ is $1024/44 \times 10^6 \approx 23\mu$sec. Δt is short enough compared with the time duration and the time interval. Moreover, we apply 2^3 as the minimum FFT size with minimum frequency resolution, $44 \times 10^6/2^3 \approx 5.5$MHz, which is narrow enough compared with the signal bandwidth, 22MHz. Common simulation parameters are summarized in Table 5.1.

At first, we verify the effect of the adjustable integer parameter β and set the proper β through computer simulation. Figure 5.14 shows RMSE($\Psi[f_c]$) as a function of SNR with different values of β. It can be seen that β gives an almost flat property against SNR. This means one proper β suffices to satisfy the given allowable DC estimation error δ. In subsequent computer simulations, we set $\beta = -1$ as it satisfies the condition (4.17).

5.6.1 RMSE in terms of DC and $|1 - \mathrm{WSDR}(v)|$

Figure 5.12 shows RMSE($\Psi[f_{\mathrm{c}}]$) as a function of SNR to confirm whether the RMSE constraint is satisfied. In Fig. 5.13, $|1 - \mathrm{WSDR}(v)|$ for every time frame as a function

Table. 5.1: Simulation parameters

Parameter	**Value**
Number of FFT samples: N_{s}	2^{10}
Segment size: v	$\{v_{\min} = 3, 4, 5, 6, 7, 8, 9, v_{\max} = 10\}$
Length of median filter: M	100
Noise Floor σ_z^2	1
SNR	[-4 10] dB
Window type	Hamming window
Allowable RMSE: δ	0.05
Target false alarm rate: $P_{\mathrm{FA,target}}$	0.01
DC: $\Psi[f],\ f \in \mathcal{H}_1$	0.5
Target probability in L-SS: $P_{\mathrm{L-SS}}$	10^{-3}

of SNR is shown to confirm the ability to find the WS. $|1 - \mathrm{WSDR}(v)|$ indicates the Mean Absolute Error (MAE) of WSDR and $|1 - \mathrm{WSDR}(v)|$ closer to zero indicates more accurate WS detection performance. In the results of Figs. 5.12 ($\mathrm{RMSE}(\Psi[f_{\mathrm{c}}])$) and 5.13 ($|1 - \mathrm{WSDR}(v)|$), five methods are evaluated: the results of L-SS and E-SS, the optimum method where the optimum FFT size satisfying (4.9) is always used, and fixed FFT size: $v = 3$, $v = 7$ and $v = 10$.

From the results of $v = 3$, $v = 7$ and $v = 10$ in Figs. 5.12 and 5.13, we can see that using constant FFT size cannot achieve proper performance when SNR is changed. When SNR $<$ 2dB in Fig. 5.12, $v = 7$ is too large to satisfy $\delta = 0.05$. In addition, $v = 10$ no longer satisfy $\delta = 0.05$ at SNR $<$ 10dB. These indicate the detection performance in low SNR and large FFT size is not very good and $v = 7$ and $v = 10$ are not adequate at SNR $<$ 2dB and SNR $<$ 10dB, respectively. On the other hand, in the case of $v = 3$ the RMSE constraint δ can be satisfied in any SNR. However, Fig. 5.13 reveals that $|1 - \mathrm{WSDR}(v)|$ with $v = 3$ is greater than that with $v = 7$ at SNR $\geq$ 2dB. This is due to reduced frequency resolution and indicates that the WS cannot be found

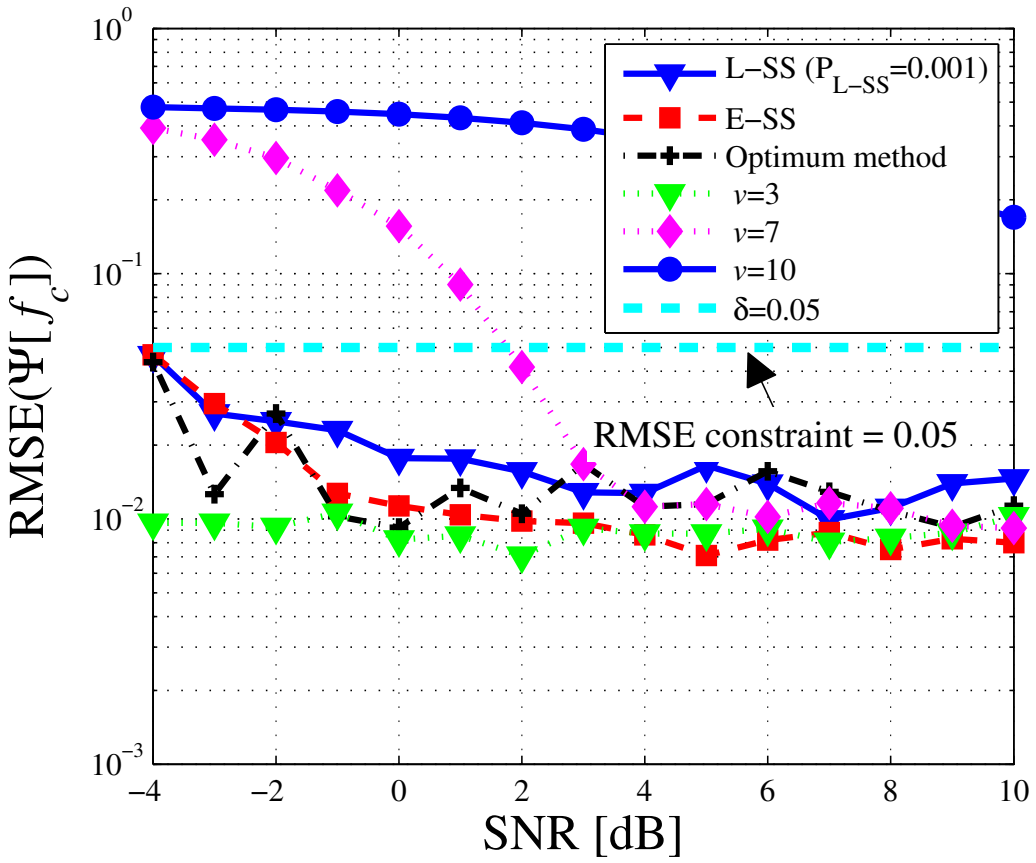

Fig. 5.12: RMSE($\Psi[f_c]$) against SNR.

properly compared with $v = 7$, and at least $v = 7$ is adequate at SNR $\geq$ 2dB.

In Fig. 5.12, the optimum method, and the results of E-SS and L-SS can always satisfy the RMSE constraint. In addition, the results of E-SS is better than that of L-SS. In Fig. 5.13, we can confirm that $|1 - \mathrm{WSDR}(v)|$ of the optimum method can achieve the best performance in any SNR. From the results of E-SS and L-SS in Fig. 5.13, we can see E-SS can achieve better $|1 - \mathrm{WSDR}(v)|$ performance in any SNR.

We can see that optimum method, E-SS and L-SS have bumpy properties in terms of RMSE. However the results of $v = 3$ and $v = 7$ have smooth curves. When 2dB $<$ SNR $\leq$ 5dB in Fig. 5.12, the index number of the optimum FFT size is $v = 7$, therefore the RMSE of $v = 7$ is equal to the RMSE of the optimum one. However, at SNR = 6 dB, the index number of the optimum FFT size is $v = 8$, so the RMSE is slightly increased

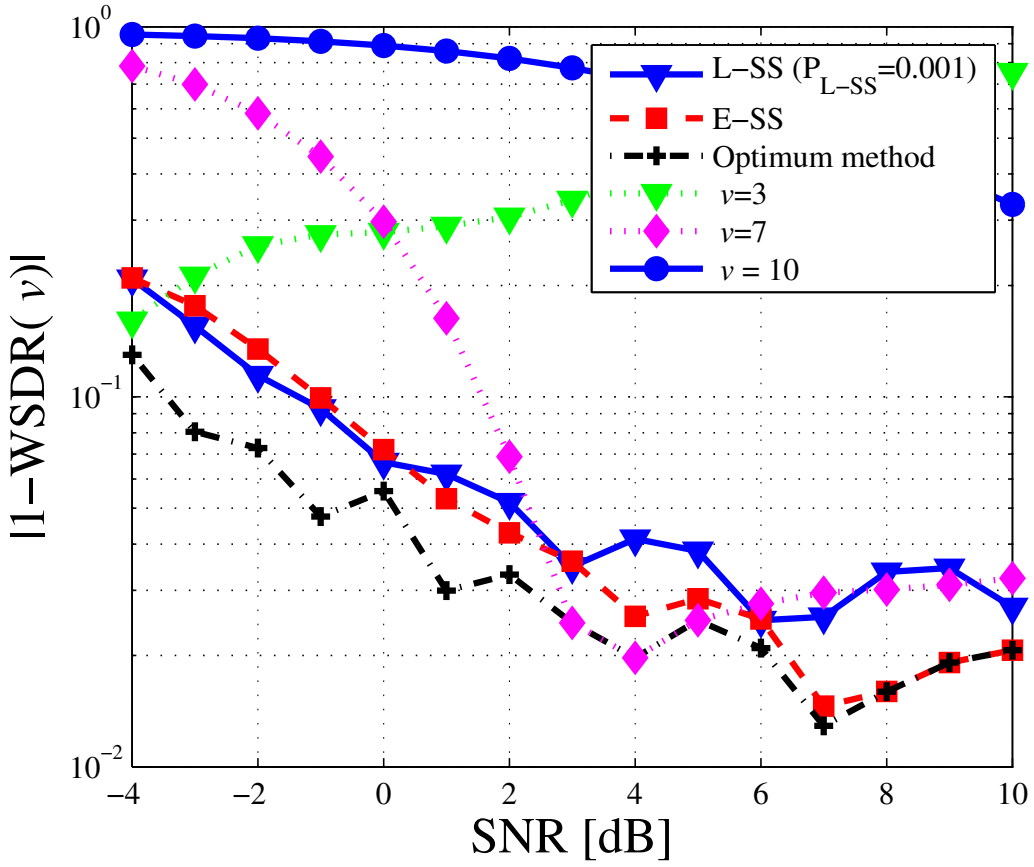

Fig. 5.13: $|1 - \mathrm{WSDR}(v)|$ in time frames against SNR.

in a discontinuous manner. Specifically, increasing SNR with fixed FFT size leads to a smooth curve, but changing FFT size causes the bumpy properties. Obviously, the three methods, i.e., L-SS, E-SS and the optimum method would change the FFT size in response to SNR which leads to this behavior.

Table. 5.2: Spectrum occupancy pattern and SNR change pattern

Index number of time frame	$1-10$	$11-20$	$21-30$	$31-40$	$41-50$	$51-60$	$61-70$	$71-80$	$81-90$	$91-100$
State	$\mathcal{H}_1$	$\mathcal{H}_0$	$\mathcal{H}_1$	$\mathcal{H}_0$	$\mathcal{H}_1$	$\mathcal{H}_0$	$\mathcal{H}_1$	$\mathcal{H}_0$	$\mathcal{H}_1$	$\mathcal{H}_0$
SNR [dB]	5	–	15	–	-3	–	9	–	1	–

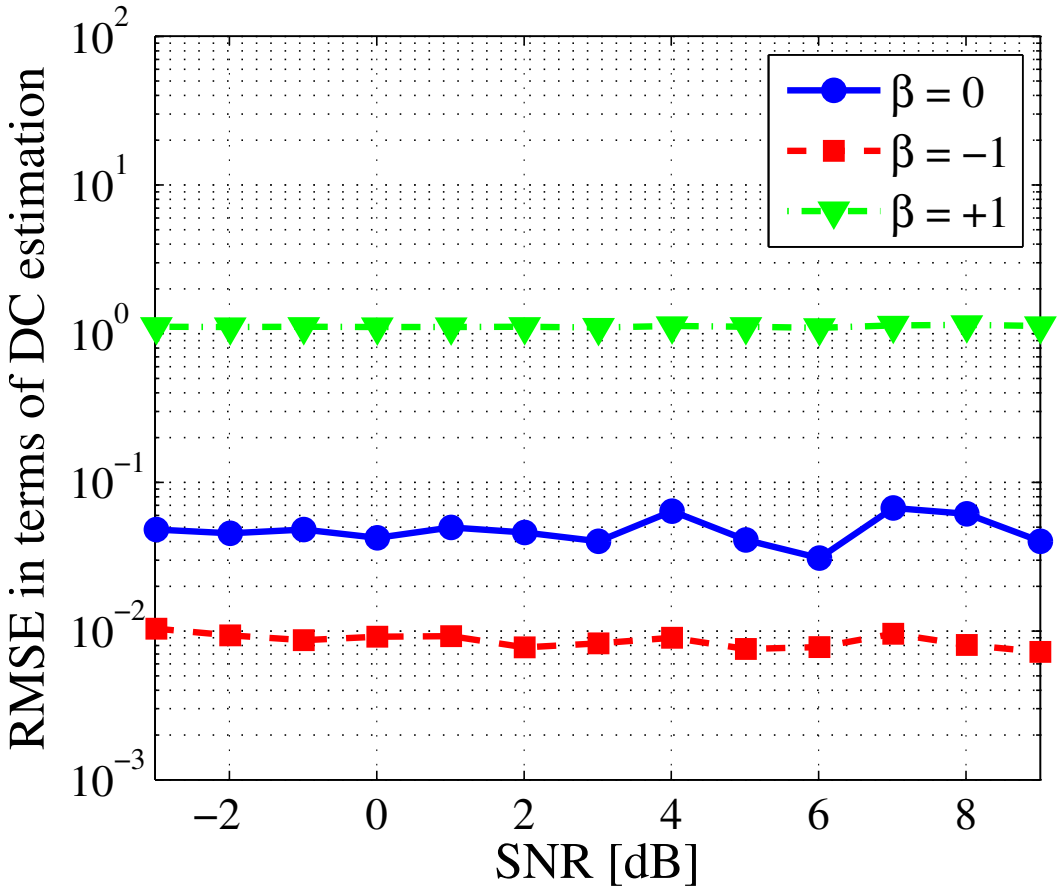

Fig. 5.14: RMSE($\Psi[f_c]$) against SNR, β

5.6.2 Computational complexity

We only evaluate the computational complexity of FFT size selection process in L-SS and E-SS. As mentioned in Subsect. 5.4 and Sect. 5.5, E-SS and L-SS consist of Welch FFT and the tentative NF estimation. Thus, the computational complexity of L-SS and E-SS is determined by the computational complexity of Welch FFT and the tentative NF estimation in L-SS and E-SS. Inherently, the computational complexity of L-SS is lower than E-SS since the numbers of executions of Welch FFT and the tentative NF estimation in L-SS are always equal to or less than ones of E-SS. The reason of this aspect is as follows. In E-SS, Welch FFT and the tentative NF estimation are performed for all possible segment sizes. On the other hand, in L-SS, Welch FFT and the tentative NF estimation are performed for a part of them and the details of L-SS are shown in Sect. 5.5.

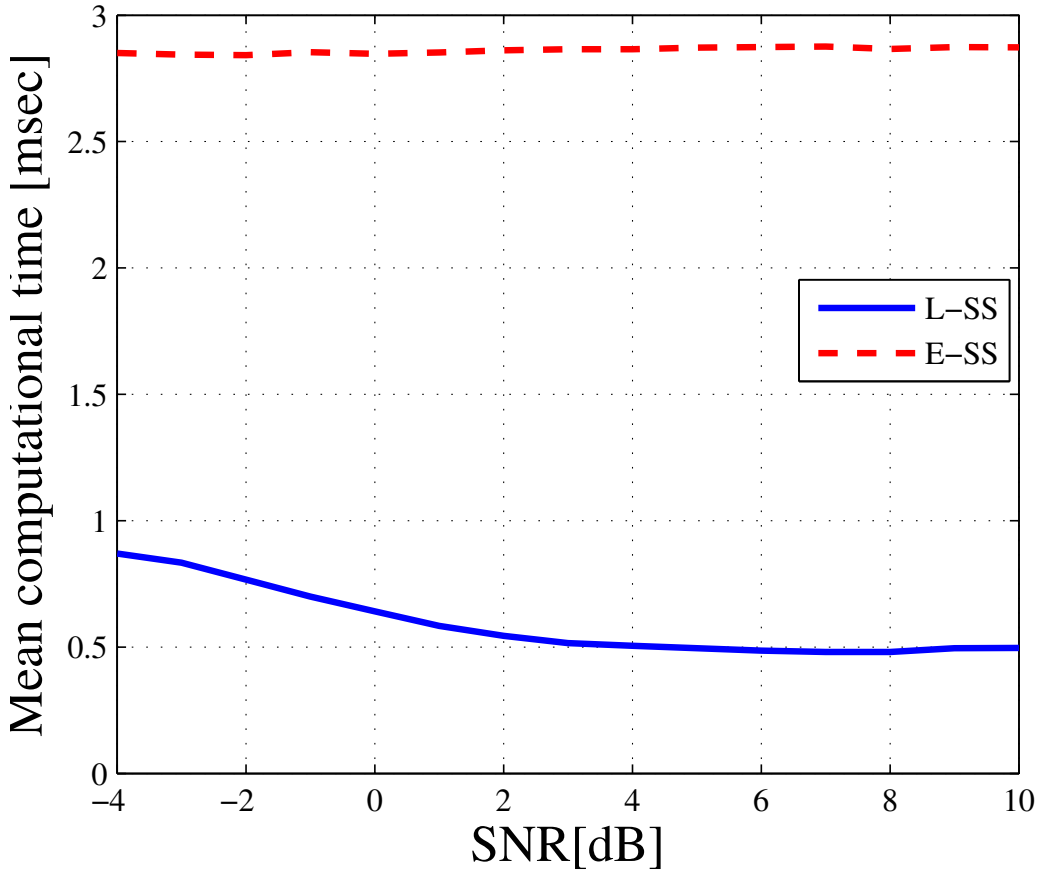

Fig. 5.15: Computational time of L-SS and E-SS. Computer specifications: Intel Core i7-2600, 3.4GHz, memory size is 8GB, and the algorithms were implemented in MATLAB.

We quantitatively evaluate the mean computational time of L-SS and E-SS (Fig. 5.15). In this evaluation, we use the same simulation parameters as used in Figs. 5.12 and 5.13. We can confirm the mean computational time of L-SS is lower than that of E-SS.

5.6.3 Adaptivity of FFT size selection with time

Finally, we observe the behavior of L-SS and E-SS in case that SNR is varied in time. Changes of spectrum occupancy state and SNR are summarized in Table 5.2.

Figure 5.16 shows ED results in time and frequency domains of L-SS (Fig. 5.16 (a)) and E-SS (Fig. 5.16 (b)), respectively. The spectrum occupancy state and SNR are

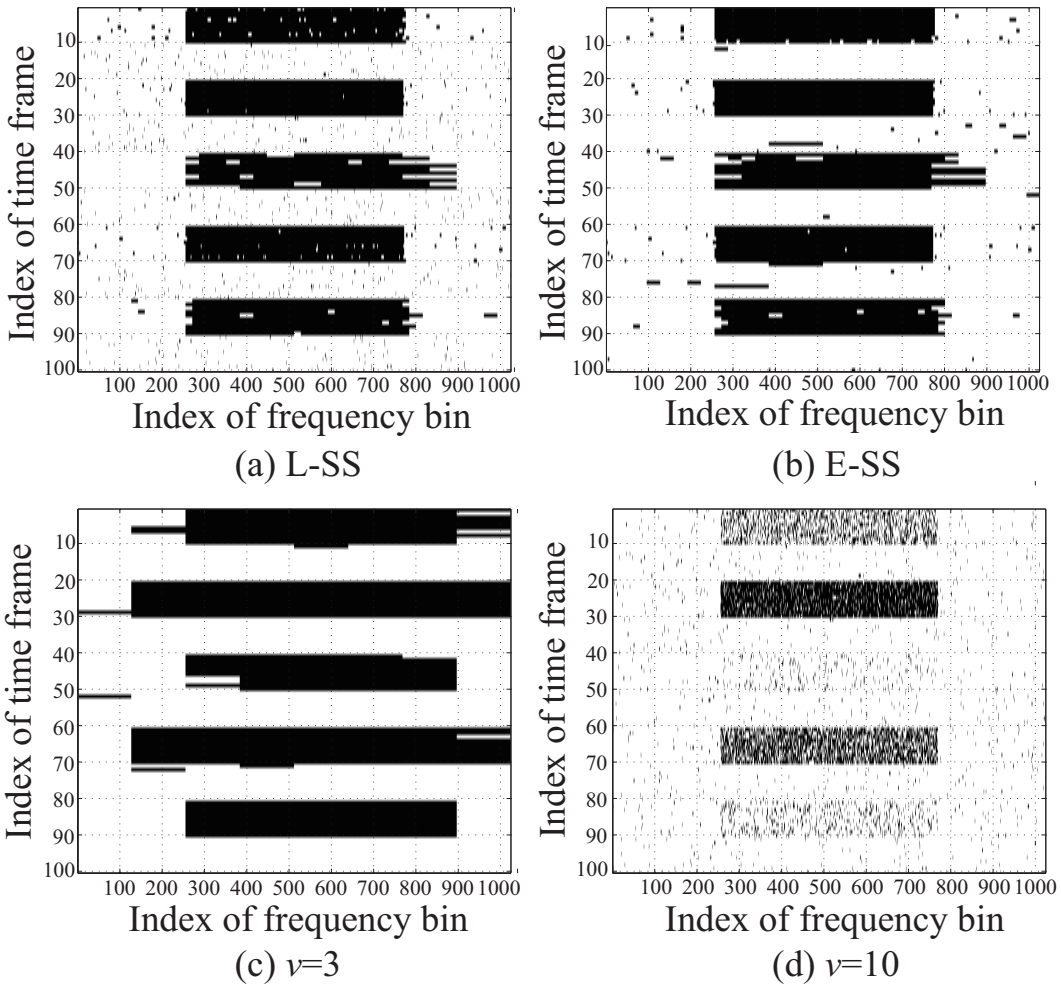

Fig. 5.16: ED detection results against time frames and frequency bins, (a) L-SS, (b) E-SS, (c) $v = 3$, (d) $v = 10$.

changed in time in Fig. 5.16 and the changes are shown in Table 5.2. For comparison, the results of $v = 3$ and $v = 10$ where segment sizes $N_{\text{seg},v} = 2^3$ and $N_{\text{seg},v} = 2^{10}$ are used during the whole observation, respectively are also shown. The PU signal exists between $f = 260$ to $f = 770$, where f is the index number of frequency bin.

In case of $v = 3$ (Fig. 5.16 (c)), the probability of detection is high at the expense of less frequency resolution. This leads to overestimation in terms of the signal bandwidth. In contrast to the case of $v = 3$, high frequency resolution is achieved but detection performance is poor in case of $v = 10$ (Fig. 5.16 (d)).

On the other hand, we can see both L-SS and E-SS can achieve enough detection

performance and this indicates both methods can adaptively select a proper FFT size, and detection performance of L-SS and E-SS are comparable in the results of Fig. 5.16 (a) and (b). One difference is frequency resolution: bandwidth of false alarm in L-SS is less than that in E-SS. This indicates that the selected FFT size for E-SS is smaller than that for L-SS. To verify this fact, Figs. 5.17 and 5.18 show the index number of FFT size selected by L-SS and E-SS, respectively. The optimum segment sizes are also plotted by dashed lines in Figs. 5.17 and 5.18. In Figs. 5.17 and 5.18, the spectrum occupancy state and SNR are changed in time as shown in Table 5.2. From these figures, both methods can select the FFT size around the optimum FFT size, but E-SS selects the smaller FFT size than that L-SS selects, especially in high SNR, i.e., SNR = 15dB. In both results, we can confirm a biased aspect. Specifically, at a certain time frame, selected segment may be higher (or lower) than the optimum one. The reason of this aspect is that the threshold, τ (L-SS) and β (E-SS) to select a FFT size is constant for whole SNR. In fact, the proper τ and β slightly depend on SNR. One important fact is that the maximum error of the FFT size selections is one at most. The error is given by the difference between index number of the optimum FFT size and index number of FFT size selected by L-SS/E-SS.

5.7 Chapter Summary

In this chapter, we investigated FFT size setting in FFT-based wide band spectrum measurement. We aimed to estimate the DC and the WS accurately via Welch FFT-based ED as it is important for spectrum measurement to provide accurate statistical information, e.g., DC to SUs. In Welch FFT-based ED, time resolution, frequency resolution and spectrum usage detection performance determine the WS detection performance in the time and frequency domains. The optimum FFT size regarding White Space Detection Ratio (WSDR) with the constraint on RMSE in terms of DC depends on the SNR which is an unknown parameter in practice as shown in previous chapter. Therefore, we proposed a FFT size selection method denoted by Exhaustive search based FFT Size Selection (E-SS) to select a proper FFT size without SNR information, but this method requires relatively high computational complexity. For this issue,

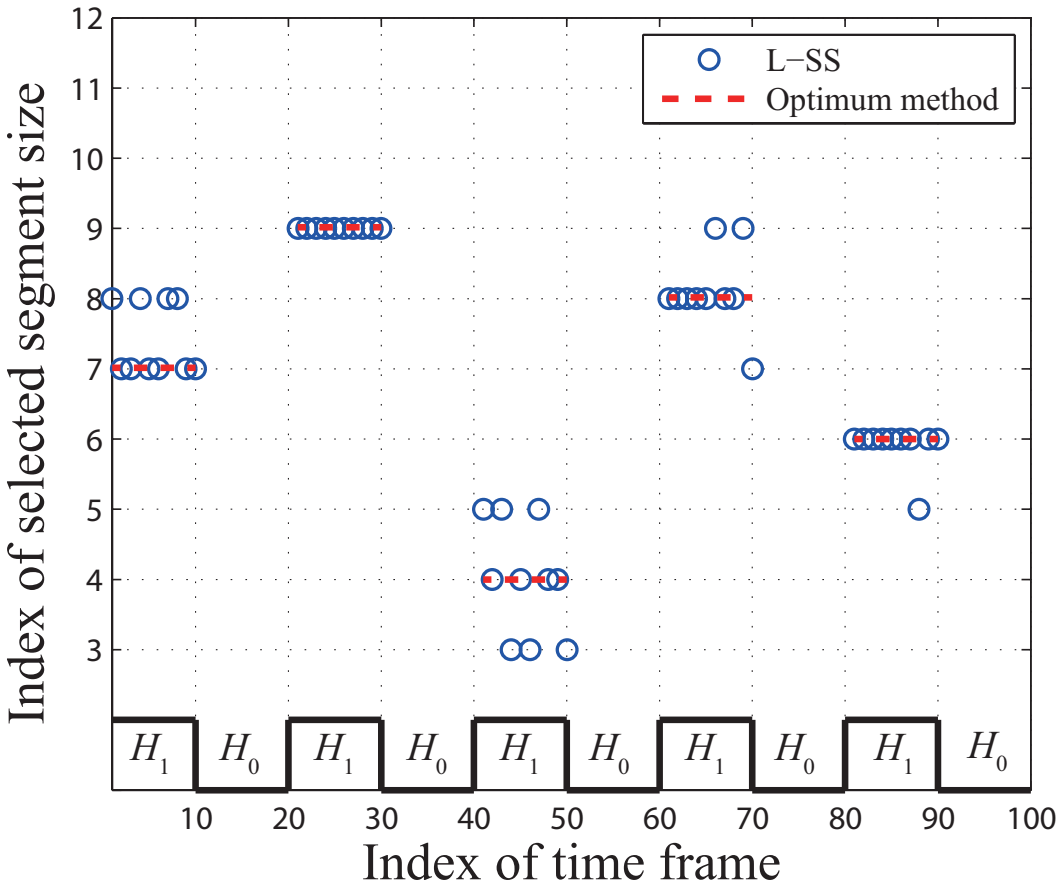

Fig. 5.17: Index number of selected FFT size for L-SS against time frames.

we proposed Limited search based FFT Size Selection (L-SS), which attempts to select the proper FFT size with high-computational efficiency. Numerical evaluations showed that L-SS can match the performance of E-SS in terms of MAE of WSDR, i.e., $|1 - \mathrm{WSDR}(v)|$ with sufficient DC estimation accuracy. On the other hand, we showed L-SS has much lower computational complexity than E-SS.

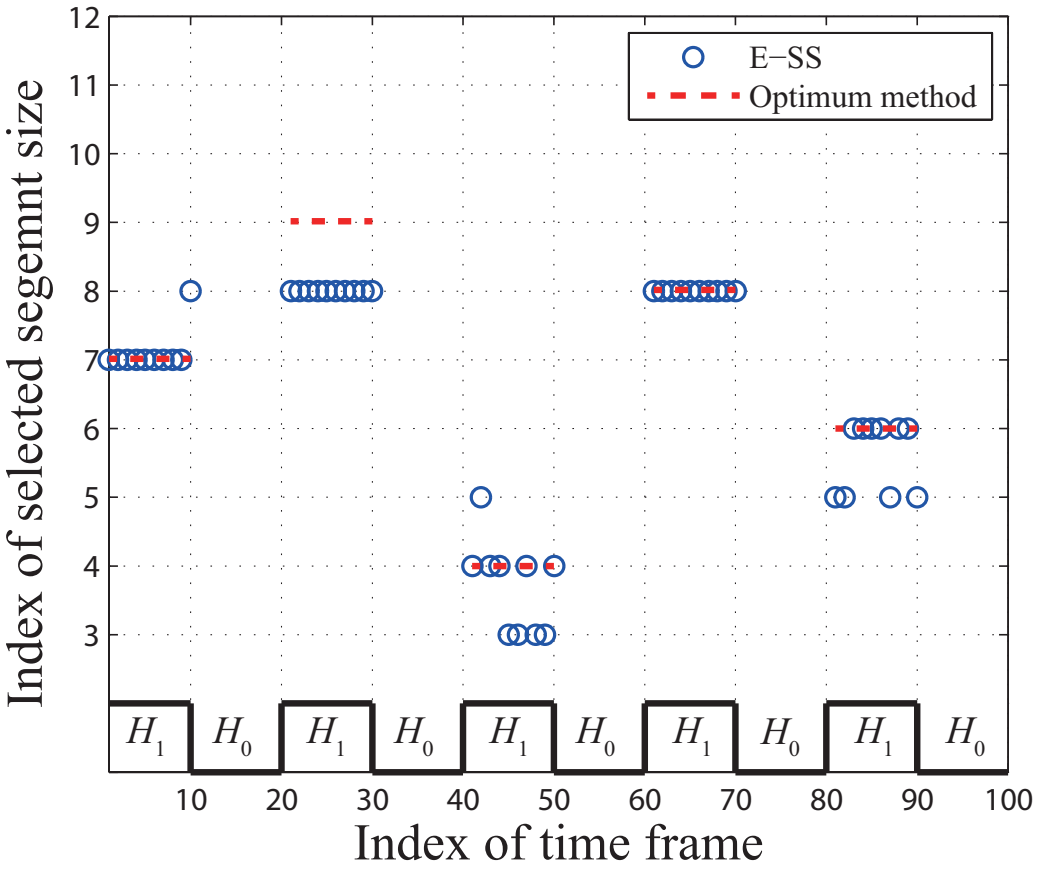

Fig. 5.18: Index number of selected FFT size for E-SS against time frames.

Chapter

6

Conclusions and Future Directions

This chapter concludes our research works on highly efficient spectrum sharing. First, we summarize the conclusion and contribution of each chapter. After that, the potential future research directions are discussed.

6.1 Conclusions

For realizing smart spectrum sharing (smart spectrum access), accurate spectrum measurements are required. To this end, we have comprehensively investigated the wideband spectrum measurement based on FFT-based ED from the viewpoint of time and frequency resolutions as well as detection performance Conclusions and contributions of this thesis are summarized below.

Chapter 1: This chapter provided the spectrum scarcity problem and its countermeasures. Especially, we focused on spectrum sharing or dynamic spectrum access and its broad models and its limitation are given. After that smart spectrum access concept is introduced for solving the issues of DSA. And then, we have mentioned the importance of accurate spectrum measurements and the motivation in this thesis. Finally, we have shown our contributions and the outline in this thesis.

Chapter 2: This chapter surveyed several spectrum measurement campaigns. Especially, we have mentioned the extracted statistics from the measurement campaigns and their weak points. From the surveys, we have verified most of the measurement campaigns exploit energy detection and do deeply not consider the detection performance, time and frequency resolutions setting problem.

Chapter 3: In this chapter, we described the spectrum measurement system in smart spectrum access. Specifically, we have shown a spectrum measurement prototype system we developed. And then, we focused on one spectrum sensor in the measurement system and introduced a basic model for spectrum measurement in the sensor.

Chapter 4: In Chapter 4, We define the optimum FFT size as the one that allows the accurate detection of the spectrum occupancy in time and frequency domains while maintaining target DC estimation accuracy and a small enough target false alarm rate. The DC estimation accuracy is quantified in terms of its root mean squared error (RMSE), which is related to signal detection performance without considering the frequency resolution. On the other hand, the detection accuracy of the spectrum occupancy in time and frequency domains is quantified by means of the white space detection ratio (WSDR), defined as the ratio of true WS to estimated WS, which also includes the effect of the frequency resolution. Furthermore, we also define a sub-optimum FFT size which is obtained analytically. The analysis reveals that the FFT size depends on SNR and DC. This indicates that FFT size selection is challenging problem since prior knowledge of SNR and DC is

impractical. Finally, extensive numerical results demonstrate that the optimum FFT size can achieve optimum WSDR performance while satisfying the RMSE constraint if SNR value is known.

Chapter 5: In this chapter, we at first reveal the noise floor estimate by FCME algorithm depends on FFT size and SNR. Thus, we verified the NF estimate which can be easily obtained in a spectrum sensor makes proper FFT size setting practical. After that, we have proposed two practical FFT size setting methods: Exhaustive-search FFT Size Setting (E-SS) method and Limited search FFT Size Setting (L-SS) method. Both methods exploit a relationship between output of NF estimation based on FCME algorithm and the FFT size for proper FFT size setting. E-SS uses NF estimation outputs for all possible segment sizes in Welch FFT, therefore it can achieve high WSDR performance but requires relatively high computational complexity. On the other hand, L-SS searches the proper FFT size while limiting the searchable FFT sizes. This limiting leads to low computational complexity in terms of FFT size setting. Finally, extensive numerical results show that E-SS and L-SS has comparable performances in terms of RMSE of DC estimate and WSDR, while computational complexity of L-SS has sufficiently lower than that of E-SS.

6.2 Future Directions

This thesis mainly aims to improve the accuracy of FFT-based spectrum measurement in only single spectrum sensor in spectrum measurement system. On the other hand, there still exist lots of research scopes for future works. At the end of this thesis, we briefly discuss the remaining and potential future works.

Extending to Multidimensional Spectrum Measurement In this thesis, we have investigated relatively long-term and wideband spectrum measurement for smart spectrum access. However, there are remaining several measurement dimensions not handled in this thesis such as geographic locations, angle, code dimensions. As for geographic location dimension, many spectrum sensors should

be installed over a large observed area of interest. This leads to several issues such as development of cost-efficient spectrum measurement system, sensor scheduling problem, measured data collection problem, to name a few. In terms of the aspect of cost, simple ideas are to install low cost but low measurement capability spectrum sensors such as smart phone and tablet terminal or rely on the power of crowd, i,e., crowd sensing. It is interesting for our to understand the power of the crowd sensing. In terms of sensor scheduling, mapping the measurement pattern in the time and frequency domains into each spectrum sensor is one of most difficult but important issues. In this mapping, we should consider several aspects such as measurement accuracy, fairness between spectrum sensors and the capability of each sensor. Finally, in terms of measured data collection, we should seek efficient data collection strategies. This problem would more difficult when the increase of the number of spectrum sensors and/or the increase of the amount of measured data each sensor sends to fusion center,

Intelligent Spectrum Measurement System In this direction, several technologies will be considered such as artificial intelligence (AI) technology and machine learning technology. Especially, deep learning or deep neural network is one of the interesting topic for intelligent spectrum measurement system because of the recent success of the deep learning over several fields. Furthermore, we expect (deep) reinforcement learning such as Q-learning is a promising approach to realizing the intelligence of spectrum measurement system. This type of learning can grow up based on own experiences and automatically go in the proper or right directions. This leads to reducing the management cost and complexity, but the selection of objects we want to achieve in the learning is a difficult problem.

Which statistical information are useful? Finally but not all, we must consider which statistical information are useful for smart spectrum access. This topic is very important but does not deeply to data. The gain bringing any statistical information changes depending on adopted spectrum sharing model. To this end, it may be beneficial to construct spectrum sharing models mathematically by a

means of for example deep neural network. Though these models, we can analyze the gain of each statistical information analytically.

References

[1] "Cisco visual networking index: Global mobile data traffic forecast update, 2016-2021," https://www.cisco.com/c/en/us/solutions/collateral/service-provider/visual-networking-index-vni/mobile-white-paper-c11-520862.pdf, accessed: 2018-11-18.

[2] "Us frequency allocation chart," https://www.ntia.doc.gov/files/ntia/publications/2003-allochrt.pdf, accessed: 2018-11-18.

[3] I. F. Akyildiz, W.-Y. Lee, M. C. Vuran, and S. Mohanty, "NeXt generation/dynamic spectrum access/cognitive radio wireless networks: A survey," *Computer Networks*, vol. 50, no. 13, pp. 2127–2159, Sep 2006.

[4] J. Abdoli, M. Jia, and J. Ma, "Filtered OFDM: A new waveform for future wireless systems," in *2015 IEEE 16th International Workshop on Signal Processing Advances in Wireless Communications (SPAWC)*. Stockholm, Sweden: IEEE, Jun 2015, pp. 66–70.

[5] M. Shafi, A. F. Molisch, P. J. Smith, T. Haustein, P. Zhu, P. D. Silva, F. Tufvesson, A. Benjebbour, and G. Wunder, "5g: A Tutorial Overview of Standards, Trials, Challenges, Deployment, and Practice," *IEEE Journal on Selected Areas in Communications*, vol. 35, no. 6, pp. 1201–1221, Jun 2017.

[6] J. G. Andrews, S. Buzzi, W. Choi, S. V. Hanly, A. Lozano, A. C. K. Soong, and J. C. Zhang, "What Will 5g Be?" *IEEE Journal on Selected Areas in Communications*, vol. 32, no. 6, pp. 1065–1082, Jun 2014.

[7] B. Farhang-Boroujeny, "OFDM Versus Filter Bank Multicarrier," *IEEE Signal Processing Magazine*, vol. 28, no. 3, pp. 92–112, May 2011.

[8] P. Banelli, S. Buzzi, G. Colavolpe, A. Modenini, F. Rusek, and A. Ugolini, "Modulation Formats and Waveforms for 5g Networks: Who Will Be the Heir of OFDM?: An overview of alternative modulation schemes for improved spectral efficiency," *IEEE Signal Processing Magazine*, vol. 31, no. 6, pp. 80–93, Nov 2014.

[9] R. Y. Mesleh, H. Haas, S. Sinanovic, C. W. Ahn, and S. Yun, "Spatial Modulation," *IEEE Transactions on Vehicular Technology*, vol. 57, no. 4, pp. 2228–2241, Jul 2008.

[10] J. Jeganathan, A. Ghrayeb, and L. Szczecinski, "Spatial modulation: optimal detection and performance analysis," *IEEE Communications Letters*, vol. 12, no. 8, pp. 545–547, Aug 2008.

[11] M. D. Renzo, H. Haas, A. Ghrayeb, S. Sugiura, and L. Hanzo, "Spatial Modulation for Generalized MIMO: Challenges, Opportunities, and Implementation," *Proceedings of the IEEE*, vol. 102, no. 1, pp. 56–103, Jan 2014.

[12] D. Bharadia, E. McMilin, and S. Katti, "Full duplex radios," p. 12.

[13] A. Sabharwal, P. Schniter, D. Guo, D. W. Bliss, S. Rangarajan, and R. Wichman, "In-Band Full-Duplex Wireless: Challenges and Opportunities," *IEEE Journal on Selected Areas in Communications*, vol. 32, no. 9, pp. 1637–1652, Sep 2014.

[14] A. Gupta and R. K. Jha, "A Survey of 5g Network: Architecture and Emerging Technologies," *IEEE Access*, vol. 3, pp. 1206–1232, 2015.

[15] Z. Ding, Z. Yang, P. Fan, and H. V. Poor, "On the Performance of Non-Orthogonal Multiple Access in 5g Systems with Randomly Deployed Users," *IEEE Signal Processing Letters*, vol. 21, no. 12, pp. 1501–1505, Dec 2014.

[16] Z. Ding, M. Peng, and H. V. Poor, "Cooperative Non-Orthogonal Multiple Access in 5g Systems," *IEEE Communications Letters*, vol. 19, no. 8, pp. 1462–1465, Aug 2015.

[17] L. Dai, B. Wang, Y. Yuan, S. Han, C. I, and Z. Wang, "Non-orthogonal multiple access for 5g: solutions, challenges, opportunities, and future research trends,"

IEEE Communications Magazine, vol. 53, no. 9, pp. 74–81, Sep 2015.

[18] E. Paolini, G. Liva, and M. Chiani, "Coded Slotted ALOHA: A Graph-Based Method for Uncoordinated Multiple Access," *IEEE Transactions on Information Theory*, vol. 61, no. 12, pp. 6815–6832, Dec 2015.

[19] A. Gupta and R. K. Jha, "Error Floor Analysis of Coded Slotted ALOHA Over Packet Erasure Channels," *IEEE Communications Letters*, vol. 19, no. 3, pp. 419–422, Mar 2015.

[20] E. Arikan, "Channel Polarization: A Method for Constructing Capacity-Achieving Codes for Symmetric Binary-Input Memoryless Channels," *IEEE Transactions on Information Theory*, vol. 55, no. 7, pp. 3051–3073, Jul 2009.

[21] I. Tal and A. Vardy, "How to Construct Polar Codes," *IEEE Transactions on Information Theory*, vol. 59, no. 10, pp. 6562–6582, Oct 2013.

[22] Q. Zhao and B. M. Sadler, "A Survey of Dynamic Spectrum Access," *IEEE Signal Processing Magazine*, vol. 24, no. 3, pp. 79–89, May 2007.

[23] J. Peha, "Sharing Spectrum Through Spectrum Policy Reform and Cognitive Radio," *Proceedings of the IEEE*, vol. 97, no. 4, pp. 708–719, Apr 2009.

[24] A. Goldsmith, S. Jafar, I. Maric, and S. Srinivasa, "Breaking Spectrum Gridlock With Cognitive Radios: An Information Theoretic Perspective," *Proceedings of the IEEE*, vol. 97, no. 5, pp. 894–914, May 2009.

[25] M. Lopez-Benitez and F. Casadevall, "Empirical time-dimension model of spectrum use based on a discrete-time markov chain with deterministic and stochastic duty cycle models," *IEEE Trans. on Veh. Technol.*, vol. 60, no. 6, pp. 2519–2533, July 2011.

[26] D. Hatfield and P. Weiser, "Property rights in spectrum: taking the next step," in *First IEEE International Symposium on New Frontiers in Dynamic Spectrum Access Networks, 2005. DySPAN 2005.* Baltimore, MD, USA: IEEE, 2005, pp. 43–55.

[27] Lin Xu, R. Tonjes, T. Paila, W. Hansmann, M. Frank, and M. Albrecht, "DRiVEing to the Internet: Dynamic Radio for IP services in Vehicular Environments," in *Proceedings 25th Annual IEEE Conference on Local Computer Networks. LCN 2000.* Tampa, FL, USA: IEEE Comput. Soc, 2000, pp. 281–289.

[28] P. Leaves, K. Moessner, R. Tafazolli, D. Grandblaise, D. Bourse, R. Tonjes, and M. Breveglieri, "Dynamic spectrum allocation in composite reconfigurable wireless networks," *IEEE Communications Magazine*, vol. 42, no. 5, pp. 72–81, May 2004.

[29] Y. Benkler, "Overcoming Agoraphobia: Building the Commons of the Digitally Networked Environment," p. 113, 1998.

[30] W. Lehr and J. Crowcroft, "Managing shared access to a spectrum commons," in *First IEEE International Symposium on New Frontiers in Dynamic Spectrum Access Networks, 2005. DySPAN 2005.* Baltimore, MD, USA: IEEE, 2005, pp. 420–444.

[31] S. Haykin, "Cognitive radio: brain-empowered wireless communications," *IEEE Journal on Selected Areas in Communications*, vol. 23, no. 2, pp. 201–220, Feb 2005.

[32] N. Wang, Y. Gao, and X. Zhang, "Adaptive Spectrum Sensing Algorithm Under Different Primary User Utilizations," *IEEE Communications Letters*, vol. 17, no. 9, pp. 1838–1841, Sep 2013.

[33] T. Nguyen, B. L. Mark, and Y. Ephraim, "Spectrum Sensing Using a Hidden Bivariate Markov Model," *IEEE Transactions on Wireless Communications*, vol. 12, no. 9, pp. 4582–4591, Sep 2013.

[34] A. Mariani, S. Kandeepan, and A. Giorgetti, "Periodic Spectrum Sensing With Non-Continuous Primary User Transmissions," *IEEE Transactions on Wireless Communications*, vol. 14, no. 3, pp. 1636–1649, Mar 2015.

[35] K. Umebayashi, K. Hayashi, and J. J. Lehtomaki, "Threshold-Setting for Spectrum Sensing Based on Statistical Information," *IEEE Communications Letters*, vol. 21, no. 7, pp. 1585–1588, Jul 2017.

[36] M. Wellens, J. Riihijarvi, and P. Mahonen, "Evaluation of Adaptive MAC-Layer Sensing in Realistic Spectrum Occupancy Scenarios," in *2010 IEEE Symposium on New Frontiers in Dynamic Spectrum (DySPAN)*. Singapore, Singapore: IEEE, Apr 2010, pp. 1–12.

[37] M. Johnston, I. Keslassy, and E. Modiano, "Channel Probing in Opportunistic Communication Systems," *IEEE Transactions on Information Theory*, vol. 63, no. 11, pp. 7535–7552, Nov 2017.

[38] K. Wang, Q. Liu, Q. Fan, and Q. Ai, "Optimally Probing Channel in Opportunistic Spectrum Access," *IEEE Communications Letters*, vol. 22, no. 7, pp. 1426–1429, Jul 2018.

[39] M. Hoyhtya, S. Pollin, and A. Mammela, "Performance improvement with predictive channel selection for cognitive radios," in *2008 First International Workshop on Cognitive Radio and Advanced Spectrum Management*. Aalborg, Denmark: IEEE, Feb 2008, pp. 1–5.

[40] K. Umebayashi, J. Lehtomaki, and Y. Suzuki, "Dynamic selection of CWmin in cognitive radio networks for protecting IEEE 802.11 primary users," in *Proceedings of the 6th International ICST Conference on Cognitive Radio Oriented Wireless Networks and Communications*. Osaka, Japan: IEEE, 2011.

[41] M. Derakhshani and T. Le-Ngoc, "Learning-Based Opportunistic Spectrum Access with Adaptive Hopping Transmission Strategy," *IEEE Transactions on Wireless Communications*, vol. 11, no. 11, pp. 3957–3967, Nov 2012.

[42] Y. Song and J. Xie, "ProSpect: A Proactive Spectrum Handoff Framework for Cognitive Radio Ad Hoc Networks without Common Control Channel," *IEEE Transactions on Mobile Computing*, vol. 11, no. 7, pp. 1127–1139, Jul 2012.

[43] Y. Xu, A. Anpalagan, Q. Wu, L. Shen, Z. Gao, and J. Wang, "Decision-Theoretic Distributed Channel Selection for Opportunistic Spectrum Access: Strategies, Challenges and Solutions," *IEEE Communications Surveys Tutorials*, vol. 15, no. 4, pp. 1689–1713, 2013.

[44] C. N. Devanarayana and A. S. Alfa, "Proactive channel access in cognitive radio networks using statistical radio environment maps," *EURASIP Journal on Wireless Communications and Networking*, vol. 2015, no. 1, Dec 2015.

[45] A. Agarwal, S. Dubey, R. Gangopadhyay, and S. Debnath, "Secondary User QoE Enhancement Through Learning Based Predictive Spectrum Access in Cognitive Radio Networks," in *Cognitive Radio Oriented Wireless Networks*, D. Noguet, K. Moessner, and J. Palicot, Eds. Cham: Springer International Publishing, 2016, vol. 172, pp. 166–178.

[46] A. Oluwaranti and S. Okegbile, "Two state Markov chain based predictive model for cognitive Radio spectrum availability: A conceptual approach," in *2016 Future Technologies Conference (FTC)*. San Francisco, CA, USA: IEEE, Dec 2016, pp. 179–186.

[47] R. Murty, R. Chandra, T. Moscibroda, and P. Bahl, "SenseLess: A Database-Driven White Spaces Network," *IEEE Transactions on Mobile Computing*, vol. 11, no. 2, pp. 189–203, Feb 2012.

[48] I. Hanif, M. Zeeshan, and A. Ahmed, "Traffic Pattern Based Adaptive Spectrum Handoff Strategy for Cognitive Radio Networks," in *2016 10th International Conference on Next Generation Mobile Applications, Security and Technologies (NGMAST)*. Cardiff, United Kingdom: IEEE, Aug 2016, pp. 18–23.

[49] R. Matheson, "Strategies for spectrum usage measurements," in *IEEE 1988 International Symposium on Electromagnetic Compatibility.* Seattle, WA, USA: IEEE, 1988, pp. 235–241.

[50] P. Vaccani, "Occupancy measurement methods in the radio frequency spectrum

and their use," in *IEEE 1988 International Symposium on Electromagnetic Compatibility.* Seattle, WA, USA: IEEE, 1988, pp. 242–246.

[51] A. Gibson, "Measurements and statistical modelling of spectrum occupancy," in *Sixth International Conference on HF Radio Systems and Techniques*, vol. 1994. York, UK: IEEE, 1994, pp. 150–154.

[52] G. Gott, "HF spectral occupancy measurements in Europe," in *IEE Colloquium on Frequency Selection and Management Techniques for HF Communications*, vol. 1996. London, UK: IEE, 1996, pp. 6–6.

[53] D. Percival, "A Markov model for HF spectral occupancy in central Australia," in *7th International Conference on High Frequency Radio Systems and Techniques*, vol. 1997. Nottingham, UK: IEE, 1997, pp. 14–18.

[54] F. Sanders, "Broadband spectrum surveys in Denver, CO, San Diego, CA, and Los Angeles, CA: methodology, analysis, and comparative results," in *1998 IEEE EMC Symposium. International Symposium on Electromagnetic Compatibility. Symposium Record (Cat. No.98CH36253)*, vol. 2. Denver, CO, USA: IEEE, 1998, pp. 988–993.

[55] M. A. McHenry, P. A. Tenhula, D. McCloskey, D. A. Roberson, and C. S. Hood, "Chicago spectrum occupancy measurements & analysis and a long-term studies proposal," in *Proceedings of the first international workshop on Technology and policy for accessing spectrum - TAPAS '06.* Boston, Massachusetts: ACM Press, 2006, pp. 1–es.

[56] M. Wellens, J. Wu, and P. Mahonen, "Evaluation of Spectrum Occupancy in Indoor and Outdoor Scenario in the Context of Cognitive Radio," in *2007 2nd International Conference on Cognitive Radio Oriented Wireless Networks and Communications.* Orlando, FL, USA: IEEE, Aug 2007, pp. 420–427.

[57] R. I. C. Chiang, G. B. Rowe, and K. W. Sowerby, "A Quantitative Analysis of Spectral Occupancy Measurements for Cognitive Radio," in *2007 IEEE 65th*

Vehicular Technology Conference - VTC2007-Spring. Dublin, Ireland: IEEE, Apr 2007, pp. 3016–3020.

[58] M. H. Islam, C. L. Koh, S. W. Oh, X. Qing, Y. Y. Lai, C. Wang, Y.-C. Liang, B. E. Toh, F. Chin, G. L. Tan, and W. Toh, "Spectrum Survey in Singapore: Occupancy Measurements and Analyses," in *2008 3rd International Conference on Cognitive Radio Oriented Wireless Networks and Communications (CrownCom 2008).* Singapore: IEEE, May 2008, pp. 1–7.

[59] M. Lopez-Benitez, A. Umbert, and F. Casadevall, "Evaluation of Spectrum Occupancy in Spain for Cognitive Radio Applications," in *VTC Spring 2009 - IEEE 69th Vehicular Technology Conference.* Barcelona, Spain: IEEE, Apr 2009, pp. 1–5.

[60] D. Miao, Z. Feng, H. Cai, and Y. Yao, "An Adaptive Threshold Method for Data Processing in Spectrum Occupancy Measurements," in *2009 IEEE 70th Vehicular Technology Conference Fall.* Anchorage, AK, USA: IEEE, Sep 2009, pp. 1–5.

[61] S. Pagadarai and A. M. Wyglinski, "A quantitative assessment of wireless spectrum measurements for dynamic spectrum access," in *2009 4th International Conference on Cognitive Radio Oriented Wireless Networks and Communications.* Hanover, Germany: IEEE, Jun 2009, pp. 1–5.

[62] K. A. Qaraqe, H. Celebi, A. Gorcin, A. El-Saigh, H. Arslan, and M.-s. Alouini, "Empirical results for wideband multidimensional spectrum usage," in *2009 IEEE 20th International Symposium on Personal, Indoor and Mobile Radio Communications.* Toyko, Japan: IEEE, Sep 2009, pp. 1262–1266.

[63] V. Valenta, Z. Fedra, R. Marsalek, G. Baudoin, and M. Villegas, "Towards cognitive radio networks: Spectrum utilization measurements in suburb environment," in *2009 IEEE Radio and Wireless Symposium.* San Diego, CA, USA: IEEE, Jan 2009, pp. 352–355.

[64] M. Wellens, J. Riih, and P. AA, "Empirical time and frequency domain models of spectrum use," *Physical Communication*, vol. 2, no. 1-2, pp. 10–32, Mar 2009.

[65] C. Ghosh, S. Pagadarai, D. P. Agrawal, and A. M. Wyglinski, "Queueing Theory Representation and Modeling of Spectrum Occupancy Employing Radio Frequency Measurements," in *2009 IEEE 70th Vehicular Technology Conference Fall*. Anchorage, AK, USA: IEEE, Sep 2009, pp. 1–5.

[66] A. Martian, I. Marcu, and I. Marghescu, "Spectrum Occupancy in an Urban Environment: A Cognitive Radio Approach," in *2010 Sixth Advanced International Conference on Telecommunications*. Barcelona, Spain: IEEE, 2010, pp. 25–29.

[67] M. Matinmikko, M. Mustonen, M. Hoyhtya, T. Rauma, H. Sarvanko, and A. Mammela, "Cooperative spectrum occupancy measurements in the 2.4 GHz ISM band," in *2010 3rd International Symposium on Applied Sciences in Biomedical and Communication Technologies (ISABEL 2010)*. Roma, Italy: IEEE, Nov 2010, pp. 1–5.

[68] ——, "Distributed and directional spectrum occupancy measurements in the 2.4 GHz ISM band," in *2010 7th International Symposium on Wireless Communication Systems*. York, United Kingdom: IEEE, Sep 2010, pp. 676–980.

[69] R. Schiphorst and C. H. Slump, "Evaluation of Spectrum Occupancy in Amsterdam Using Mobile Monitoring Vehicles," in *2010 IEEE 71st Vehicular Technology Conference*. Taipei, Taiwan: IEEE, 2010, pp. 1–5.

[70] Y. H. Y. Wen, W. Tang, and S. Li, "Spectrum Occupancy Measurement:Focus on the TV Frequency," *nd International Conference on Signal Processing Systems*, p. 5, 2010.

[71] M. Lopez-Benitez, "Spectrum Occupancy in Realistic Scenarios and Duty Cycle Model for Cognitive Radio," vol. 1, no. 1, p. 9, 2010.

[72] C. Ghosh, S. Pagadarai, D. Agrawal, and A. Wyglinski, "A framework for statistical wireless spectrum occupancy modeling," *IEEE Transactions on Wireless Communications*, vol. 9, no. 1, pp. 38–44, Jan 2010.

[73] R. Bacchus, T. Taher, K. Zdunek, and D. Roberson, "Spectrum utilization study

in support of dynamic spectrum access for public safety," in *Proc. DySPAN*. IEEE, Apr. 2010, pp. 1–11.

[74] L. Mendes, L. Goncalves, and A. Gameiro, "GSM downlink spectrum occupancy modeling," in *2011 IEEE 22nd International Symposium on Personal, Indoor and Mobile Radio Communications*. Toronto, ON, Canada: IEEE, Sep 2011, pp. 546–550.

[75] K. Patil, R. Prasad, and K. Skouby, "A Survey of Worldwide Spectrum Occupancy Measurement Campaigns for Cognitive Radio," in *2011 International Conference on Devices and Communications (ICDeCom)*. Mesra, Ranchi, India: IEEE, Feb 2011, pp. 1–5.

[76] K. A. Qaraqe, N. Rahimian, H. Celebi, and C. N. Georghiades, "Spatio-temporal measurement and model for number of occupied channels," in *2011 18th International Conference on Telecommunications*. Ayia Napa, Cyprus: IEEE, May 2011, pp. 33–37.

[77] T. M. Taher, R. B. Bacchus, K. J. Zdunek, and D. A. Roberson, "Long-term spectral occupancy findings in Chicago," in *2011 IEEE International Symposium on Dynamic Spectrum Access Networks (DySPAN)*. Aachen, Germany: IEEE, May 2011, pp. 100–107.

[78] N. Q. B. Vo, Q. C. Le, Q. P. Le, D. T. Tran, T. Q. Nguyen, and M. T. Lam, "Vietnam spectrum occupancy measurements and analysis for cognitive radio applications," in *The 2011 International Conference on Advanced Technologies for Communications (ATC 2011)*. Da Nang, Vietnam: IEEE, Aug 2011, pp. 135–143.

[79] G. Noorts, J. Engel, J. Taylor, D. Roberson, R. Bacchus, T. Taher, and K. Zdunek, "An RF spectrum observatory database based on a Hybrid Storage System," in *2012 IEEE International Symposium on Dynamic Spectrum Access Networks*. Bellevue, WA, USA: IEEE, Oct 2012, pp. 114–120.

[80] S. Rocke and A. M. Wyglinski, "Estimation of spectrum occupancy in heterogeneous radio access environments using random spectral sampling," in *2012 35th IEEE Sarnoff Symposium*. Newark, NJ, USA: IEEE, May 2012, pp. 1–6.

[81] Sixing Yin, Dawei Chen, Qian Zhang, Mingyan Liu, and Shufang Li, "Mining Spectrum Usage Data: A Large-Scale Spectrum Measurement Study," *IEEE Transactions on Mobile Computing*, vol. 11, no. 6, pp. 1033–1046, Jun 2012.

[82] D. Chen, J. Yang, J. Wu, H. Tang, and M. Huang, "Spectrum occupancy analysis based on radio monitoring network," in *2012 1st IEEE International Conference on Communications in China (ICCC)*. Beijing, China: IEEE, Aug 2012, pp. 739–744.

[83] M. Kamarudin, M. Dzulkifli, and T. Rahman, "Spectrum occupancy of Malaysia radio environment for cognitive radio application," in *IET International Conference on Wireless Communications and Applications (ICWCA 2012)*. Kuala Lumpur, Malaysia: Institution of Engineering and Technology, 2012, pp. 022–022.

[84] J. Kokkoniemi and J. Lehtomaeki, "Spectrum Occupancy Measurements and Analysis Methods on the 2.45 GHz ISM Band," in *Proceedings of the 7th International Conference on Cognitive Radio Oriented Wireless Networks*. Stockholm, Sweden: IEEE, 2012.

[85] V. Kone, L. Yang, X. Yang, B. Y. Zhao, and H. Zheng, "The Effectiveness of Opportunistic Spectrum Access: A Measurement Study," *IEEE/ACM Transactions on Networking*, vol. 20, no. 6, pp. 2005–2016, Dec 2012.

[86] M. Mehdawi, N. Riley, M. Ammar, and M. Zolfaghari, "Comparing historical and current spectrum occupancy measurements in the context of cognitive radio," in *2012 20th Telecommunications Forum (TELFOR)*. Belgrade, Serbia: IEEE, Nov 2012, pp. 623–626.

[87] A. Palaios, J. Riihijarvi, P. Mahonen, V. Atanasovski, L. Gavrilovska, P. Van Wesemael, A. Dejonghe, and P. Scheele, "Two days of European spectrum: Preliminary analysis of concurrent spectrum use in seven European sites in GSM and

ISM bands," in *2013 IEEE International Conference on Communications (ICC)*. Budapest, Hungary: IEEE, Jun 2013, pp. 2666–2671.

[88] A. Palaios, J. Riihijarvi, O. Holland, and P. Mahonen, "A week in London: Spectrum usage in metropolitan London," in *2013 IEEE 24th Annual International Symposium on Personal, Indoor, and Mobile Radio Communications (PIMRC)*. London: IEEE, Sep 2013, pp. 2522–2527.

[89] K. Patil, S. Barge, K. Skouby, and R. Prasad, "Evaluation of spectrum usage for GSM band in indoor and outdoor scenario for Dynamic Spectrum Access," in *2013 International Conference on Advances in Computing, Communications and Informatics (ICACCI)*. Mysore: IEEE, Aug 2013, pp. 655–660.

[90] L. F. Pedraza, F. Forero, and I. Paez, "Metropolitan Spectrum Survey in Bogota Colombia," in *2013 27th International Conference on Advanced Information Networking and Applications Workshops*. Barcelona: IEEE, Mar 2013, pp. 548–553.

[91] L. F. Pedraza, A. Molina, and I. Paez, "Spectrum occupancy statistics in Bogota-Colombia," in *2013 IEEE Colombian Conference on Communications and Computing (COLCOM)*. Medell n , Colombia: IEEE, May 2013, pp. 1–6.

[92] J. Xue, Z. Feng, and K. Chen, "Beijing Spectrum Survey for Cognitive Radio Applications," in *2013 IEEE 78th Vehicular Technology Conference (VTC Fall)*. Las Vegas, NV, USA: IEEE, Sep 2013, pp. 1–5.

[93] K.-L. A. Yau, A. Azizan, H. Mohamad, W. Hashim, N. Ramli, and H. J. Lee, "Cognitive radio activities in Malaysia: Spectrum utilization and open issues," in *2013 IEEE 11th Malaysia International Conference on Communications (MICC)*. Kuala Lumpur, Malaysia: IEEE, Nov 2013, pp. 51–56.

[94] R. Aguilar-Gonzalez, M. Cardenas-Juarez, U. Pineda-Rico, and E. Stevens-Navarro, "Spectrum Occupancy Measurements below 1 GHz in the City of San Luis Potosi, Mexico," in *2013 IEEE 78th Vehicular Technology Conference (VTC Fall)*. Las Vegas, NV, USA: IEEE, Sep 2013, pp. 1–5.

[95] S. Barnes, P. Jansen van Vuuren, and B. Maharaj, "Spectrum occupancy investigation: Measurements in South Africa," *Measurement*, vol. 46, no. 9, pp. 3098–3112, Nov 2013.

[96] C. Hammerschmidt and H. Ottke, "Spectrum occupancy results from several surveys," in *2013 IEEE International Symposium on Electromagnetic Compatibility.* Denver, CO, USA: IEEE, Aug 2013, pp. 76–81.

[97] M. Hoyhtya, J. Lehtomaki, J. Kokkoniemi, M. Matinmikko, and A. Mammela, "Measurements and analysis of spectrum occupancy with several bandwidths," in *2013 IEEE International Conference on Communications (ICC).* Budapest, Hungary: IEEE, Jun 2013, pp. 4682–4686.

[98] A. H. Jaber, N. M. Aripin, and N. Salaim, "Evaluation of spectrum occupancy in Kuala Lumpur of UHF TV band for cognitive radio applications," in *2013 IEEE Student Conference on Research and Developement.* Putrajaya, Malaysia: IEEE, Dec 2013, pp. 491–494.

[99] G. M. Kagarura, D. K. Okello, and R. N. Akol, "Evaluation of Spectrum Occupancy: A Case for Cognitive Radio in Uganda," in *2013 IEEE 9th International Conference on Mobile Ad-hoc and Sensor Networks.* Dalian, China: IEEE, Dec 2013, pp. 167–174.

[100] P. Kumar, N. Rakheja, A. Sarswat, H. Varshney, P. Bhatia, S. R. Goli, V. J. Ribeiro, and M. Sharma, "White space detection and spectrum characterization in urban and rural India," in *2013 IEEE 14th International Symposium on "A World of Wireless, Mobile and Multimedia Networks" (WoWMoM).* Madrid: IEEE, Jun 2013, pp. 1–6.

[101] J. J. Lehtomaki, R. Vuohtoniemi, and K. Umebayashi, "On the Measurement of Duty Cycle and Channel Occupancy Rate," *IEEE Journal on Selected Areas in Communications*, vol. 31, no. 11, pp. 2555–2565, Nov 2013.

[102] M. Lopez-Benitez and F. Casadevall, "Time-Dimension Models of Spectrum Usage for the Analysis, Design, and Simulation of Cognitive Radio Networks," *IEEE*

Transactions on Vehicular Technology, vol. 62, no. 5, pp. 2091–2104, Jun 2013.

[103] M. Mehdawi, N. Riley, K. Paulson, A. Fanan, and M. Ammar, "Spectrum Occupancy Survey In HULL-UK For Cognitive Radio Applications: Measurement & Analysis," vol. 2, no. 4, p. 6, 2013.

[104] S.-M. Qu, Q.-L. Shi, and X. Liu, "Study on Calculation Method of Spectrum Occupancy Threshold Based on Cognitive Radio Access," in *2014 International Conference on Wireless Communication and Sensor Network*. Wuhan, China: IEEE, Dec 2014, pp. 65–71.

[105] T. Taher, R. Attard, A. Riaz, D. Roberson, J. Taylor, K. Zdunek, J. Hallio, R. Ekman, J. Paavola, J. Suutala, J. Roning, M. Matinmikko, M. Hoyhtya, and A. MacKenzie, "Global Spectrum Observatory Network Setup and Initial Findings," in *Proceedings of the 9th International Conference on Cognitive Radio Oriented Wireless Networks*. Oulu, Finland: ICST, 2014.

[106] V. Velisavljevic, B. Allen, and E. Chatziantoniou, "A Statistical Framework for Channel Availability Modelling in the Polarisation Domain," in *IET Colloquium on Antennas, Wireless and Electromagnetics 2014*. London, UK: Institution of Engineering and Technology, 2014, pp. 9–9.

[107] T. Zhang, N. Leng, and S. Banerjee, "A vehicle-based measurement framework for enhancing whitespace spectrum databases," in *Proceedings of the 20th annual international conference on Mobile computing and networking - MobiCom '14*. Maui, Hawaii, USA: ACM Press, 2014, pp. 17–28.

[108] P. Balina, K. Garg, and S. V. R. K. Rao, "Spectrum occupancy measurements and analysis in a rural area setting," in *2014 International Conference on Parallel, Distributed and Grid Computing*. Solan, India: IEEE, Dec 2014, pp. 412–416.

[109] A. A. Cheema and S. Salous, "High resolution temporal occupancy measurements to characterize idle time window in ISM band," in *2014 XXXIth URSI General Assembly and Scientific Symposium (URSI GASS)*. Beijing, China: IEEE, Aug 2014, pp. 1–4.

[110] S. Subramaniam, H. Reyes, and N. Kaabouch, "Spectrum occupancy measurement: An autocorrelation based scanning technique using USRP," in *2015 IEEE 16th Annual Wireless and Microwave Technology Conference (WAMICON)*. Cocoa Beach, FL, USA: IEEE, Apr 2015, pp. 1–5.

[111] A. Al-Hourani, V. Trajkovic, S. Chandrasekharan, and S. Kandeepan, "Spectrum occupancy measurements for different urban environments," in *2015 European Conference on Networks and Communications (EuCNC)*. Paris, France: IEEE, Jun 2015, pp. 97–102.

[112] O. Babalola, E. Garba, I. Oladimeji, A. Bamiduro, N. Faruk, O. Sowande, O. Bello, A. Ayeni, and M. Muhammad, "Spectrum occupancy measurements in the TV and CDMA bands," in *2015 International Conference on Cyberspace (CYBER-Abuja)*. Abuja, Nigeria: IEEE, Nov 2015, pp. 192–196.

[113] W. Balid, S. A. Rajab, and H. H. Refai, "Comprehensive study of spectrum utilization for 802.11b/g/n networks," in *2015 International Wireless Communications and Mobile Computing Conference (IWCMC)*. Dubrovnik, Croatia: IEEE, Aug 2015, pp. 1526–1531.

[114] D. Das and S. Das, "A Survey on Spectrum Occupancy Measurement for Cognitive Radio," *Wireless Personal Communications*, vol. 85, no. 4, pp. 2581–2598, Dec 2015.

[115] S. Depatla, A. Muralidharan, and Y. Mostofi, "Occupancy Estimation Using Only WiFi Power Measurements," *IEEE Journal on Selected Areas in Communications*, vol. 33, no. 7, pp. 1381–1393, Jul 2015.

[116] H. Elshafie, N. Fisal, M. Abbas, W. Hassan, H. Mohamad, N. Ramli, S. Jayavalan, and S. Zubair, "A survey of cognitive radio and TV white spaces in Malaysia: A survey of cognitive radio and TV white spaces in Malaysia," *Transactions on Emerging Telecommunications Technologies*, vol. 26, no. 6, pp. 975–991, Jun 2015.

[117] H. E. A. Elshafie, N. Fisal, S. K. Syed-Yusof, H. Mohamad, N. B. Ramli, S. Jayavalan, W. A. Hassan, and S. Zubair, "VHF Band Utilization Measure-

ment for Cognitive Radio Application in Malaysia," *Wireless Personal Communications*, vol. 85, no. 4, pp. 2727–2747, Dec 2015.

[118] M. Fadda, V. Popescu, M. Murroni, P. Angueira, and J. Morgade, "On the Feasibility of Unlicensed Communications in the TV White Space: Field Measurements in the UHF Band," *International Journal of Digital Multimedia Broadcasting*, vol. 2015, pp. 1–8, 2015.

[119] the Department of Telecommunication Science, University of Ilorin, Nigeria, A. A. Ayeni, N. Faruk, O. W. Bello, O. A. Sowande, and M. Y. Muhammad, "Spectrum Occupancy Measurements and Analysis in the 2.4-2.7 GHz Band in Urban and Rural Environments," *International Journal of Future Computer and Communication*, vol. 5, no. 3, pp. 142–147, 2016.

[120] M. Umehira, S. Rachi, and S. Takeda, "Experimental evaluation of a spectrum occupancy rate measurement method based on LSE estimation of Gaussian noise CDF," in *2016 22nd Asia-Pacific Conference on Communications (APCC)*. Yogyakarta, Indonesia: IEEE, Aug 2016, pp. 404–408.

[121] E. Wiles, B. Hill, F. A. da Silva, and K. Negus, "Measurement and analysis of spectrum occupancy from 140 to 1000 MHz in rural western Montana," in *2016 10th European Conference on Antennas and Propagation (EuCAP)*. Davos, Switzerland: IEEE, Apr 2016, pp. 1–4.

[122] A. Agarwal, A. S. Sengar, R. Gangopadhyay, and S. Debnath, "A real time measurement based spectrum occupancy investigation in north-western india for Cognitive Radio applications," in *2016 International Conference on Wireless Communications, Signal Processing and Networking (WiSPNET)*. Chennai, India: IEEE, Mar 2016, pp. 2035–2039.

[123] S. Barnes, P. Botha, and B. Maharaj, "Spectral occupation of TV broadcast bands: Measurement and analysis," *Measurement*, vol. 93, pp. 272–277, Nov 2016.

[124] M. Cardenas-Juarez, M. A. Diaz-Ibarra, U. Pineda-Rico, A. Arce, and E. Stevens-Navarro, "On spectrum occupancy measurements at 2.4 GHz ISM band for cognitive radio applications," in *2016 International Conference on Electronics, Communications and Computers (CONIELECOMP)*. Cholula: IEEE, Feb 2016, pp. 25–31.

[125] Y. Chen and H.-S. Oh, "Spectrum measurement modelling and prediction based on wavelets," *IET Communications*, vol. 10, no. 16, pp. 2192–2198, Nov 2016.

[126] Y. Chen and H. Oh, "A Survey of Measurement-Based Spectrum Occupancy Modeling for Cognitive Radios," *IEEE Communications Surveys & Tutorials*, vol. 18, no. 1, pp. 848–859, 2016.

[127] N. Faruk, O. W. Bello, O. Sowande, S. Onidare, M. Muhammad, and A. Ayeni, "Large scale spectrum survey in rural and urban environments within the 50 MHz – 6 GHz bands," *Measurement*, vol. 91, pp. 228–238, Sep 2016.

[128] A. Gupta, S. Agarwal, and S. De, "A New Spectrum Occupancy Model for 802.11 WLAN Traffic," *IEEE Communications Letters*, vol. 20, no. 12, pp. 2550–2553, Dec 2016.

[129] M. Hoyhtya, A. Mammela, M. Eskola, M. Matinmikko, J. Kalliovaara, J. Ojaniemi, J. Suutala, R. Ekman, R. Bacchus, and D. Roberson, "Spectrum Occupancy Measurements: A Survey and Use of Interference Maps," *IEEE Communications Surveys & Tutorials*, vol. 18, no. 4, pp. 2386–2414, 2016.

[130] J. Jacob and B. R. Jose, "Spectrum occupancy measurement and analysis in Kochi-India from a cognitive radio perspective," in *2016 Sixth International Symposium on Embedded Computing and System Design (ISED)*. Patna, India: IEEE, Dec 2016, pp. 328–333.

[131] B. E. Khamlichi, C. Abdelaali, L. Ahmed, and J. E. Abbadi, "A quantitative investigation of spectrum utilization in UHF and VHF bands in Morocco: The road to cognitive radio networks," in *2016 11th International Conference on In-*

telligent Systems: Theories and Applications (SITA). Mohammedia, Morocco: IEEE, Oct 2016, pp. 1–6.

[132] M. Lopez-Benitez and F. Casadevall, "Space-dimension models of spectrum usage for cognitive radio networks," *IEEE Transactions on Vehicular Technology*, pp. 1–1, 2016.

[133] S. A. Rajab, W. Balid, and H. H. Refai, "Toward enhanced wireless coexistence in ISM band via temporal characterization and modelling of 802.11b/g/n networks: Enhanced wireless coexistence via temporal characterization/modelling," *Wireless Communications and Mobile Computing*, vol. 16, no. 18, pp. 3212–3229, Dec 2016.

[134] A. Martian, R. Craciunescu, A. Vulpe, G. Suciu, and O. Fratu, "Access to RF White Spaces in Romania: Present and Future," *Wireless Personal Communications*, vol. 87, no. 3, pp. 693–712, Apr 2016.

[135] G. Ding, Y. Jiao, J. Wang, Y. Zou, Q. Wu, Y. Yao, and L. Hanzo, "Spectrum inference in cognitive radio networks: Algorithms and applications," *IEEE Communications Surveys Tutorials*, vol. 20, no. 1, pp. 150–182, Firstquarter 2018.

[136] R. Aguilar-Gonzalez, V. Ramos, A. Prieto-Guerrero, M. Cardenas-Juarez, U. Pineda-Rico, and E. Stevens-Navarro, "An analysis of spectrum occupancy upon the analog switch-off in the City of San Luis Potosi, Mexico," in *2017 IEEE 9th Latin-American Conference on Communications (LATINCOM)*. Guatemala City: IEEE, Nov 2017, pp. 1–6.

[137] A. De Sabata, C. Balint, P. Bechet, and S. Miclaus, "USRP based HF spectrum occupancy measurements at two locations in central and Western Romania," in *2017 International Symposium on Signals, Circuits and Systems (ISSCS)*. Iasi, Romania: IEEE, Jul 2017, pp. 1–4.

[138] H. Haralambous and H. Papadopoulos, "24-h HF Spectral Occupancy Characteristics and Neural Network Modeling Over Northern Europe," *IEEE Transactions on Electromagnetic Compatibility*, vol. 59, no. 6, pp. 1817–1825, Dec 2017.

[139] F. Kiftaro, M. El-Tarhuni, and K. Assaleh, "UHF Spectrum Occupancy Measurements in Sharjah - UAE," p. 5, 2017.

[140] M. G. Mostafa, E. Tsolaki, and H. Haralambous, "HF Spectral Occupancy Time Series Models Over the Eastern Mediterranean Region," *IEEE Transactions on Electromagnetic Compatibility*, vol. 59, no. 1, pp. 240–248, Feb 2017.

[141] A. Palaios, J. Riihijarvi, O. Holland, and P. Mahonen, "Detailed Measurement Study of Spatial Similarity in Spectrum Use in Dense Urban Environments," *IEEE Transactions on Vehicular Technology*, vol. 66, no. 10, pp. 8951–8963, Oct 2017.

[142] I. A. Sikiru, N. Faruk, S. I. Popoola, Y. Imam-Fulani, A. A. Oloyede, L. A. Olawoyin, and N. T. Surajudeen-Bakinde, "Effects of detection threshold and frame size on duty cycle in GSM bands," in *2017 IEEE 3rd International Conference on Electro-Technology for National Development (NIGERCON)*. Owerri: IEEE, Nov 2017, pp. 343–346.

[143] P. D. Welch, "The use of fast Fourier transform for the estimation of power spectra: A method based on time averaging over short, modified periodograms," *IEEE Trans. Audio Electroacoust.*, vol. 15, pp. 70–73, Jun. 1967.

[144] J. Lehtomäki, M. López-Benítez, K. Umebayashi, and M. Juntti, "Improved channel occupancy rate estimation," *IEEE Trans. Commun.*, vol. 63, no. 3, pp. 643–654, Mar. 2015.

[145] "Recommendation ITU-R SM.328-10. Spectra and bandwidth of emissions," 1992.

[146] S. Wang, F. Patenaude, and R. J. Inkol, "Computation of the normalized detection threshold for the FFT filter bank-based summation CFAR detector," *Journal of Computers*, vol. 2, no. 6, pp. 35–48, Aug. 2007.

[147] J. Lehtomäki, R. Vuohtoniemi, and K. Umebayashi, "On the measurement of duty cycle and channel occupancy rate," *IEEE J. Sel. Areas Commun.*, vol. 31,

no. 11, pp. 2555–2565, Nov. 2013.

[148] S. Geirhofer, L. Tong, and B. M. Sadler, "A measurement-based model for dynamic spectrum access in WLAN channels," in *in Proc. MILCOM*, Oct. 2006, pp. 1–7.

[149] H. Urkowitz, "Energy detection of unknown deterministic signals," *Proc. IEEE*, vol. 55, no. 4, pp. 523–531, Apr. 1967.

[150] M. López-Benítez and F. Casadevall, "Methodological aspects of spectrum occupancy evaluation in the context of cognitive radio," *European Trans. Telecommun.*, vol. 21, no. 8, pp. 680 – 693, Dec. 2010.

[151] D. Torrieri, "The radiometer and its practical implementation," in *in Proc. MILCOM*. IEEE, Nov. 2010, pp. 304–310.

[152] H. Saarnisaari, P. Henttu, and M. Juntti, "Iterative multidimensional impulse detectors for communications based on the classical diagnostic methods," *IEEE Trans. Commun.*, vol. 53, pp. 395–398, Mar. 2005.

[153] J. J. Lehtomäki, R. Vuohtoniemi, K. Umebayashi, and J.-P. Mäkelä, "Energy detection based estimation of channel occupancy rate with adaptive noise estimation," *IEICE Trans. Commun.*, vol. E95-B, no. 4, pp. 1076–1084, Apr 2012.

[154] S. M. Kay, "Fundamentals of statistical signal processing," *Prentice Hall PTR*, 1998.

[155] K. Umebayashi, R. Takagi, N. Ioroi, Y. Suzuki, and J. Lehtomäki, "Duty cycle and noise floor estimation with welch FFT for spectrum usage measurements," in *in Proc. CROWNCOM*, Jun. 2014, pp. 73–78.

Appendix

Derivation of the condition that $0 \leq P_{\mathrm{D1}} \leq 1$

In this appendix, we will show the condition that $0 \leq P_{\mathrm{D1}} \leq 1$ at $0 \leq \Psi[f_c] \leq 1$.

At first, we will prove that the condition (4.17) satisfies $P_{\mathrm{D1}} \leq 1$. The condition $P_{\mathrm{D1}} \leq 1$ is given by (4.16) as

$$1 + \frac{b}{2a} \leq \frac{\sqrt{b^2 - 4ac}}{2a}, \tag{6.1}$$

where a, b and c are given by (4.15). Finally, (6.1) is given as the following inequality

$$-4a(a + b + c) \geq 0. \tag{6.2}$$

Then, a is always larger than or equal to zero because $a = \Psi[f_c](\Psi[f_c] - \frac{1}{M})$ and $0 \leq \Psi[f_c] \leq \frac{1}{M}$ is not defined for $m_{\mathcal{H}_1}$-*out-of*-M Model. Therefore, (6.2) is satisfied when $a + b + c \leq 0$.

On the other hand, $(a + b + c)$ becomes a quadratic equation with respect to $\Psi[f]$ as

$$\begin{aligned} & a + b + c \\ = \; & P_{\mathrm{FA,target}}^2 \Psi[f_c]^2 \\ & + \left[\left(\frac{1}{M} - 2 \right) P_{\mathrm{FA,target}}^2 - \frac{1}{M} P_{\mathrm{FA,target}}^2 \right] \Psi[f_c] \\ & + \frac{P_{\mathrm{FA,target}}(1 - P_{\mathrm{FA,target}})}{M} + P_{\mathrm{FA,target}}^2 - \delta^2. \end{aligned} \tag{6.3}$$

$(a+b+c)$ is monotonic and decreasing at $0 \leq \Psi[f_c] \leq 1$ because $(a+b+c)$ is a convex function with respect to $\Psi[f_c]$ and the axis $\Psi[f_c]_{\mathrm{axis}}$ takes $\Psi[f] \geq 1$ as follows,

$$\Psi[f_c]_{\mathrm{axis}} = 1 + \frac{1 - P_{\mathrm{FA,target}}}{2M P_{\mathrm{FA,target}}}. \tag{6.4}$$

From the above results, if $a+b+c \leq 0$ is satisfied at $\Psi[f_c]=0$, $a+b+c \leq 0$ is always satisfied at $0 \leq \Psi[f_c] \leq 1$. Therefore, the condition that satisfies $P_{\mathrm{D1}} \leq 1$ is given as (6.5) by substituting $\Psi[f_c]=0$ for (6.3),

$$\frac{P_{\mathrm{FA,target}}(1-P_{\mathrm{FA,target}})}{M}+P_{\mathrm{FA,target}}^2-\delta^2 \leq 0. \tag{6.5}$$

By solving (6.5) with respect to δ, the obtained condition is given as

$$\delta \geq \sqrt{P_{\mathrm{FA,target}}^2+\frac{P_{\mathrm{FA,target}}(1-P_{\mathrm{FA,target}})}{M}}. \tag{6.6}$$

This condition is logical because the estimated DC is always overestimated as much as $P_{\mathrm{FA,target}}$.

Next, we will prove that the condition (4.18) satisfies $P_{\mathrm{D1}} \geq 0$ under the condition (4.17) or (6.6) approximately.

The condition $P_{\mathrm{D1}} \geq 0$ is given by (4.16) and the fact that $a \geq 0$ as

$$c \geq 0, \tag{6.7}$$

where c is given by (4.15). Then, by substituting the condition (6.6) into δ in c, we obtain the following inequality,

$$\begin{aligned} c &\leq (1+P_{\mathrm{FA,target}})^2\Psi[f_c]^2 \\ &- \left[\left(2-\frac{1}{M}\right)P_{\mathrm{FA,target}}^2+\left(2+\frac{1}{M}\right)P_{\mathrm{FA,target}}\right]\Psi[f_c]. \end{aligned} \tag{6.8}$$

If we set allowable DC estimation error δ and target false alarm rate $P_{\mathrm{FA,target}}$ that hold the equation for (6.6) subject to $P_{\mathrm{FA,target}} \ll 1$ and $P_{\mathrm{FA,target}} \ll M$, the area of DC to be $c \geq 0$ is approximately given as follows,

$$\begin{aligned} \Psi[f_c] &\geq \frac{\left(2-\frac{1}{M}\right)P_{\mathrm{FA,target}}^2+\left(2+\frac{1}{M}\right)P_{\mathrm{FA,target}}}{1+P_{\mathrm{FA,target}}} \\ &\approx 2P_{\mathrm{FA,target}}. \end{aligned} \tag{6.9}$$

From the above condition, we see that $P_{D1} \geq 0$ with high probability because we set small enough probability of false alarm according to (6.6).

Publications

Journal Papers

[1] H. Iwata, K. Umebayashi, J. J. Lehtomaki, and S. Narieda, "Welch FFT Segment Size Selection Method for FFT Based Wide Band Spectrum Measurement," IEICE Trans. Commun., vol. E101-B, no. 7, pp.1733-1743, July 2018 (Chapter 5, Contribution [C3]).

[2] H. Iwata, K. Umebayashi, S. Tiiro, J. J. Lehtomaki, M. Lopez-Benitez, and Y. Suzuki, "Welch FFT Segment Size Selection Method for Spectrum Awareness System," IEICE Trans. Commun., vol. E99-B, no. 8, pp. 1813-1823, Aug. 2016 (Chapters 4 and 5, Contributions [C1], [C2] and [C3]).

[3] K. Umebayashi, K. Moriwaki, R. Mizuchi, H. Iwata, S. Tiiro, J. J. Lehtomaki, M. Lopez-Benitez, and Y. Suzuki, "Simple Primary User Signal Area Estimation for Spectrum Measurement," IEICE Trans. Commun., vol. E99-B, no. 2, pp. 523-532, Feb. 2016.

Refereed International Conference Papers

[1] H. Iwata, K. Umebayashi, J. J. Lehtomaki, M. Lopez-Benitez and S. Narieda, "Development of A Smart Specrum Access Prototype," in Proc. European Conference on Networks and Communications (EuCNC), Oulu, Finland, June 2017.

[2] K. Umebayashi, H. Iwata, J. J. Lehtomaki and M. Lopez-Benitez, "Study on Simple Signal Area Estimation for Efficient Spectrum Measurements," in Proc. Eu-

ropean Conference on Networks and Communications (EuCNC), Oulu, Finland, June 2017.

[3] H. Iwata, K. Umebayashi, S. Tiiro, J. J. Lehtomaki, and Y. Suzuki, "A study on Welch FFT Segment Size Selection Method for Spectrum Awareness," in Proc. IEEE Wireless Communications and Networking Conference Workshops (WCNCW), IEEE, Doha, Qatar, Apr. 2016.

[4] H. Iwata, K. Umebayashi, S. Tiiro, J. J. Lehtomaki, and Y. Suzuki "Optimum Welch FFT Segment Size for Duty Cycle Estimation in Spectrum Awareness System", in Proc. IEEE Wireless Communications and Networking Conference Workshops (WCNCW), IEEE, pp.229-234, New Orleans, USA, Mar. 2015.

Non-Refereed International Conference Papers

[1] H. Iwata, K. Umebayashi, A. Al-Tahmeesschi, M. Lopez-Benitez, "[Poster Presentation] Neural Network-based Channel Occupancy Rate Prediction," in Proc. IEICE International Workshop on Smart Wireless Communications (SmartCom), Bangkok, Thailand, Oct. 2018.

[2] K. Umebayashi, R. Mizuchi, H. Iwata, K. Hayashi, M. Kobayashi, S. Tiiro, Y. Tamaki, T. Maruyama, J. J. Lehtomaki, M. Lopez-Benitez, and Y. Suzuki, "[Technology Exhibit] Spectrum Awareness System Prototype for Smart Spectrum Access", in Proc. IEICE International Workshop on Smart Wireless Communicarions (SmartCom), Tokyo, Japan, Oct. 2015.

[3] H. Iwata, K. Umebayashi, R. Mizuchi, T. Maruyama, K. Moriwaki, S. Tiiro, J. J. Lehtomaki, and Y. Suzuki, "[Technology Exhibit] Development of A Measurement System for Spectrum Awareness DC Estimation based on Welch-FFT ", in Proc. IEICE International Workshop on Smart Wireless Communicarions (SmartCom), vol. 114, no. 284, SR2014-89, pp. 171-177, Singapore, Oct. 2014.

Domestic Conference Papers (in Japanese)

［1］岩田 大輝, 梅林 健太, 佐藤 遼, 山田 健斗, 大川 航平, 笠原 芳樹, Janne Lehtomaki, Miguel Lopez-Benitez, ”［技術展示］スマートスペクトラムアクセスのための周波数利用観測システムプロトタイプの開発 周波数利用率の予測 ”, 電子情報通信学会技術報告, vol. 118, no. 58, SR2018-17, pp. 99-106, 東京, May 2018.

［2］岩田 大輝, 梅林 健太, Janne Lehtomaki, Miguel Lopez-Benitez, ”周波数利用観測のための時間-周波数変動するノイズフロア推定法”, 電子情報通信学会技術報告, vol. 117, no. 410, SR2017-101, pp. 43-50, 福岡, Jan. 2018.

［3］岩田 大輝, 梅林 健太, 玉木 義孝, 長 大樹, 佐藤 遼, 成枝 秀介, ”［技術展示］スマートスペクトラムアクセスプロトタイプの開発”, 電子情報通信学会技術報告, vol. 117, no. 56, SR2017-16, pp. 97-104, 東京, May 2017.

［4］岩田 大輝, 梅林 健太, Janne J. Lehtomaki, 鈴木 康夫, ”周波数利用観測のための低コストな Welch FFT セグメントサイズ選択法の解析”, 電子情報通信学会技術報告, vol. 115, no. 411, SR2015-72 , pp. 1-8, 長崎, Jan. 2016.

［5］岩田 大輝, 梅林 健太, Samuli Tiiro, Janne J. Lehtomaki, 鈴木 康夫, ”Duty Cycle 推定に適した Welch FFT のセグメントサイズ選択法”, 電子情報通信学会技術報告, vol. 114, no. 435, SR2014-110, pp. 101-108, 函館, Jan. 2015.

Award

［1］ The 2nd International Workshop on Smart Spectrum at IEEE Wireless Communications and Networking Conference 2016, Best Paper Award. (関連論文 [1])